Catalytic Membrane Reactors

Università della Calabria

Dottorato di Ricerca in Ingegneria Chimica e dei Materiali

SCUOLA DI DOTTORATO " PITAGORA " IN SCIENZE INGEGNERISTICHE

Tesi

Analysis of Membrane Reactor Integration in Hydrogen Production Process

Settore Scientifico Disciplinare CHIM07 – Fondamenti chimici delle tecnologie

Supervisori

Ch.mo Prof. Enrico DRIOLI

Dr. Ing. Giuseppe BARBIERI

Il Coordinatore del Corso di Dottorato

Ch.mo Prof. Raffaele MOLINARI

Dottoranda

Ing. Ilaria Mirabelli

Ciclo XXVII

A.A. 2013-2014

Contents

Abstract

In the H_2 production field, the membrane reactor (MR) technology is considered a promising and interesting technology. In this thesis work the integration in a small scale hydrogen generator of an MR, to carry out the water gas shift reaction (WGS), has been studied. In particular, the effect of MR integration from a systems perspective, i.e. specifically assessing the impact of MR on the whole process, has been investigated. A preliminary design of a pilot scale MR to produced 5 Nm^3/h of H_2 by reformate stream upgrading has been performed. A CO conversion of 95% and an hydrogen recovery yield of 90% have been fixed as minimum performance target of the WGS-MR. Depending on the system considered to promote the driving force for the permeation, three scenarios have been proposed: base, vacuum and sweep scenario. On the basis of results from a preliminary scenario screening, the required membrane area (ca. 0.179 m^2), for vacuum and sweep scenarios, has been estimated by means of an MR modelling and simulation. The results obtained from the pilot scale have been used for the scale-up of the WGS-MR integrated in the 100 Nm^3/h hydrogen production unit. The plant for the integrated process (reformer and WGS-MR) has been simulated by using the commercial simulation tool Aspen Plus®.

The MR integration, actually, implies a re-design of the process downstream the WGS reactor. Since more than 90% of the produced H_2 is directly recovered in the permeate stream, the PSA unit can be removed, leading to a more compact system. For the retentate stream post processing, the possibility to recover the CO_2, by means of membrane gas separation technology has been proposed. The results for a two stages membrane separation unit confirmed the technological feasibility of the CO_2 capture, achieving the CO_2 purity target.

Pursuing the logic of process intensification, the comparison with the reference technology (reformer, high temperature shift, PSA) showed as the WGS-MR integrated system results in a more "intensified" process since a higher H_2 productivity, a smaller plant and an enhanced exploitation of raw materials are obtained. In addition, since the MR delivers a high-pressure CO_2-rich stream, it provides an opportunity for small-scale CO_2 capture and thus possible emission reduction.

The possibility to extend the spectrum of MR application in reactions of industrial interest, where hydrogen is produced as by-product, has been also studied. In particular, as case study, the direct conversion of n-butane to isobutene has been analysed, showing as, from a thermodynamic point of view, better performance (equilibrium conversion up to seven times higher than the one of a traditional reactor) can be obtained.

Abstract

Nel campo della produzione di H_2, quella dei reattori a membrana (MR) è considerata una tecnologia promettente e interessante. In questo lavoro di tesi si è studiata l'integrazione all'interno di un generatore di idrogeno su piccola scala (100 Nm^3/h di H_2) di un reattore a membrane, usato per condurre la reazione di water gas shift (WGS). In particolare è stato studiato l'effetto dell'integrazione del MR dal punto di vista dell'intero processo, valutando cioè l'impatto e le ricadute dell'integrazione su tutto il processo. È stata effettuata prima la progettazione del reattore a membrana su scala pilota, per la produzione di 5 Nm^3/h di H_2. Una conversione di CO del 95% ed un recupero di idrogeno del 90% sono stati fissati come valori minimi delle prestazioni del WGS-MR.

A seconda del sistema considerato per promuovere la forza spingente per la permeazione, sono stati proposti tre scenari: base, vacuum and sweep. Sulla base dei risultati ottenuti da uno screening preliminare sugli scenari, per quello vacuum e quello sweep si è proceduto alla valutazione della superficie di membrana richiesta (pari a ca. 0.18 m^2) mediante la modellazione e simulazione del MR. I risultati di simulazione ottenuti su scala pilota sono stati utilizzati per lo scale-up del WGS-MR per la produzione di 100 Nm^3/h di idrogeno.

L'impianto per il processo integrato (reformer e WGS-MR) è stato simulato usando come software di simulatione l' AspenPlus®. L'integrazione del reattore a membrana implica in pratica, una ri-progettazione del processo a valle del reattore stesso. Poiché più del 90% dell' H_2 prodotto è recuperato direttamente nella corrente di permeato, l'unità per la purificazione dell'idrogeno può essere rimossa, ottenendo di conseguenza un sistema più compatto. Per il post-processing della corrente di retentato è stata proposta e analizzata la possibilità di recuperare la CO_2, per mezzo di tecnologie a membrana per separazione gassose. I risultati ottenuti con un sistema costituito da due unità di separazione a membrana hanno confermato la fattibilità tecnologica della cattura della CO_2, consentendo di raggiungere il target sulla purezza della CO_2 recuperata.

Perseguendo la logica definita dalla "Process intensification", il confronto con la tecnologia di riferimento (reforming, shift ad alta temperatura, PSA) ha mostrato come il sistema integrato con il WGS-MR risulti in un processo più "intensificato" poiché si ottengono una maggiore produttività di idrogeno, un impianto più piccolo e una migliore sfruttamento delle materie prime. Inoltre, poiché in uscita dal reattore a membrana si ottiene una corrente di retentato compressa e ricca in CO_2, ciò offre la possibilità di catturare anche su piccola scala la CO_2, e perciò una possibile riduzione delle emissioni.

è stato inoltre oggetto di studio la possibilità di estendere lo spettro di applicazione dei reattori a membrana in reazioni di interesse industriale, in cui si produce idrogeno come sottoprodotto. In particolare, come caso di studio, è stata analizzata la conversione diretta di n-butano ad isobutene, mostrando come possano essere ottenute, da un punto di vista termodinamico, migliori prestazioni, con conversione all'equilibrio fino a sette volte superiore a quella di un reattore tradizionale.

Problem statement, objectives and work structure

The idea developed in the following thesis is based on the study of membrane reactor (MR) integration to produce hydrogen in a more efficient way, following the process intensification strategy. The attention has been addressed toward hydrogen production since the hydrogen, as a potential energy carrier, will play a very important role in future energy systems. For this reason many companies and academic institutions are focusing their efforts in trying to improve the H_2 production process. This is also the subject of several research projects, such as the European project DEMCAMER (Design and Manufacturing of Catalytic Membrane Reactors by developing new nano-architectured catalytic and selective membrane materials) under which this thesis has been developed. In the H_2 production field, the membrane reactor (MR) technology is considered a promising and interesting technology. MR systems, to carry out some typical reactions for hydrogen production (e.g., reforming, water gas shift), have been extensively investigated in the open literature, proving MR capability in improving conversion, yield and selectivity. Most of these studies, however, have been mainly focused on the enhanced achievable MR performance, at experimental and theoretical level. The effect of MR integration from a systems perspective, i.e. specifically assessing the impact of MR on the whole process, has been poorly investigated.

The focus of this research work has been therefore addressed to deeper investigate and quantify the benefits of WGS-MR integration into small-scale H_2 production, since the MR technology could be a good candidate in distributed hydrogen production. The main objective of this work was to re-design the traditional hydrogen production process in a more compact and efficient way, by means of membrane technology application.
In the global re-design of process scheme, the opportunity of possible cheaper small-scale CO_2 separation, by means of membrane gas separation technology, has also been examined.

The integration of a novel WGS catalyst, developed by DEMCAMER partner project, with a commercial Pd-base membrane has been also studied from an experimental point of view.

The possibility to extend the spectrum of MR application in reactions of industrial interest, where hydrogen is produced as by-product, has been also studied; the direct conversion of n-butane to isobutene, by dehydroisomerization reaction, has been analysed as case study.

The applied methodology and structure of the work are as follows:

i. Design of a pilot scale WGS-MR to produce H_2 by reformate stream upgrading: selection of suitable configurations, modelling of MR configurations, definition of operating conditions and MR design (chapter 1).

ii. Scale up of the WGS-MR, as defined in i., integration of the WGS-MR in small scale H_2 generator (100 Nm^3/h H_2) and process plant simulation. Comparison between selected scenarios and comparison with conventional technology (chapter 2).

iii. Post processing of WGS-MR retentate stream by membrane gas separation technology application for CO_2 recovery (chapter 3).

iv. Experimental reaction investigation on a novel WGS catalyst integrated in a membrane reactor (chapter 4).

v. Analysis of the potentiality of MR integration in process involving H_2 production (chapter 5).

vi. Overall conclusions.

.

Chapter 1

Pilot scale water gas shift membrane reactor design

Introduction

The water-gas shift (WGS) reaction (Eq. 1) is a well-known step for upgrading carbon monoxide to hydrogen: the CO content, present in the syngas mixtures, is reduced by steam, producing more hydrogen.

$$H_2O + CO \leftrightarrow CO_2 + H_2 \qquad \Delta H_{RX, 298 \, K} = -41 \text{ kJ/mol}$$

<div align="right">Eq. 1</div>
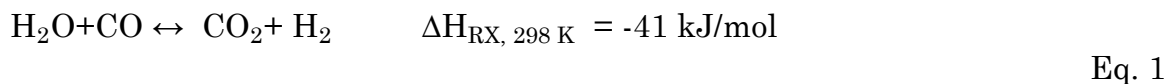
The WGS is an exothermic equilibrium-limited reaction characterized by no variation of mole number. From a thermodynamic point of view the equilibrium conversion is favoured at lower temperatures and it is not affected by the pressure.

Reported for the first time in literature by the end of the 19th century, the WGS reaction found initial industrial application in the production of synthesis gas from coal and coke. The gas shift reaction was commonly performed at temperatures around 450-600 °C, using iron oxide catalyst [1] in a single stage. The introduction of a second stage operating at lower temperature, by means of Cu-based low-temperature (LT) shift catalysts, allows the reduction of CO content to less than 0.5%. The integration of the WGS reaction was dependent on the origin of the synthesis gas, principally coal at the time of its first industrial applications. With the increasing industrial demand for hydrogen, new production processes based on hydrocarbons reforming have been investigated. In particular, fuel processing of natural gas is the most common hydrogen production method in commercial use today.

In a typical industrial operation, Ni-based catalysts are primarily used for the steam reforming of natural gas at high temperatures (>700 °C) using high steam to carbon ratios (S/C), at least 3-5. Then, the cooled gas from the reformer is fed into a high temperature (HT) CO-shift converter, commonly in the temperature range of 320-360 °C and at a total pressure between 10 and 60 bar, containing a Fe-based oxide catalyst [2]. Depending on the feedstock and the performance of the HT CO-shift reactor, an outlet stream with a CO concentration between 1 and 5% is typically obtained at a temperature around 400-450 °C. The stream is then cooled by thermal quenching with water or by an inter-cooler system between stages. In some operations, water is injected between the stages to adjust the S/C ratio before entering into a low temperature CO-shift reactor, operating in the range of 190-250 °C. A CO concentration less than 0.5% is usually obtained in the outlet stream from the low temperature shift [3].

Moving from the initial WGS industrial application to the current shift process, many aspects related to the catalysts, reaction mechanisms and kinetics has been investigated. In most recent times, the growing H_2 demand (for instance high purity hydrogen stream used in polymeric electrolyte membrane (PEM) fuel cells) has brought in a new dimension the WGS process role [4]. For the production of high-purity H_2 stream the advantages offered by membrane reactor technology applications have been clearly shown and proved in the literature [5, 6, 7].

Fundamentally, a membrane reactor is a system where reaction and separation are performed in the same unit by means of a permselective membrane that allows the selective removal of some products from the reaction volume. In the field of hydrogen production, the application of a membrane reactor to carry out WGS reaction has been extensively investigated by several research groups [5, 8, 9, 10, 11, 12, 13]. These studies showed as the removal of hydrogen from the reaction side allows to shift the reaction toward further CO conversion and to recover, in dependence on the membrane used, a rich/pure H_2 stream in the permeate side. In most of the cases, H_2 selective membranes such as Pd, Pd-Ag alloys, or microporous silica

have been tested [11]. Recently, studies using CO_2 selective membranes have also appeared in literature [14, 15]. In these studies the possibility of using a CO_2 selective membrane to enhance the CO conversion and to increase the H_2 purity on the high pressure side of the membrane reactor has been investigated. In addition to experimental studies, the modelling and simulation of membrane reactors has been also largely studied. The relevant literature concerning membrane reactors models is wide; thus we will mention here some selected examples only. MR models are described in the literature with various level of complexity: one [11, 17, 18, 19] or two-dimensional models [20, 21], in steady-state or transient condition. Regarding the configuration, the tube and shell reactor configuration is the most used. Some models assume isothermal MR operation while others include heat balances, allowing to simulate non-isothermal or adiabatic operation. The majority of the papers on Pd-alloy MR modelling refers to tubular plug-flow MRs for steady-state operations. Barbieri and Di Maio [22] proposed a non-isothermal steady-state model of a plug-flow tubular MR for the methane steam reforming (MSR) reaction in co-current and counter-current mode, studying in particular, the configuration effects. Basile et al. [23] proposed 1D steady-state model for the partial oxidation of methane, water gas shift and MSR in dense Pd MR. Using a 1D isothermal model Harold et al. [24] simulated a packed-bed annular MR for the methanol decomposition, methanol steam reforming, and methanol partial oxidation.

From a more general point of view there are many studies on small scale membrane reactor systems to carry out reactions of industrial interest such as reforming, water gas shift, dehydrogenation of hydrocarbons, proving the capability of MRs in improving conversion, yield and selectivity [25]. This is the scenario where the DEMCAMER project [26] is set in, aiming to develop innovative multifunctional catalytic membrane reactors based on novel catalysts and selective membranes to improve their performance, durability, cost effectiveness and sustainability over four selected chemical processes (Autothermal Reforming (ATR), Fischer-Tropsch Synthesis (FTS), Water Gas

Shift (WGS), and Oxidative Coupling of Methane (OCM) for pure hydrogen, liquid hydrocarbons and ethylene production.

The activity described in the following, performed in the framework of DEMCAMER project, has been addressed to design a pilot scale MR to carry out the water gas shift reaction, producing 5 Nm³/h of hydrogen. The results, obtained from the pilot scale design, have been used as input in the analysis of this novel reactor integrated into a small scale natural gas reforming system for H_2 production (presented in chapter 2).

1.1   Pilot scale definition

The size for the pilot scale WGS membrane reactor has been defined following the target specified in the framework of the DEMCAMER project. A hydrogen production of 5 Nm³/h, with a minimum purity of 99.99 %, has been fixed. Moreover, the integration of WGS-MR has been associated downstream to a hydrocarbon reformer unit. Figure 1 shows a scheme of the considered system. The feed composition for the membrane reactor has been defined on the basis of the typical composition of a stream coming out from a natural gas steam reformer. The composition is reported in Table 1. On the basis of the water molar fraction presents in the reformer outlet stream, the steam to CO ratio is equal to 3.7. Being the typical steam to carbon ratio for the shift reaction in the range 3-5 [27], no further adjustment to the steam amount has been considered. Moreover, as reported in the literature, a membrane reactor due to the equilibrium shift effect, consequence of the hydrogen extraction, can operate at lower steam to carbon ratio with respect to the traditional reactor.
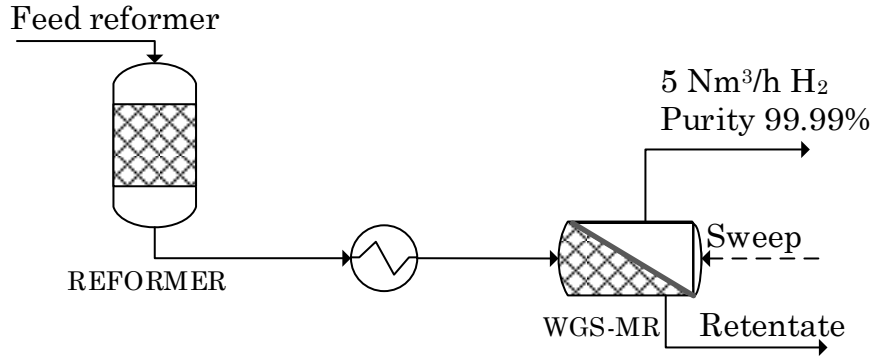
Figure 1 Scheme of the downstream integrated WGS – MR associated to a hydrocarbon reformer unit.

In a conventional H_2 production process by steam methane reforming the syngas stream coming out from the reformer is fed to a shift reactor to convert the remaining CO and then sent to a hydrogen purification unit, usually a pressure swing adsorption unit (PSA).

The aim of the WGS membrane reactor integration in H_2 production plant is to substitute the traditional shift reactor and hydrogen separation system with one single unit able to convert the CO present in the reformate stream and to recover directly the produced hydrogen. As a consequence, a minimum H_2 recovery yield value of 90% has been fixed as target value. The H_2 recovery yield is defined as the amount of hydrogen recovered in the permeate side with respect to the maximum hydrogen producible, that is the sum of hydrogen and carbon monoxide in the MR feed stream (Eq. 2)

$$\text{Hydrogen recovery yield} = H_2 \, RY = \frac{H_2 \text{ recovered in the permeate side}}{\text{Maximum } H_2 \text{ producible}}$$

Eq. 2

A minimum CO conversion target, higher than 95%, has been also set in the framework of the project.

Table 1 Feed molar fraction composition of WGS-MR

Molar fraction composition, -					
H_2	H_2O	CO	CO_2	CH_4	N_2
0.448	0.347	0.092	0.047	0.038	0.028

1.2   Case studies identification

The starting point for the pilot scale WGS-MR design was the identification of possible scenarios, in term of operating pressures and flow configuration.

As previously introduced, a membrane reactor is a system having a permselective membrane that divides the reactor in a reaction side, where the reaction happens, and a permeation side, where the selectively removed products are recovered. The selective removal of products from the reaction volume by means of the permselective membrane occurs under the effect of a driving force that is a function of the partial pressures of the species on the reaction and permeate sides. In particular, it can be created by means of an inert sweep gas in the permeate compartment (nitrogen, water, etc.), or with the application of a pressure difference between the retentate and the permeate compartments or by their combination. Depending on the system considered to promote the driving force for the permeation three scenarios have been selected for the pilot scale WGS-MR:

- a base scenario
- a vacuum scenario
- a sweep scenario.

The base scenario is the simplest one: in the reaction side the membrane reactor operates at the same pressure of the reformer unit upstream, and, in the permeation side, a pressure slightly above the atmospheric pressure value, ca. 1.2 bar_a, has been chosen. For the vacuum scenario the possibility to reduce the pressure on the permeation side, applying a vacuum pump, is proposed. As already mentioned, by decreasing the permeate pressure, the

driving force for the permeation increases. An other strategy to improve the permeation by reducing the hydrogen partial pressure on the permeation side by feeding a sweep gas, usually steam, is proposed in the sweep scenario. In this case, a dilute hydrogen stream is recovered in the permeate. For the sweep scenario the flow configuration has t be also defined. The sweep gas can be fed in co-current with the reformate feed or in counter current. The configurations are similar to the ones in the heat exchangers. The benefits of counter current configuration are well known [13, 28]; it is more efficient since allows a better exploitation of the membrane area. Several case studies have been selected within the described scenarios. They are reported in Table 2. For the base scenario, only one case study has been defined, assuming, as described above, to operate at 1.2 bar_a in the permeate side and at the same pressure of the reformer in the retentate side. A pressure value of 7 bar_a, has been considered, since this value was fixed in the framework of the project on the basis of operating constrains for the pilot scale MR testing.

In the sweep scenario the retentate and permeate pressures are the same of the base scenario; however, the presence of a sweep stream introduces an additional degree of freedom. It is usually saturated fixing the sweep factor defined for a closed MR as the ratio of the mole number of the sweep gas to the mole number of the reference component, both evaluated at the starting time [16]. In this analysis, since we was interested to perform a preliminary screening of the defined case studies on the basis of the maximum performance achievable at equilibrium condition (see next paragraph), the additional degree of freedom for the sweep scenario was saturated by fixing the equilibrium sweep molar fraction. It represents the ratio between the molar flow rate of sweep gas fed in the permeate side and the total permeate stream molar flow rate at equilibrium condition. Fixing the equilibrium sweep fraction corresponds to fix the equilibrium hydrogen partial pressure, as expressed in Eq. 3:

$$p_{hydrogen}^{Equilibrium} = y_{hydrogen}^{Equilibrium} \; p^{Permeate\,side} = \left(1 - y_{sweep}\right) p^{Permeate\,side}$$

Eq. 3

As far as the vacuum scenario concerns, two value of vacuum pressure has been considered (case study 5 and 6).

Table 2 MR operating condition: case studies specifics

Scenario	Case study	Feed/retentate	Permeate	H_2 equilibrium partial pressure, bar_a	Equilibrium sweep molar fraction
		Pressure, bar_a			
Base	1	7	1.20	1.20	-
Sweep	2	7	1.20	0.96	0.2
	3			0.60	0.5
	4			0.24	0.8
Vacuum	5	7	0.50	0.50	-
	6		0.25	0.25	-

A scheme of the analysed scenarios is shown in Figure 2.
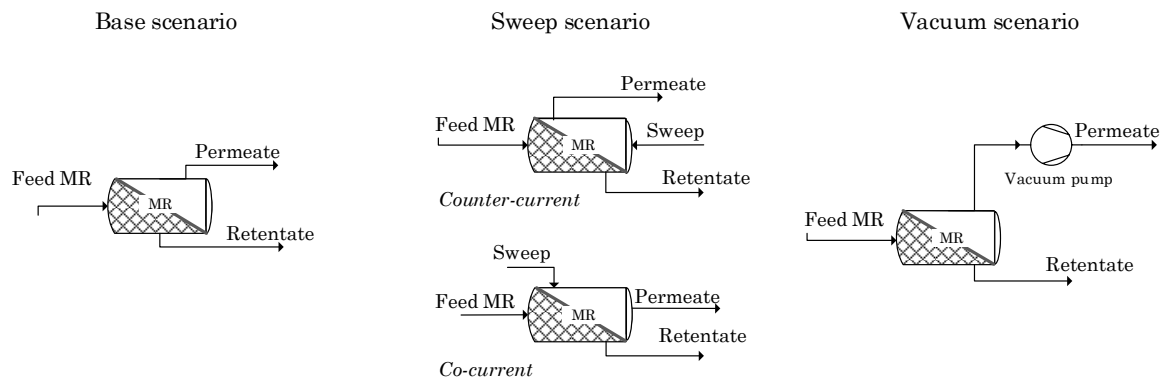
Figure 2 Schemes of the analysed scenarios.

1.3   Screening case studies

A preliminary screening of the case studies has been performed to evaluate the maximum achievable CO conversion and hydrogen recovery. On the basis of operating condition defined for each case study, a thermodynamic equilibrium calculation for a membrane reactor has been done. Thermodynamic analysis of an MR is similar to that of a traditional reactor. A membrane reactor can be considered as composed by two sections: reaction and permeation volume. In an equilibrium membrane reactor system both sections are kept closed at a constant pressure and only some specific gases can be transported between the two volumes. In this case, the hydrogen selective membrane allows the removal of the hydrogen from the reaction volume. A part of the produced hydrogen permeates through the membrane into the permeation side. As long as the hydrogen partial pressure in the reaction volume is higher than the partial pressure in the permeate side, there is permeating flux. When the partial pressures of hydrogen, on both membrane sides, are equal, no hydrogen permeation happens, and then permeative equilibrium is reached [29, 30]. In the permeative equilibrium state, the partial pressure of hydrogen on both membrane sides is also equal to the partial pressure of hydrogen at equilibrium; this condition is expressed by Eq. 4. Therefore, the thermodynamic equilibrium in an MR also depends on the permeative equilibrium in addition to the reactive equilibrium.

$$p_{\text{hydrogen}}^{\text{Equilibrum}} \;=\; p_{\text{hydrogen}}^{\text{Permeate side}} \;=\; p_{\text{hydrogen}}^{\text{Reaction side}}$$

Eq. 4

Table 3 summarizes the mass balance for the species involved in the shift reaction, also including the information for hydrogen permeation through the variable "z", which is the fraction of hydrogen in the permeation side compared to the total hydrogen produced. Therefore, the number of moles of each species at equilibrium, reactive and permeative, is a function of the reaction conversion degree (x_{eq}) and the hydrogen fraction permeated (z). In addition, the energy balance (Eq. 8) has to be associated to the material

balance to determine the maximum conversion, that can be achieved in a exothermic reaction carried out adiabatically [31]. The adiabatic temperature and equilibrium composition of the MR is thus calculated through the material and energy balances also including the constraint, introduced by Eq. 4, for the permeative equilibrium state. Table 4 reports the mathematical set of equations to be solved, with feed temperature and composition, reaction pressure and hydrogen equilibrium partial pressure as input values.

Table 3 Molar balance to calculate the equilibrium composition in a membrane reactor

moles	CO	H_2O	CO_2	H_2
Initial state	n_{CO}	n_{H2O}	n_{CO2}	n_{H2}
Reactive State	$- n_{CO}x_{eq}$	$-n_{CO}x_{eq}$	$+n_{CO}x_{eq}$	$+n_{CO}x_{eq}$
Permeation State	-	-	-	$\left(n_{H2}+n_{CO}x_{eq}\right) z$
Permeative and Reactive Equilibrium State	$n_{CO}\,(1\text{-}x_{eq})$	$(n_{H2O}\text{-}n_{CO}x_{eq})$	$(n_{CO2}+n_{CO}x_{eq})$	$\left(n_{H2}+n_{CO}x_{eq}\right)(1\text{-}z)$

Total moles number on reaction side $n_{total}^{\text{Reaction side}} = n_{tot,feed} - \left(n_{H2}+n_{CO}x_{eq}\right) z$

Total moles number on permeation side $n_{total}^{\text{Permeation side}} = n_{sweep} + \left(n_{H2}+n_{CO}x_{eq}\right) z$

Table 4 Set of equations for equilibrium conversion and H_2 recovery calculation

$$K_{eq} = \exp\left(\frac{4577.8}{T\,[K]} - 4.33\right) \qquad \text{Eq. 5}$$

$$K_{eq} = \frac{n_{CO2}n_{H2}}{n_{CO}n_{H2O}} = \frac{y_{CO2}y_{H2}}{y_{CO}y_{H2O}} = \frac{y_{CO2}}{y_{CO}y_{H2O}}\,\frac{p_{H_2}^{\text{Equilibrium}}}{p^{\text{Reaction side}}} =$$

$$= \frac{(n_{CO_2}^{\text{feed}}+n_{CO}^{\text{feed}}\,x_{eq})}{n_{CO}^{\text{feed}}\,(1-x_{eq})(\,n_{H_2O}^{\text{feed}}-n_{CO}^{\text{feed}}x_{eq})}\,\left[n_{\text{tot,feed}}-\left(n_{H_2}^{\text{feed}}+n_{CO}^{\text{feed}}x_{eq}\right)z\,\right]\frac{p_{H_2}^{\text{Equilibrium}}}{p_{\text{Reaction}}} \qquad \text{Eq. 6}$$

$$p_{\text{hydrogen}}^{\text{Equilibrium}} = y_{H_2}p^{\text{Reaction}} = \frac{\left(n_{H_2}^{\text{feed}}+n_{CO}^{\text{feed}}x_{eq}\right)(1-z)}{\left[n_{\text{tot,feed}}-\left(n_{H_2}^{\text{feed}}+n_{CO}^{\text{feed}}x_{eq}\right)z\,\right]}\,p^{\text{Reaction}} \qquad \text{Eq. 7}$$

$$-\Delta H_{Rx}(T)\,x_{eq} = \sum\left(\frac{n_i^{\text{feed}}}{n_{CO}^{\text{feed}}}\right)\,c_{p_i}(T-T_{\text{feed}}) \qquad \text{Eq. 8}$$
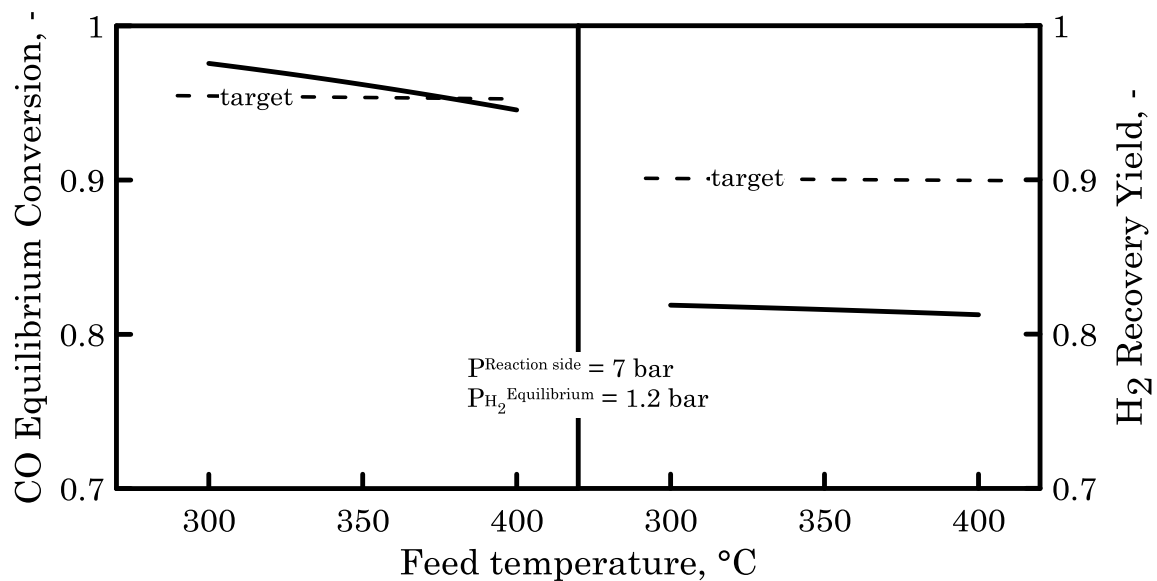
Figure 3 CO equilibrium conversion and H_2 Recovery Yield as a function of MR feed temperature.

For the case study 1 (base scenario) the membrane reactor equilibrium composition has been evaluated, at different feed temperatures (see Figure 3). Due to the exothermicity of the reaction, the CO conversion decreases

increasing the temperature. At low temperature, feed temperature less than 370°C, the target conversion is exceeded. On the other hand, the hydrogen recovery is lower than the target value in the whole temperature range investigated. The results show therefore as the operating conditions for base scenario are not suitable, because target value of the hydrogen recovery can not be obtained, even at equilibrium condition. Analogous analysis has been done for the other case studies. Conversion and H_2 recovery yield at equilibrium condition for all case studies are reported in Table 5, considering a feed temperature of 330°C. The results show as the maximum CO conversion achievable is higher than the target value for all case studies. The main constrain is related to the hydrogen recovery. It can not be reached for case study 1 (p^{Feed} = 7 bar, $p_{hydrogen}^{Equilibrium}$ = 1.2 bar) and case study 4 (p^{Feed} = 7 bar, $p_{hydrogen}^{Equilibrium}$ = 0.96 bar). The result for case study 4 requires however a more detailed analysis. As previously described, for the sweep scenario two configurations can be used: co-current and counter-current configurations. Since they are flow configurations, from a thermodynamic point of view, they should not affect the performance at equilibrium conditions. Nevertheless, the approach used to describe the equilibrium of a membrane reactor is valid only for a co-current configuration. In fact, in a counter-current configuration with an infinite membrane area, theoretically all the carbon monoxide can be converted and all the hydrogen recovered.

From the preliminary screening, only the base scenario can be excluded from the further analysis, being the target values surely not reachable.

Table 5 Summary results of an adiabatic equilibrium membrane reactor for the different case studies

	Target value	Case study 1	Case study 2	Case study 3	Case study 4	Case study 5	Case study 6
CO equilibrium conversion	> 95	96.8	99.5	98.2	97.8	98.8	99.3
H_2 RY, %	> 90	81.7	96.9	91.7	86.0	93.2	96.7
p^{Feed}, bar_a		7	7	7	7	7	7
$p^{Permeate\ side}$, bar_a		1.2	1.2	1.2	1.2	0.5	0.25
$p_{hydrogen}^{Equilibrium}$		1.2	0.24	0.6	0.96	0.5	0.25
Sweep Fraction, -		-	0.8	0.5	0.2	-	-

However, to analyse the possible benefit to operate at a higher feed pressure, the minimum feed to permeate pressure ratio required to reach the conversion and recovery target values has been evaluated. In a membrane reactor, operating as an extractor with no sweep stream, the pressure ratio is, in fact, one of the most important and significant parameters affecting the performance of the membrane unit. It provides an indication about the driving force for the permeation and about the maximum extraction achieved by the membrane unit. As shown in Figure 4, the minimum pressure ratio to obtain an H_2 recovery yield of 90% is 17. Therefore for the base scenario, where no vacuum is applied and the minimum operating permeate pressure is 1.2 bar_a, the required feed pressure is higher than 20 bar_a. The possibility to consider a case study with this feed pressure value has been excluded, since this pressure value is quite higher then the one defined as reference value for the pilot scale reactor (feed pressure of 7 bar_a). A summary of the equilibrium molar compositions for all case studies is reported in Table 6.
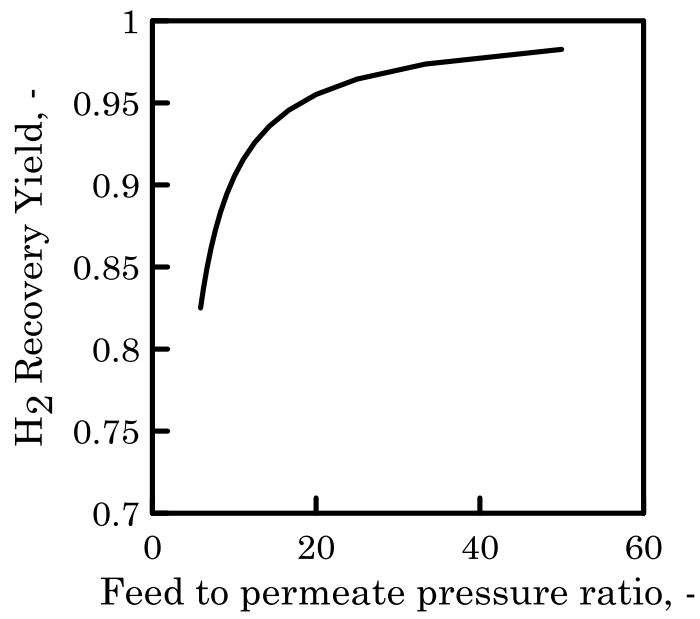
Figure 4 H_2 Recovery Yield as a function of feed to permeate pressure ratio ($p^{Feed}/p^{Permeate}$).

Table 6 Summary of the equilibrium molar compositions for all case studies

	Feed	Case Study 1		Case Study 2		Case Study 3		Case Study 4		Case Study 5		Case Study 6	
		R[a]	P[b]	R	P	R	P	R	P	R	P	R	P
Temperature[c], °C	330	429.4		358.8		405.2		410.7		431.5		432.0	
Pressure, bar$_a$	7	7	1.2	7	1.2	7	1.2	7	1.2	7	0.5	7	0.25
Molar composition, -													
CH_4	0.038	0.068	0.000	0.080	0.000	0.075	0.000	0.071	0.000	0.079	0.000	0.082	0.000
CO	0.092	0.005	0.000	0.001	0.000	0.003	0.000	0.004	0.000	0.002	0.000	0.001	0.000
CO_2	0.047	0.243	0.000	0.291	0.000	0.272	0.000	0.256	0.000	0.278	0.000	0.290	0.000
H_2	0.448	0.171	1.000	0.034	0.200	0.086	0.500	0.137	0.800	0.071	1.000	0.036	1.000
N_2	0.028	0.050	0.000	0.059	0.000	0.055	0.000	0.052	0.000	0.056	0.000	0.059	0.000
H_2O	0.347	0.462	0.000	0.536	0.800	0.508	0.500	0.480	0.200	0.514	0.000	0.533	0.000

[a] R means retentate, [b] P means permeate. [c] In the permeate side the same temperature of retentate side has been assumed.

1.4 Preliminary estimation of membrane area

On the basis of the accomplished screening, a preliminary estimation of the membrane area required to obtain the hydrogen production target of 5 Nm³/h has been done. Theoretically, the flux of hydrogen diffusing through an infinite hydrogen selective membrane is given by:

$$J_{H_2} = \frac{dF_{H_2}}{dA^{Membrane}} = \frac{Permeability_{H_2}}{Thickness} \text{ Driving force}$$

Eq. 9

In Pd-based membranes, hydrogen atoms permeate through the membrane by a solution–diffusion mechanism; the permeating flux can be expressed by Sieverts law (Eq. 10) when the rate determining step is the diffusion through the membrane:

$$J_{H_2} = \frac{Permeability_{H_2}}{Thickness} \left(\sqrt{p_{H_2}^{Retentate\ side}(z)} - \sqrt{p_{H_2}^{Permeate\ side}(z)} \right)$$

Eq. 10

The hydrogen amount permeated through a given membrane area can be thus determined by integrating Eq. 10 along the membrane surface. The hydrogen partial pressure profile, in retentate and permeate side, are required to integrate the equation. Alternatively, the average hydrogen flow through the membrane can be very accurately estimated (Eq. 11) defining the driving force by means of logarithmic mean driving force equation [32] (LMDF, Eq. 12).

$$H_2 \text{average flow rate on permeation side } = \frac{Permeability_{H_2}}{thickness} \ A^{Membrane} \ LMDF$$

Eq. 11

$$LMDF = \frac{DF_{inlet} - DF_{outlet}}{\ln\left(\frac{DF_{inlet}}{DF_{outlet}}\right)}$$

Eq. 12

Where DF_{inlet} is the inlet (feed) driving force and DF_{outlet} is the output retentate (exit) gas driving force defined respectively:

$$DF_{inlet}= \left(\sqrt{p_{H_2}^{\text{Retentate side}}}\bigg|_{inlet} - \sqrt{p_{H_2}^{\text{Permeate side}}}\bigg|_{inlet}\right)$$

Eq. 13

$$DF_{outlet}= \left(\sqrt{p_{H_2}^{\text{Retentate side}}}\bigg|_{outlet} - \sqrt{p_{H_2}^{\text{Permeate side}}}\bigg|_{outlet}\right)$$

Eq. 14

By means of Eq. 11 the membrane area can be thus expressed as:

$$A^{\text{Membrane}}= \frac{H_2 \text{molar flow rate on permeation side}}{\text{Permeance}_{H_2} \ \text{LMDF}}$$

Eq. 15

where

$$\text{Permeance}_{H_2} = \frac{\text{Permeability }_{H_2}}{\text{thickness}}$$

Eq. 16

Hence, for the different case studies, the membrane area has been estimated by means of Eq. 15. In particular, the mass and energy balances on the membrane reactor have been solved for fixed H_2 recovery yield values (RY_{H2}, see Eq. 2). The retentate and permeate composition have been evaluated assuming that the reactor approaches the equilibrium composition (Eq. 5 and Eq. 17).

$$K_{eq} = \frac{n_{CO2}n_{H2}}{n_{CO}n_{H2O}} =$$

$$= \frac{(n_{CO_2}^{\text{Feed}}+n_{CO}^{\text{Feed}}x_{eq})}{n_{CO}^{\text{Feed}} (1\text{-}x_{eq})(n_{H_2O}^{\text{Feed}} - n_{CO}^{\text{Feed}}x_{eq})} \left[(n_{H_2}^{\text{Feed}}+ n_{CO}^{\text{Feed}}x_{eq}) - H_2RY \ (n_{H_2}^{\text{Feed}}+ n_{CO}^{\text{Feed}}x_{eq}) \right]$$

Eq. 17

The following equation represents the energy balance on the membrane reactor:

$$F^{\text{Feed}} \ \Delta H^{\text{Feed}}+F^{\text{Sweep}} \ \Delta H^{\text{Sweep}} - F^{\text{Permeate}} \ \Delta H^{\text{Permeate}} - F^{\text{Retentate}} \ \Delta H^{\text{Retentate}} =$$

$$= F^{Feed}\left[\overline{C_{P_{Feed}}}\left(T_{Feed} - T_{rif}\right) + \sum y_i^{Feed}\Delta H_{i,f}^0\right]$$

$$+ F^{Sweep}\left[\overline{C_{P_{Sweep}}}\left(T_{Sweep} - T_{rif}\right) + \sum y_i^{Sweep}\Delta H_{i,f}^0\right]$$

$$- F^{Permeate}\left[\overline{C_{P_{Permeate}}}\left(T_{Permeate} - T_{rif}\right) + \sum y_i^{Permeate}\Delta H_{i,f}^0\right]$$

$$- F^{Retentate}\left[\overline{C_{P_{Retentate}}}\left(T_{Retentate} - T_{rif}\right) + \sum y_i^{Retentate}\Delta H_{i,f}^0\right] = 0$$

<div align="right">Eq. 18</div>

The energy balance has been solved for feed temperatures on retentate and permeate side (T_{Feed} and T_{Sweep}) equal to 330 °C. Moreover, the outlet temperature of the permeate stream ($T_{Permeate}$) has been assumed equal to the outlet temperature of the retentate stream ($T_{Retentate}$), for all case studies (Eq. 19).

$$T_{Permeate} = T_{Retentate}$$

<div align="right">Eq. 19</div>

A hydrogen permeance value of 0.18 Nm³/ m² h Pa$^{0.5}$ has been considered, being this value defined as a target for the membranes developed in the framework of the DEMCAMER project.

The driving force has been calculated using the logarithmic mean driving force equation, described above. For the sweep scenario, in analogy to the heat exchanger, the driving force for a co-current and counter-current configuration has been expressed respectively as:

$$\Delta p|_{\text{Co-current}} = \frac{\left(\sqrt{p_{H2}^{Feed}} - \sqrt{p_{H2}^{Sweep}}\right) - \left(\sqrt{p_{H2}^{Retentate}} - \sqrt{p_{H2}^{Permeate}}\right)}{\ln\dfrac{\sqrt{p_{H2}^{Feed}} - \sqrt{p_{H2}^{Sweep}}}{\sqrt{p_{H2}^{Retentate}} - \sqrt{p_{H2}^{Permeate}}}}$$

<div align="right">Eq. 20</div>

$$\Delta p|_{\text{Counter-current}} = \frac{\left(\sqrt{p_{H2}^{Feed}} - \sqrt{p_{H2}^{Permeate}}\right) - \left(\sqrt{p_{H2}^{Retentate}} - \sqrt{p_{H2}^{Sweep}}\right)}{\ln\dfrac{\sqrt{p_{H2}^{Feed}} - \sqrt{p_{H2}^{Permeate}}}{\sqrt{p_{H2}^{Retentate}} - \sqrt{p_{H2}^{Sweep}}}}$$

<div align="right">Eq. 21</div>

The membrane area required for different hydrogen recovery yield values, for all the case studies, is reported in Table 7. It was assumed to feed 10.3 Nm³/h of a reformate stream gas, with a composition as defined in Table 1, and a feed temperature of 330 °C. The value of feed flow rate has been defined considering the feed required to obtain the H_2 production target, 5 Nm³/h, with an MR H_2 recovery yield of 90%.

$$\text{Feed flow rate} = \frac{H_2 \text{ production target}}{H_2 \text{ recovery yield target} \left(x_{H2}^{feed} + x_{CO}^{feed}\right)} = \frac{5 \text{ Nm}^3/\text{h}}{0.90\,(0.448 + 0.092)}$$

Eq. 22

A comparison of the membrane area required for the different case studies is presented in Figure 5 - Figure 8. The base scenario needs the highest membrane surface (Figure 5); for an H_2 recovery yield of 80% a membrane area three times larger than the one for vacuum scenario, operating at 0.5 bar, is required. Looking at the performance with vacuum scenario, as expected, operating at lower pressure smaller membrane area are required to rich the hydrogen recovery target: 0.2 m² and 0.125 m² at 0.5 and 0.25 bar, respectively.
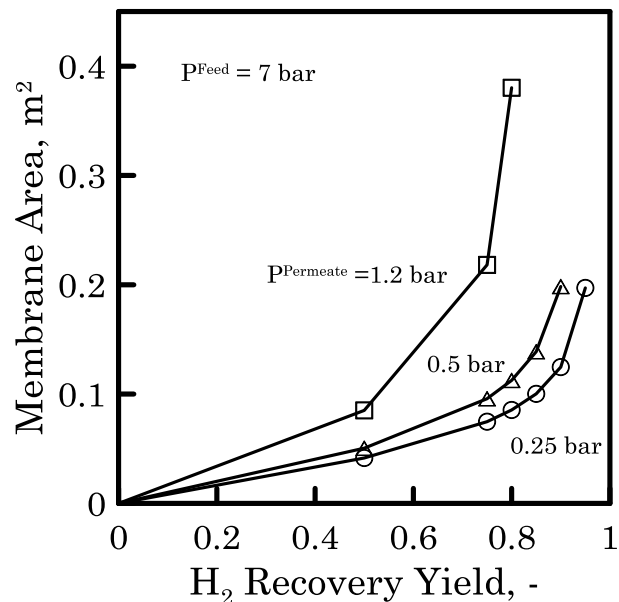
Figure 5 Required membrane area as a function of H_2 recovery yield for base scenario (case study 1) and vacuum scenario (case studies 5 and 6).

For the sweep scenario, Figure 6 shows a reduction of membrane surface when the sweep fraction increases. In addition, for high H_2 RY, the difference between the membrane area values of each case study increases. The same behaviour is shown in Figure 7 where, for a sweep fraction of 0.8, the co-current and counter-current configuration are compared. At low recovery value, vacuum and sweep scenario require quite similar membrane surface. However, comparing both scenario at higher hydrogen recovery (see Figure 8) the difference in term of required membrane area increases, showing as H_2 RY > 95 % can be reached only operating with sweep scenario.
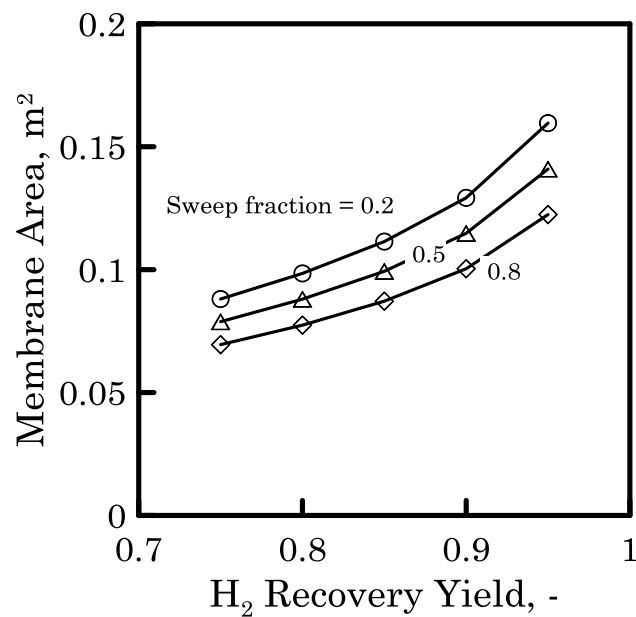
Figure 6 Required membrane area as a function of H_2 recovery yield at different sweep fraction (case studies 2, 3 and 4). Sweep scenario, counter-current configuration.
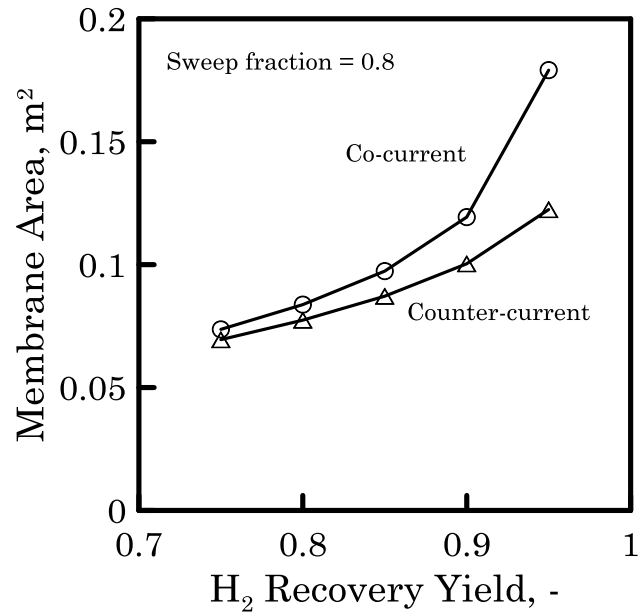
Figure 7 Required membrane area as a function of H_2 recovery yield with co-current (dots) and counter-current (triangles) configuration. Sweep scenario, sweep fraction 0.8 (case study 2).
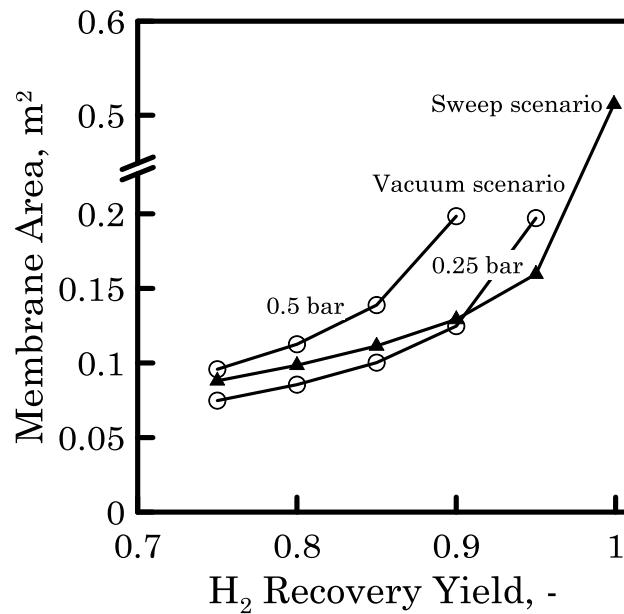
Figure 8 Required membrane area as a function of H_2 recovery yield for sweep scenario (solid triangles, sweep fraction 0.8) and vacuum scenario (open dots).

Table 7 Membrane area [m²] required at fixed H_2 recovery yield values

	Base scenario	Sweep scenario			Vacuum scenario	
H_2 RY, %	Case Study 1	Case Study 2	Case Study 3	Case Study 4	Case Study 5	Case Study 6
99		0.356	0.430	0.512	Not Reachable	Not Reachable
95	Not Reachable	0.122	0.141	0.150		0.197
90 (Target)		0.100	0.115	0.129	0.198	0.125
85		0.087	0.099	0.111	0.139	0.100
80	0.380	0.077	0.088	0.098	0.113	0.085
75	0.218	0.069	0.079	0.088	0.096	0.075
50	0.085	0.041	0.046	0.051	0.051	0.042

On the basis of this preliminary screening it has been concluded that:

- The base scenario is not suitable because the H_2 recovery yield target cannot be reached. (A reaction pressure higher than 20 bar should be applied and it is not feasible for the pilot scale reactor testing).

- The vacuum and sweep scenarios both can meet the target requirements.

- A minimum membrane area in the range of 0.1-0.2 m^2, depending on the considered scenario, should be required to produce and recover 5 Nm^3/h of hydrogen, achieving the CO conversion and H_2 recovery targets.

To accomplish a complete design of the pilot scale WGS-MR and define the final operating condition a deeper analysis on membrane reactor performance is required. Thus, the modelling and simulation of the membrane reactor has been performed for both vacuum and sweep scenario, as following reported.

1.5   Modelling and simulation of WGS-MR

The general structure of a mathematical model of MR is based on momentum, mass, and energy balances, the same as that of traditional reactors but for an MR these equations are written for the reaction and permeate volumes. The local velocity field can be considered known/assigned in most cases. The mass balance on the reaction side contains in addition to the other know terms, the one related to the ith permeating species through the membrane. In the mass balance for the permeate side, the same permeation term has to be considered with the opposite sign with respect to the reaction side. The permeating flux law depends on the permeation mechanism (solution-diffusion in dense or metallic membranes, viscous, or Knudsen flux in porous membranes, etc.). For Pd-based membranes, the only permeating species is the hydrogen (infinite membrane selectivity) and the permeating flux can be expressed, as above reported, with Sieverts law (see Eq. 10)

The majority of the Pd-alloy membrane reactor refers to tubular plug-flow MRs. Generally, a tubular MR is a tube-in-tube device in which the inner tube is a permselective membrane promoting the selective mass transfer of reactants/products between the reaction and permeation sides. On both sides, species compositions, temperature, and pressures change along the reactor length and radial direction; in addition, the permeation rate through the membrane changes along the reactor length. Therefore, in general, these systems must be described by partial differential equations (PDEs). However, a one-dimensional (1D) mathematical model provides satisfactory description of systems in which radial gradients can be neglected.

The WGS pilot scale membrane reactor has been modelled as a tubular packed bed membrane reactor implementing a one dimensional model for gas-phase reactions [16, 33]. We assumed to operate the reactor adiabatically. A tubes in tube configuration has been considered: the MR consists of an outer tube, the shell, and of N inner tubes, the Pd-alloy membranes; the catalyst is packed in the shell side (see Figure 9). The presented mathematical model is based on the following hypotheses, common to most of the models present in the open literature:

- Axial dispersion and radial profiles negligible.
- Assigned velocity field: plug flow on both membrane sides (only mass and energy balances will be considered).
- Pseudo-homogeneous description of heterogeneous catalytic reactions.
- Pd-alloy membranes with ideal behaviour: infinite H_2 selectivity.
- H_2 permeation diffusion-controlled: H_2-permeating flux expressed by Sieverts law.
- Isobaric condition on the permeate side.
- Ideal gas mixtures behaviour.
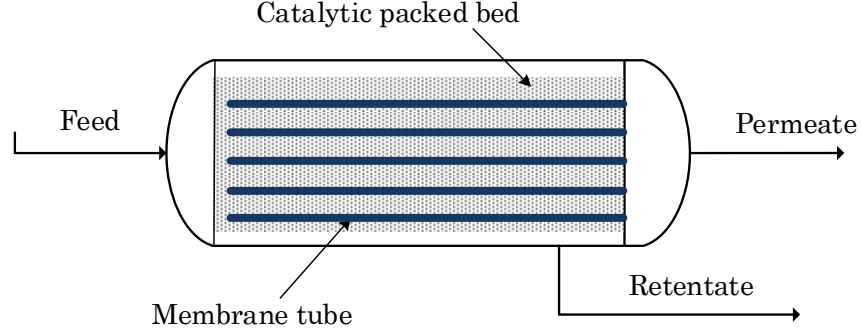
Figure 9 Packed bed tubular membrane reactor scheme.

1.5.1 Mass balance

The mass balances on both membrane sides for a tubular MR is written for a differential reference volume, dV, of length dz (Figure 10). The mass balance equations for hydrogen (Eq. 24) and the other species (Eq. 23), on the reaction volume, are the following:
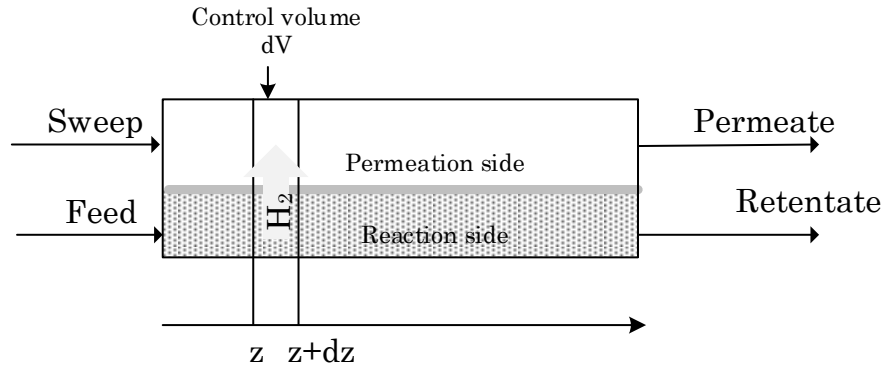
Figure 10 Control volume scheme of a tubular Pd membrane reactor.

$$-\frac{dF_i^{\text{Reaction side}}}{dz} + \nu_i r_{\text{WGS}} \, S_{\text{shell}} = 0 \quad \text{for i} \neq H_2$$

Eq. 23

$$-\frac{dF_{H_2}^{\text{Reaction side}}}{dz} + \nu_{H_2} r_{\text{WGS}} \, S_{\text{shell}} - \frac{A^{\text{Membrane}}}{L_{\text{Reactor}}} J_{H_2}^{\text{Permeating}} = 0$$

Eq. 24

where ν_i is the stoichiometric coefficient for species i. The boundary condition is expressed as follows:

$$F_i^{\text{Reaction side}}\Big|_{z=0}=F_i^{\text{Feed}}$$

Eq. 25

In the mass balance the first term is the convective flux variation of the ith specie along the reactor length, the second term is the reaction and the third term is the gases permeation through the membrane. In the mass balance equation for the permeation side the terms are the same of Eq. 23 except for the reaction term, no more included. The term of the permeating flux through the membrane has a positive sign because in this case the H_2 enters in the permeation volume. Mass balances and boundary condition (B.C.) on the permeation side are given by following equations:

$$-\frac{dF_i^{\text{Permeate side}}}{dz}=0 \quad \text{for i} \neq H_2$$

Eq. 26

$$-\frac{dF_{H_2}^{\text{Permeate side}}}{dz}+\frac{A^{\text{Membrane}}}{L_{\text{Reactor}}}\,J_{H_2}^{\text{Permeating}}=0$$

Eq. 27

$$F_i^{\text{Permeate side}}\Big|_{z=0}=0$$

Eq. 28

When the presence of a sweep stream is considered in the co-current configuration only the boundary condition changes (Eq. 29, Eq. 30).

$$F_i^{\text{Permeate side}}\Big|_{z=0}=0$$

Eq. 29

$$F_{\text{Sweep}}^{\text{Permeate side}}\Big|_{z=0}=F_{\text{Sweep}}^{\text{Feed}}$$

Eq. 30

For the counter-current tubular MR the model equations are the same of the co-current mode; the only difference is the sign of the term related to convective flux on the permeate side (Eq. 31). The B.C.s for this set of equations are defined at the two ends of the membrane module (Eq. 32 and Eq. 33).

$$+\frac{dF_{H_2}^{\text{Permeate side}}}{dz}+\frac{A^{\text{Membrane}}}{L_{\text{Reactor}}}\,J_{H_2}^{\text{Permeating}}=0$$

Eq. 31

$$F_i^{\text{Permeate side}}\Big|_{z=L}=0$$

$$F_{\text{Sweep}}^{\text{Permeate side}}\Big|_{z=L}=F_{\text{Sweep}}^{\text{Feed}}$$

1.5.2 Energy balance

The mass balance equations have to be solved simultaneously with the energy balances in order to describe the behaviour of the adiabatic MR. In fact, the energy transport and the temperature profiles developing along the reactor axis have a significant importance on the thermodynamics, the kinetics and the transport properties. The energy balance takes into account the heat production by chemical reaction, the heat exchanged with the permeation side and the convective flux of energy. Moreover, an additional term related to energy associated with the permeating flux is considered. The following equations represent the energy balance (Eq. 34 and Eq. 36) and boundary conditions (Eq. 35 and Eq. 37) for reaction and permeation sides, respectively.

$$r_{\text{WGS}}(\text{-}\Delta H_{\text{RX}})S_{\text{shell}} + \frac{A^{\text{Membrane}}}{L_{\text{Reactor}}}\ U^{\text{Membrane}}\ \left(T^{\text{Reaction side}} - T^{\text{Permeate side}}\right)$$
$$-\frac{A^{\text{Membrane}}}{L_{\text{Reactor}}}\ J_{\text{H2}}^{\text{Permeating}}\ \Delta H_{\text{H2}}^{\text{Permeating}}$$
$$=\sum_{i=1}^{N_{\text{species}}}\ F_i^{\text{Reaction side}}\ cp_i\ \frac{dT^{\text{Reaction side}}}{dz}$$

$$T^{\text{Reaction side}}\Big|_{z=0}=T^{\text{Feed}}$$

$$+\frac{A^{\text{Membrane}}}{L_{\text{Reactor}}}\ U^{\text{Membrane}}\ \left(T^{\text{Reaction side}} - T^{\text{Permeate side}}\right)$$
$$+\frac{A^{\text{Membrane}}}{L_{\text{Reactor}}}J_{\text{H2}}^{\text{Permeating}}\ \Delta H_{\text{H2}}^{\text{Permeating}}$$
$$=\sum_{i=1}^{N_{\text{species}}}\ F_i^{\text{Permeate side}}cp_i\ \frac{dT^{\text{Permeate side}}}{dz}$$

$$T^{\text{Permeate side}}\Big|_{z=0}=T^{\text{Feed}}$$

When the presence of a sweep stream is considered, as described above for the mass balance, the boundary conditions on the permeation side have to be modified (Eq. 38) as

$$T^{\text{Permeate side}}\big|_{z=0} = T^{\text{Feed}}_{\text{Sweep}}$$

Eq. 38

When the counter-current mode is considered, the energy balance equation for the reaction side will be the same as the co-current mode, but for the permeate side the sign of convective heat flux changes (Eq. 39). Moreover, the B.C. for the permeate side is defined at the other extremity of the MR (Eq. 40).

$$\frac{A^{\text{Membrane}}}{L_{\text{Reactor}}} U^{\text{Membrane}} \left(T^{\text{Reaction side}} - T^{\text{Permeate side}}\right) +$$
$$\frac{A^{\text{Membrane}}}{L_{\text{Reactor}}} J^{\text{Permeating}}_{\text{H2}} \Delta H^{\text{Permeating}}_{\text{H2}} = -\sum_{i=1}^{N_{\text{species}}} F_i^{\text{Permeate side}} cp_i \frac{dT^{\text{Permeate side}}}{dz}$$

Eq. 39

$$T^{\text{Permeate side}}\big|_{z=L} = T^{\text{Feed}}_{\text{Sweep}}$$

Eq. 40

The overall membrane heat transfer coefficient has been evaluated considering a resistance series system [34]. The coefficient is expressed as:

$$\frac{1}{U^{\text{Membrane}}} = \frac{1}{h^{\text{Shell}}} + \frac{OD^{\text{Tube}}}{2k^{\text{Membrane}}} \ln\left(\frac{OD^{\text{Tube}}}{ID^{\text{Tube}}+2\delta^{\text{Support}}}\right) + \frac{OD^{\text{Tube}}}{2k^{\text{Support}}} \ln\left(\frac{ID^{\text{Tube}}+2\delta^{\text{Support}}}{ID^{\text{Tube}}}\right) + \frac{OD^{\text{Tube}}}{ID^{\text{Tube}}} \frac{1}{h^{\text{Tube}}}$$

Eq. 41

The thermal conductivity of the porous support k^{Support} is calculated as

$$k^{\text{Support}} = \left(1 - \varepsilon_{\text{Support}}\right) k_{\text{Ceramic}} + \varepsilon_{\text{Support}} k^{\text{Permeate side}}_{\text{Mix}}$$

Eq. 42

where k_{ceramic} and $k^{\text{Perm}}_{\text{Mix}}$ are the thermal conductivities of the ceramic membrane support and the gaseous mixture in the permeate side, respectively; $\varepsilon_{\text{Support}}$ is the porosity of the membrane support. The heat transfer coefficient between the fluid in the bed and the membrane, h^{Shell}, is calculated as [35]

$$h^{\text{Shell}} = 0.17 \, \frac{k_{\text{Mix}}^{\text{Retentate side}}}{d_{\text{P}}} \left(\frac{Pr}{0.7}\right)^{1/3} \text{Re}_{\text{P}}^{0.79}, \qquad \text{Re}_{\text{P}} = \frac{G \; d_P}{\mu_{\text{Mix}}^{\text{Reaction}}}$$

<div align="right">Eq. 43</div>

In the permeation side, where no catalyst pellets are present, the following expression is used for the heat transfer coefficient [36].

$$h^{\text{Tube}} = 1.86 \, \frac{k_{\text{Mix}}^{\text{Permeate side}}}{D_{Eq}} + \left(\frac{D_{Eq}}{L^{\text{Membrane}}} \, \text{Re} \, Pr\right)^{1/3}, \text{ laminar flow}$$

<div align="right">Eq. 44</div>

1.5.3 Permeation flux equation

The H$_2$ permeation flux through the membrane was determined by the Sieverts law using the parameters of a supported Pd-membrane developed in the framework of DEMCAMER project (Eq. 45).

$$J_{\text{H}_2}^{\text{Permeating}} = \text{Permeance}_{\text{H}_2} \quad \text{Driving Force} \quad =$$

$$= \frac{\text{Permeability}_0 \; e^{(-E_a/RT)}}{\text{Thickness}} \left(\sqrt{p_{\text{H}_2}^{\text{Reaction side}}} - \sqrt{p_{\text{H}_2}^{\text{Permeation side}}}\right) =$$

$$= 9.06 \, \frac{\text{mmol}}{\text{m}^2 \, \text{s} \; \text{Pa}^{0.5}} \, e^{\left(\frac{-8000\frac{\text{kJ}}{\text{kmol}}}{RT}\right)} \left(\sqrt{p_{\text{H}_2}^{\text{Reaction side}}} - \sqrt{p_{\text{H}_2}^{\text{Permeation side}}}\right)$$

<div align="right">Eq. 45</div>

The effect of CO inhibition has been neglected since the CO partial pressure is low and the operating temperature is higher than 300 °C. The inhibition phenomenon, in fact, affects the permeation only at low temperature (< 270-280 °C) and at higher CO partial pressure [37, 38]. The effect of concentration polarization has been considered by mean of a concentration polarization coefficient (CPC) as reported in the literature [39, 40, 41, 42]. This coefficient evaluates the concentration polarization effect in term of permeance reduction. The term (1- CPC) is the ratio between the permeance in presence of concentration polarization limitation and the intrinsic permeance of the membrane, whose value can be obtained by pure H$_2$ permeation test. The permeance reduction term (1-CPC) has been estimated from literature data [42] available for a hydrogen permeator, operating at similar pressures and flow regime (Reynold number). In particular, from the literature data an

expression for CPC as a function of the H_2 molar fraction on the retentate side has been derived (Eq. 46):

$$\text{CPC} = f(x_{H_2}^{\text{Reaction side}})$$

Eq. 46

The general trend of concentration polarization coefficient, as reported in literature, reveals as decreasing the hydrogen molar fraction increases the CPC value. In the simulation performed taking into account also the concentration polarization effect, the permeation flux equation has been expressed as:

$$J_{H_2}^{\text{Permeating}} = (1 - \text{CPC})$$
$$* 9.06 \, \frac{\text{mmol}}{\text{m}^2 \, \text{s} \, \text{Pa}^{0.5}} e^{\left(\frac{-8000 \, \text{kJ/kmol}}{RT}\right)} \left(\sqrt{p_{H_2}^{\text{Reaction side}}} - \sqrt{p_{H_2}^{\text{Permeation side}}}\right)$$

Eq. 47

The estimated permeance reduction value (1-CPC) varied within a range of 0.2-0.4. It has to be noticed that, evaluating the CPC coefficient from permeator system data, the concentration polarization effect in membrane reactor is actually overestimated. The results from rigorous modelling, performed in the framework of DEMCAMER project, on concentration polarization effect in packed bed membrane showed lower permeance reduction values. For the pilot scale design a larger concentration polarization effect has been assumed since this approach assures that a conservative design is kept.

1.5.4 Kinetic equation

A kinetic equation from the literature [43] is considered. This equation has been determined for an iron–chromium based commercial catalyst and the kinetic study was directed to assessing the performance of the catalyst also in membrane reactor. In particular, the effects of CO, CO_2, H_2O and H_2 concentration on WGS reaction rate has been determined over the catalyst using selected gas compositions that might be encountered in both traditional

and membrane reactors. The experiments were performed in a differential reactor at a constant temperature of 450 °C.

The considered reaction rate follows a power-law:

$$-r_{CO} = 4.56 \exp\left(\frac{-88}{RT}\right) p_{CO}^{0.9}\ p_{H2O}^{0.31}\ p_{CO2}^{-0.156}\ p_{H2}^{-0.05} \left(1 - \frac{p_{CO2} p_{H2}}{p_{CO} p_{H2O} K_{eq}}\right)$$

Eq. 48

where R is the universal gas constant (kJ mol^{-1} K^{-1}), T is the reaction temperature (K) and K_{eq} is the equilibrium constant for the WGS reaction [44]:

$$K_{eq} = \exp\left(\frac{4577.8}{T} - 4.33\right)$$

Eq. 49

Reaction rate unit is mol/ (g_{cat} s) and pressures are expressed in kPa. The diffusion limitation in the catalytic pellets is also considered by means of "effectiveness factor", defined in term of observable Thiele modulus. The effectiveness factor for a catalyst pellet diameter of 1 cm has been evaluated on the basis of the intrinsic reaction rate and experimental condition defined in the literature [43] as free from the mass transfer limitations.

The actual reaction rate (Eq. 50), expressed as mol/(m$^3_{Reactor}$ s), is evaluated considering an effectiveness factor equal to 0.2, a catalyst density of 1500 kg/m^3 and a bed void fraction of 0.5.

$$r_{WGS} = \eta\,(-r_{CO}\,)(\text{catalyst density})\,(1 - \text{ bed void fraction})$$

Eq. 50

1.5.5 Pressure drop

The pressure drop on the feed side was calculated using Ergun's law (Eq. 51), while a constant pressure is assumed on the permeate side.

$$\frac{dp^{\text{Reaction side}}}{dz} = -\frac{G^{\text{Reaction side}}}{d_P}\frac{1-\varepsilon}{\varepsilon^3}\left(\frac{150(1-\varepsilon)\mu_{\text{Mix}}^{\text{Reaction}}}{d_P} + 1.75\,G^{\text{Reaction side}}\right)$$

Eq. 51

$$p^{\text{Reaction side}}\big|_{z=0} = p^{\text{Feed}}$$

Eq. 52

The obtained system of coupled ordinary differential equations was solved by means of a simulation tool.

1.5.6 Simulation condition

The feed composition considered in the simulations is the one defined in Table 1. As described above, the composition of a syngas stream produced by natural gas steam reforming has been taken into account. Both vacuum and sweep scenario have been simulated, choosing the operating parameters and configuration on the basis of the results of the preliminary case studies screening. Three permeate pressure values within 0.25 and 0.5 bar have been considered for the vacuum scenario and three sweep factor values have been selected for the sweep scenario. The sweep factor is defined as the ratio of the flow rate of the sweep gas to the flow rate of the feed [16].

$$\text{Sweep factor} = \text{I} = \frac{F_{\text{Sweep}}}{F_{\text{Feed}}}$$

Eq. 53

The sweep factor values have been set on the basis of results from the analysis at fixed H_2 recovery yield (RY_{H2}). In particular, with a counter current configuration, it has been shown that the conversion and H_2 recovery target values can be obtained operating even at low sweep fraction, equal to 0.2. The sweep flow rate to be fed to the MR has been therefore calculated by means of the following equation, assuming a sweep fraction of 0.2:

$$F_{\text{Sweep}} = F_{\text{H2}}^{\text{Permeate}} \frac{\text{Sweep factor}}{(1\text{-} \text{Sweep factor})} = F_{\text{Feed}}\left(x_{\text{H2}}^{\text{Feed}} + x_{\text{CO}}^{\text{Feed}}\right) RY_{\text{H2}} \frac{\text{Sweep factor}}{(1\text{-} \text{Sweep factor})}$$

Eq. 54

For an H_2 RY of 0.9 the corresponding sweep flow rate is 0.055 kmol/h. This corresponds to a sweep factor equal to 0.12, since:

$$\text{Sweep factor} = \text{I} = \frac{F_{\text{Sweep}}}{F_{\text{Feed}}} = \frac{0.055 \text{ kmol/h}}{0.46 \text{ kmol/h}} = 0.12$$

Three sweep factor values have been fixed assuming as upper value 0.24 and as lower value 0.06. The MR geometric characteristic and the operating

conditions are reported in Table 8 and Table 9, respectively. The membrane area range has been selected on the basis of the estimated membrane surface for the different case studies, as describe in paragraph 1.4.

Table 8 Simulated MR geometric characteristics

Membrane outer diameter, m	0.01
Membrane area, m^2	0.11 – 0.22

Table 9 Simulated operating conditions

	Vacuum scenario	Sweep scenario
Feed pressure, bar	7	
Permeate pressure, bar	0.25,0.35,0.5	1.2
Feed temperature, °C	330, 360, 380, 400	
Feed molar flow rate, mol/min	7.6	
Sweep factor	-	0.06, 0.12, 0.24
Configuration	-	Counter-current

1.6 Simulation results and discussion

To investigate the effect on MR performance and to define the final operating condition of the pilot scale reactor, the behaviour of the adiabatic packed bed membrane reactor as a function of the operating variables has been simulated for both scenarios. The most important variables to be evaluated for describing the MR performance are the CO conversion and the hydrogen recovery yield. The CO conversion was calculated as

$$\text{CO conversion} = \frac{F_{CO}^{Feed} - F_{CO}^{Retentate}}{F_{CO}^{Feed}}$$

The hydrogen permeated through the membrane and recovered in the permeate side was evaluated in term of H_2 recovery yield, as already defined in Eq. 2.

$$H_2 \, RY \quad = \frac{F_{H2}^{Permeate}}{F_{H2}^{Feed} + F_{CO}^{Feed}}$$

1.6.1 Results for vacuum scenario

For the vacuum scenario the effect of the permeate pressure on the MR performance has been evaluated. CO conversion and H_2 recovery yield have been calculated at 0.25, 0.35 and 0.5 bar, for different membrane area. As expected, increasing the permeate pressure, conversion and recovery decrease because the hydrogen permeation driving force decreases. Figure 11 shows as the hydrogen recovery yield is more affected by the permeate pressure, with respect to the CO conversion. Operating at 0.25 bar an H_2 recovery of 88% is obtained, with a membrane area of 0.11 m². At 0.5 bar, for the same area, the hydrogen recovered decreases to 78%. The MR performance has been analysed also for several membrane surface. Increasing the membrane area, higher conversion and H_2 recovery are obtained. In addition, at higher membrane area the difference between the CO conversion values reachable at different vacuum pressure decreases. Operating at 0.35 bar with a membrane area of 0.135 m², the conversion and recovery target values can be reached. When the permeate pressure is further decreased, to 0.25 bar, the improvement in term of conversion and hydrogen recovery are less than 3%. In addition, considering also at the vacuum pump power required, lower permeate pressure seems to be less convenient. Therefore, on the basis of the simulation results obtained, a permeate pressure equal to 0.35 bar has been chosen as a reference value for the operating condition.
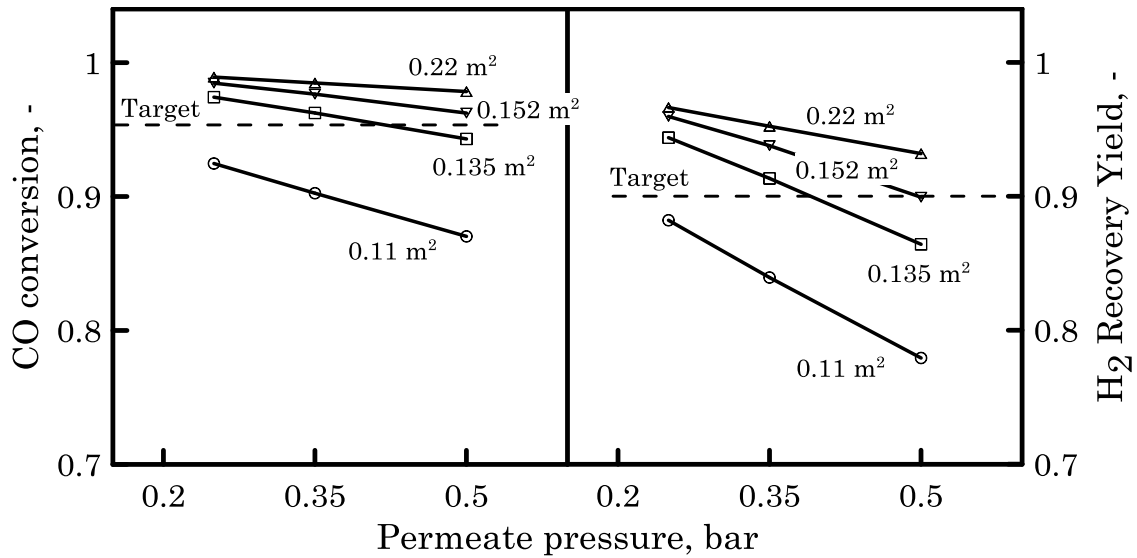
Figure 11 CO conversion and H_2 Recovery yield as a function of permeate pressure for different membrane area. Feed temperature 330 °C.

The effect of feed temperature has been also investigated. Results, in Figure 12, show the conversion and H_2 recovery yield as a function of feed temperature for an MR with 0.152 m^2 of membrane area, operating at 0.35 bar as permeate pressure. Increasing the feed temperature the conversion slightly decreases. The negative effect on the equilibrium, being the reaction exothermic, is overbalanced by the increased H_2 permeation that promotes the CO conversion. Increasing the temperature the membrane permeance increases thus a larger hydrogen flux is obtained.
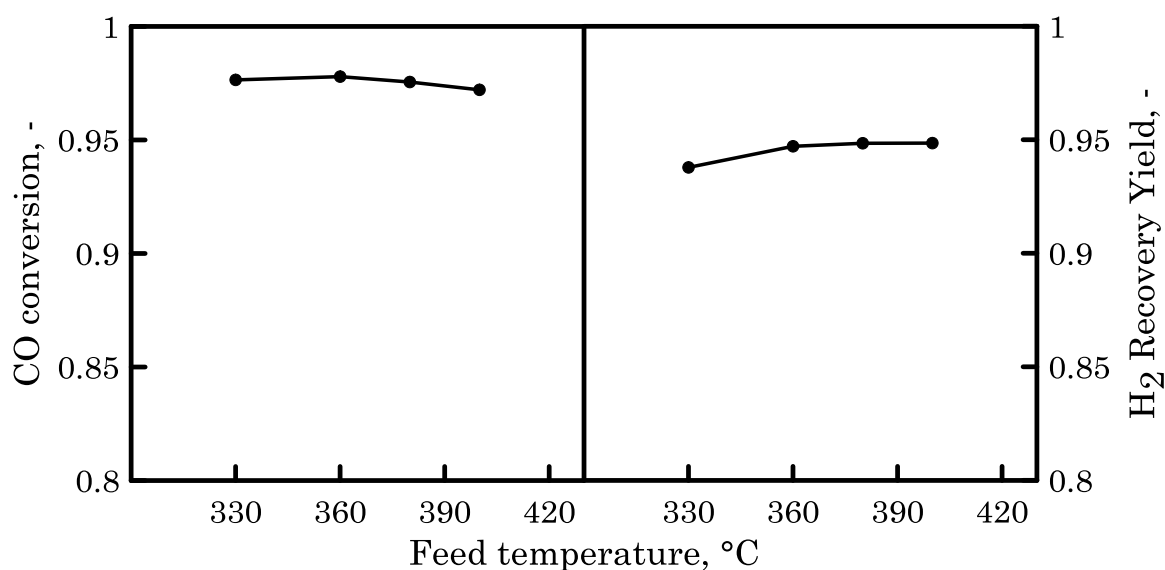
Figure 12 CO conversion and H_2 Recovery yield as a function of feed temperature. Permeate pressure 0.35 bar, membrane area 0.152 m^2.

Table 10 CO conversion and retentate outlet temperature for different feed temperature. Permeate pressure 0.35 bar, membrane area 0.152 m^2

Feed temperature, °C	Retentate outlet temperature, °C	H_2 recovery yield, -
330	427.1	0.938
360	453.6	0.947
380	472.8	0.948
400	492.4	0.948

The results show as for feed temperature higher than 360 °C no further significant improvements in H_2 recovery are obtained. Increasing the feed temperature the retentate outlet temperature also increases (Table 10), moving towards temperature values more severe for both membrane and catalyst. In particular, low-medium temperature WGS catalyst was the target set for the novel catalyst to be developed within the framework of DEMCAMER project. Consequentially, aiming to integrate in the actual pilot

reactor the novel catalyst, 360 °C has been considered as the reference value for the operating feed temperature.

Finally, simulations for different membrane tubes number were performed in order to find the minimum number needed to reach the conversion and H_2 recovery target values, for the selected operating condition (feed temperature 360 °C, permeate pressure 0.35 bar). The MR geometric characteristics have been selected by taking into account the membrane tube specifications (membrane tube unit length and membrane tube diameter) defined by the membrane producer partner. Table 11 reports the MR geometric characteristics used in the simulations, where, the concentration polarization effect has been considered by means of a permeance reduction coefficient, as described above (see 1.5.3 Permeation flux equation).

Table 11 Simulated MR geometric characteristics

Reactor length, m	0.44
Membrane outer diameter, m	0.01
Membrane tubes number	$10 - 13$
Membrane area, m^2	$0.138 - 0.180$

Figure 13 shows the results, in terms of CO conversion and H_2 recovery: the minimum tube number required to reach the target value is 11 tubes. Consequentially, for the final design 12 tubes have to be considered, assuring to be over the target.

Table 12 reports the gas streams molar composition, CO conversion and H_2 recovery of a membrane reactor equipped with 12 membrane tubes, operating at 0.35 bar and 360 °C, as permeate pressure and feed temperature respectively.
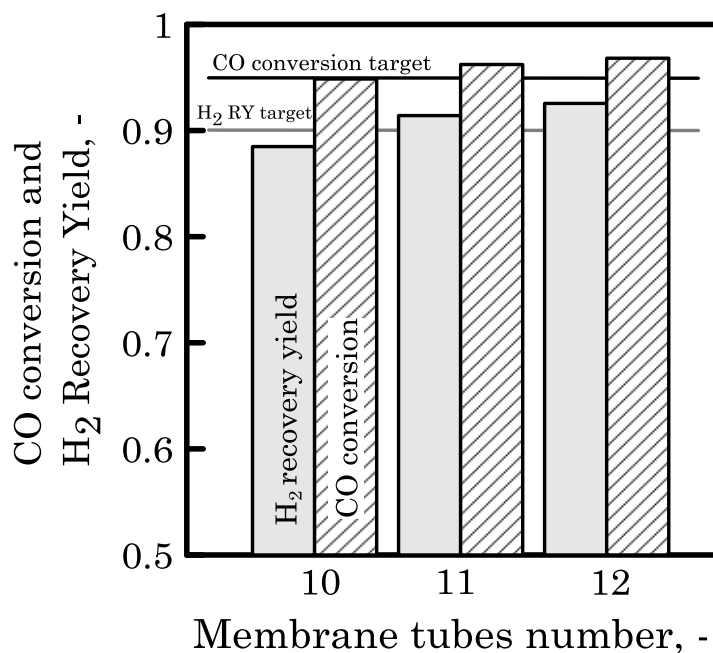
Figure 13 CO conversion and H_2 Recovery yield as a function of membrane tubes number. Permeate pressure 0.35 bar, feed temperature 360 °C.

The calculated molar flow rate and temperature profile along the reactor length are also shown in Figure 14 and Figure 15. As expected, the molar flow rate of carbon monoxide and water (reaction reagents) decreases along the reactor length whereas the CO_2 one (reaction product) increases. Also the hydrogen, that is a reaction product, is expected to increases along the reactor length. However in the MR, the hydrogen, permeating through the membrane, is extracted from the reaction volume. Figure 14 shows as, in the reaction side, the overall H_2 molar flow along the reactor length decreases. Moreover, having a permeation driving force at the inlet of reactor yet (ca 45% of the hydrogen is present in the feed stream), hydrogen begins to permeate already at z=0, decreasing up to reach a constant value (no more significant permeation).

The temperature profile (see Figure 15) on reaction side increases, especially on the first part of the reactor, due to the heat generated by reaction, finally reaching a plateau value around 450°C. The heat exchanged with the reaction side and the latent heat associated with the H_2 permeating flux contribute to

the temperature increasing in the permeation side. The permeate outlet temperature tends to the same temperature value of retentate outlet stream.

Table 12 Gas streams molar composition, CO conversion and H_2 Recovery, for vacuum scenario. Permeate pressure 0.35 bar, membrane tubes number 12 ($A^{Membrane}$ = 0.166 m^2)

	Feed	Retentate	Permeate
Temperature, °C	360	454	451
Pressure, bar	7	7	0.35
Total molar flow rate, mol/min	7.6	3.78	3.82
Composition: molar flow rate, mol/min			
CH_4	0.29	0.29	0
CO	0.70	0.02	0
CO_2	0.36	1.04	0
H_2	3.40	0.25	3.82
N_2	0.21	0.21	0
H_2O	2.64	1.93	0
CO conversion, %	96.8		
H_2 Recovery yield, %	92.5		
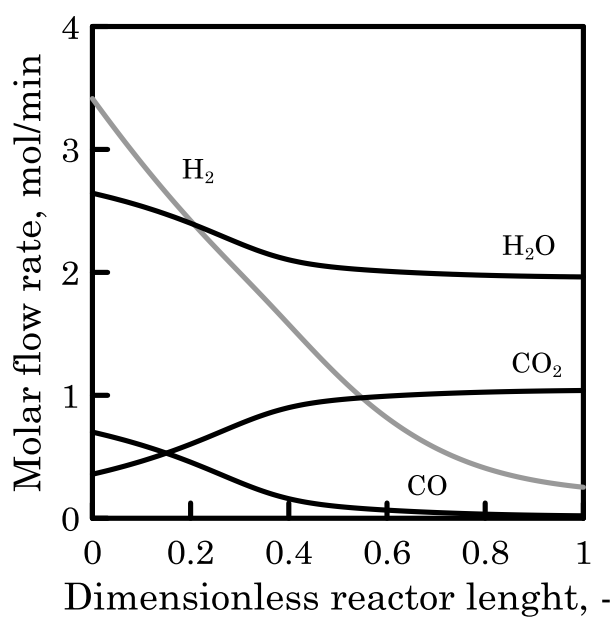
Figure 14 Molar flow rate profiles on reaction side along the reactor length. Membrane area 0.166 m^2 (12 membrane tubes), permeate pressure 0.35 bar, feed temperature 360 °C.
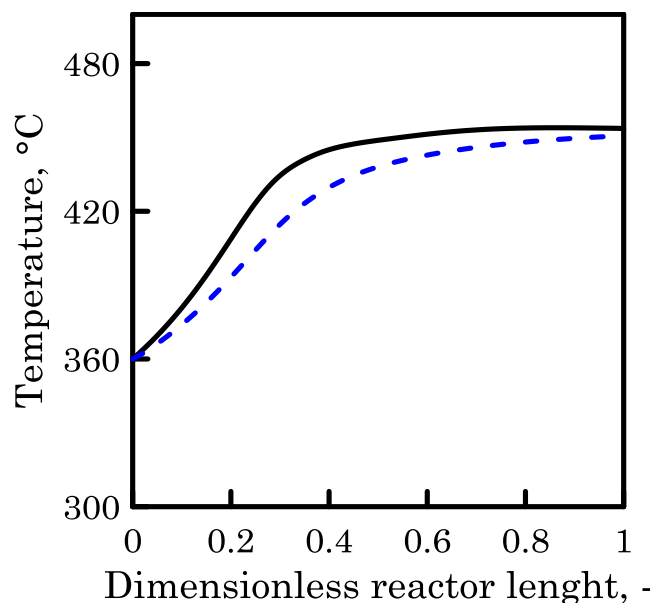
Figure 15 Temperatures profiles, on reaction side (solid line) and permeation side (dashed line), along the reactor length. Membrane area 0.166 m² (12 membrane tubes), permeate pressure 0.35 bar, feed temperature 360 °C.

1.6.2 Results for sweep scenario

For the sweep scenario, the steam has been considered as sweep gas because a pure H_2 stream can be easily obtained condensing the steam in the permeate stream. The effect of different sweep molar flow rate on the MR performance has been evaluated. CO conversion and H_2 recovery have been calculated for the three sweep factor value: 0.06, 0.12 and 0.24. Results are shown in Figure 16. At higher sweep factor corresponds higher conversion and recovery. Increasing the sweep factor the hydrogen molar fraction on the permeate side decreases, so the H_2 partial pressure. As a consequence, the permeation driving force is improved. This allows recovering more hydrogen and shifting the equilibrium toward higher CO conversion. A CO conversion of 92% is obtained operating with a sweep factor 0.06 for a membrane area of 0.135 m². When higher molar flow rate is fed, at sweep factor 0.24 for instance, the carbon monoxide converted increases to 98%, for the same area. Same trend is observed for the H_2 recovery, which rises from 85% up to 97%.

The MR performance has been analysed also for several membrane surfaces. As expected, increasing the membrane area, higher conversion and recovery are obtained. The minimum area required to reach 90% of H_2 recovery with a sweep factor of 0.12 is 0.135 m^2. Operating at higher sweep flow rate less membrane area is required to have the same MR performance. Feeding in the permeate side 0.11 kmol/h of steam, which means a sweep factor of 0.24, 95 % of CO conversion and 90% of H_2 recovery can be obtained with a membrane area of 0.11 m^2. On the other hand, we have to consider that a sweep factor of 0.24 means a steam flow rate which doubles the one at 0.12. Therefore, even though the membrane area required is reduced of 20%, considering the energy required to produce this amount of steam, operate at higher sweep flow rate does not seem to be much convenient.
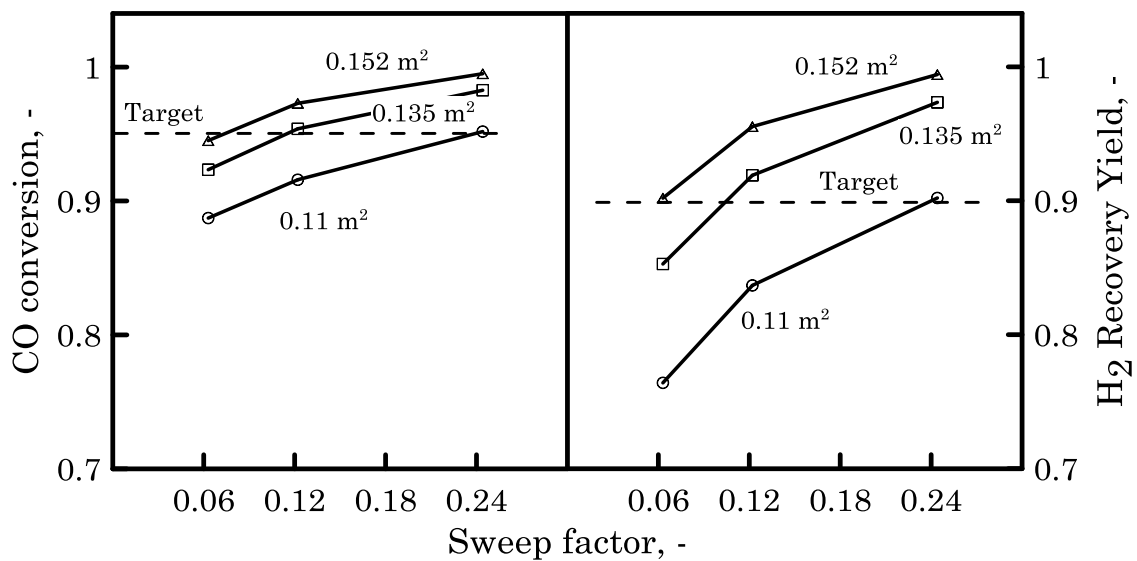
Figure 16 CO conversion and H_2 Recovery yield as a function of sweep factor for different membrane area. Feed temperature 330 °C.
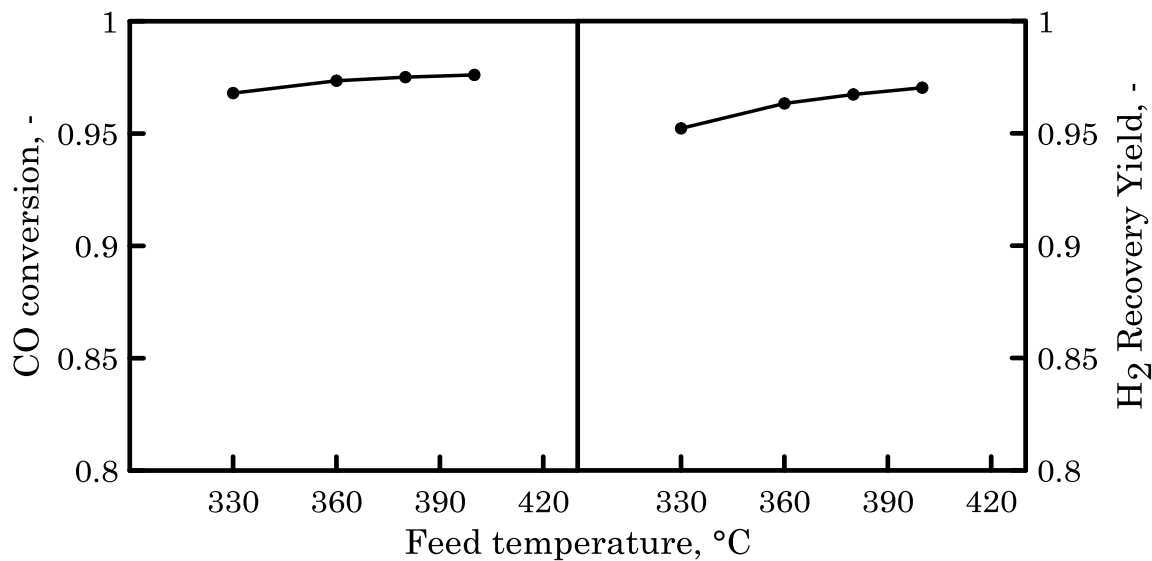
Figure 17 CO conversion and H_2 Recovery yield as a function of feed temperature. Sweep factor 0.12, membrane area 0.152 m^2.

The effect of feed temperature has been also investigated. Figure 17 shows the conversion and H_2 recovery as a function of feed temperature for an MR with 0.152 m^2 of membrane area, operating at 0.12 sweep factor. The trend for the CO conversion is similar to the one obtained for vacuum scenario. The H_2 recovery increases from 95% to 97 % in the feed temperature range within 330 and 400 °C. However, increasing the feed temperature the retentate outlet temperature also increases. Therefore, as previously discussed for the vacuum scenario, on the basis of the obtained simulation results, 360 °C has been considered as operating feed temperature also in the sweep scenario.

Considering the operating condition selected above and taking into account the concentration polarization effect, the performance of an MR has been evaluated following the same approach described for the vacuum scenario. The MR geometric characteristics used in the simulations are the same reported in Table 11. In the case of the sweep scenario, the minimum membrane tubes number needed to reach the conversion and H_2 recovery target values is 12 (see Figure 18). To be over the target, 13 membrane tubes have to be considered in the final design. The gas streams molar composition, CO conversion and H_2 recovery achievable in a membrane reactor with 13 membrane tubes, operating at sweep factor 0.12 and a feed temperature of

360 °C are reported in Table 13. The calculated molar flow rate and temperature profile along the reactor length are also shown in Figure 19 and Figure 20, respectively.
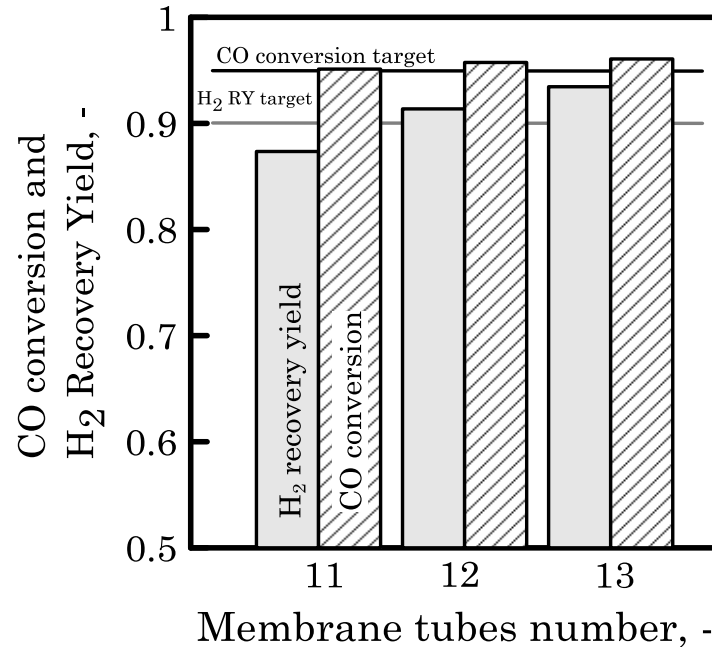
Figure 18 CO conversion and H_2 Recovery yield as a function of membrane tubes number. Sweep factor 0.12, feed temperature 360 °C.

The molar flow rate profiles are quite similar to the ones described for the vacuum scenario. Only the H_2 profile shows a different behaviour close to end of reactor (z=L). In the vacuum scenario the slope of the H_2 profile is about zero because no more appreciable permeation occurs. This is due to reduction of the permeation driving force since the hydrogen partial pressure in the reaction side approaches the fixed permeate pressure value. On the other hand, in the sweep scenario due to the counter-current configuration at the end of reactor a significant permeation driving force exists.

The temperature profiles in reaction and permeation side show a similar shape, with an almost constant temperature in the central part of the reactor and lower values at the extremes. Due to the counter-current configuration, the reaction side temperature increases in the first part of reactor, as a consequence of the heat generated by reaction. Then the temperature decreases because of the heat exchanges with the permeate stream, that flows

in counter-current at lower temperature. On the permeation side, the sweep stream is fed at the outlet of reactor at 360 °C. The heat exchanged with the reaction side and the latent heat associated with the H_2 permeating flux contribute to the permeate temperature increasing. Then, close the the inlet of reactor the temperature decreases because of the heat exchanges with the retentate stream at lower temperature.

Table 13 Gas streams mole composition, CO conversion and H_2 Recovery for sweep factor 0.12 and membrane area 0.180 m² (13 membrane tubes).

	Feed	Sweep (Steam)	Retentate	Permeate
Temperature, °C	360	360	480	411.5
Pressure, bar	7	1.2	7	1.2
Total molar flow rate, mol/min	7.6	0.93	3.79	4.74
Composition: molar flow rate, mol/min				
CH_4	0.29	0	0.29	0
CO	0.70	0	0.03	0
CO_2	0.36	0	1.03	0
H_2	3.40	0	0.26	3.81
N_2	0.21	0	0.21	0
H_2O	2.64	0.93	1.97	0.93
CO conversion, %	96.1			
H_2 Recovery, %	93.4			
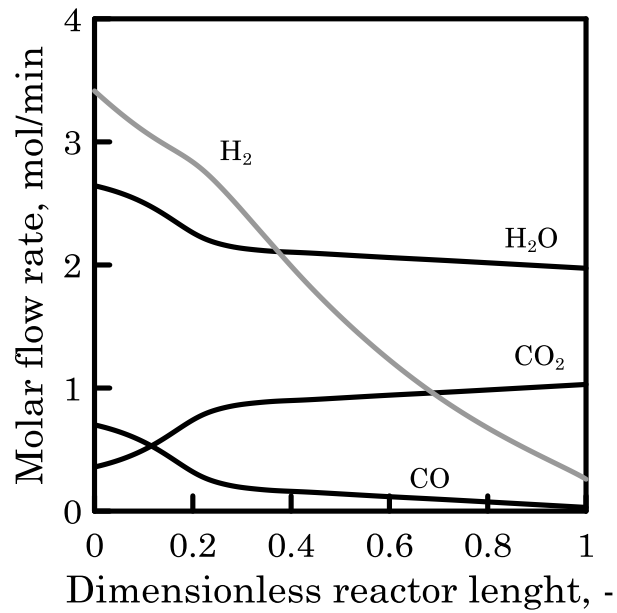
Figure 19 Molar flow rate profiles on reaction side along the reactor length. Membrane area 0.180 m² (13 membrane tubes), sweep factor 0.12, feed temperature 360 °C.
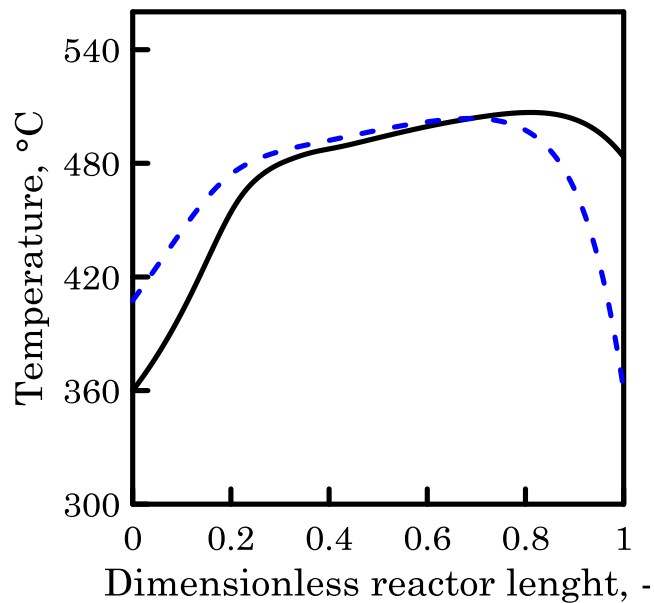
Figure 20 Temperatures profiles, on reaction side (solid line) and permeation side (dashed line), along the reactor length. Membrane area 0.180 m² (13 membrane tubes), sweep factor 0.12, feed temperature 360 °C.

1.7   Conclusion

The design of a pilot scale WGS-MR to produce 5 Nm³/h of hydrogen by reformate stream upgrading has been performed.

The production volume and the reaction pressure have been fixed in the framework of DEMCAMER project. Moreover, the minimum required MR performance, in terms of CO conversion and H_2 recovery, has been defined as project target.

The application of the WGS-MR has been associated to a conventional technology for H_2 production such as the natural gas steam reforming.

Depending on the system considered to promote the driving force for the permeation, three scenarios have been proposed: base, vacuum and sweep scenario. The preliminary screening of the MR performance at equilibrium condition showed that only for the base scenario (reaction pressure 7 bar, permeate pressure 1.2 bar) the H_2 recovery yield target value (H_2 RY equal to 90%) is not reachable. Operating at 1.2 bar on the permeate side, without a sweep gas stream, a reaction pressure higher than 20 bar should be needed to recover 90% of the maximum hydrogen producible. The vacuum and sweep scenario have been further investigated, considering different vacuum pressures and sweep factors. For the defined case studies a first estimation of the membrane area, required to obtain the hydrogen production target, has been done. Then a complete design of the MR has been performed by means of MR modelling and simulation. On the basis of the simulation results, the final operating conditions (feed temperature, sweep factor and permeate vacuum pressure) and required membrane tubes number have been calculated. To define the exact membrane tubes number the concentration polarization effect has been also taken into account by means of a permeance reduction coefficient, estimated from literature data. The permeance reduction, due to the concentration polarization effect, accounts for an additional membrane area equal to the 22% of value estimated without concentration polarization. However, this membrane surface area is actually overestimated since results obtained in the framework of DEMCAMER

project have shown as the permeance reduction, estimated from literature data for a hydrogen extractor membrane system, is higher than the real one occurring in membrane reactor.

Comparing for each scenario the required membrane area, in term of membrane tubes number, at quite similar performance there is only a slight difference: 13 tubes are needed for the sweep scenario and 12 tubes for the vacuum one.

To define the best option between vacuum and sweep scenario, other factors related, for instance, to the operating cost, to ease of designing and operating, have to be considered. Moreover, a different MR downstream post-processing follows from each scenario.

In the analysis of WGS-MR integration in a small scale H_2 generator, presented in the next chapter, both scenarios have been investigated. The results obtained from the pilot scale have been used for the design of the WGS-MR integrated in a 100 Nm^3/h hydrogen production unit.

Nomenclature

List of symbols

A	membrane area or heat exchange surface
C_p	specific molar heat
D_{Eq}	equivalent diameter
d_P	mean pellet diameter
Ea	activation energy
F	molar flow rate
G	superficial mass velocity
h	heat transfer coefficient
$J_{H2}^{Permating}$	H_2 permeating flux
ID , OD	inner, outer diameter
k	thermal conductivity
K_{eq}	equilibrium constant
$L_{Reactor}$	reactor length
n	number of mole
p	pressure
Pe_0	permeance pre exponential factor
$-r_{CO}$	intrinsic reaction rate, mol CO/(weight$_{catalyst}$ time)
r_{WGS}	reaction rate, mol CO/(Volume$_{Reactor}$ time)
R	ideal gas constant
S_{shell}	shell cross section
T	temperature
U	overall heat transfer coefficient
V	volume
y	molar fraction
z	axial coordinate along reactor length

Greek symbol

δ	thickness
$-\Delta H_{RX}$	enthalpy of reaction
$\Delta H_{H2}^{Permeating}$	enthalpy associated with the H_2 permeating flux
ε	void fraction/porosity
η	catalyst effectiveness factor
$\mu_{Mix}^{Reaction}$	viscosity of reaction mixture
v_i	stoichiometric coefficient of species i

Subscripts and superscripts

Catalyst	catalyst referred to
eq	equilibrium referred to
Feed	membrane module inlet stream referred to
i	ith species referred to
Membrane	membrane referred to
Permeation	membrane module permeation stream referred to
Reaction	membrane module stream on the reaction side referred to
Shell	membrane module shell referred to
Sieverts	Sieverts law referred to
Sweep	membrane module inlet stream on permeate side referred to
Tube	membrane module tube side referred to

Acronyms

HT-WGS	high temperature water gas shift
LT-WGS	low temperature water gas shift
MR	membrane reactor
TR	traditional reactor
MREC	membrane reactor equilibrium conversion
TREC	traditional reactor equilibrium conversion
H_2 RY	hydrogen recovery yield

References

1. R.P. Quirk. In Kirk-Othmer Encyclopedia of Chemical Engineering Technology, Vol 2, Wiley-VCH: 1963.

2. D.S. Newsome. Catal. Rev.-Sci. Eng., 1980; 21(1), 275–318.

3. Ruettinger W.F., Ilinich. O., In Encyclopedia of Chemical Processing (Ed.: S. Lee), Taylor & Francis, 2006, pp.3205-3215.

4. Babita K., Sridhar S., Raghavan K.V., Int. J. Hydrogen energy, 2011, 36, 6671-6688.

5. Dittmeyer R., Hollein and Daub K., J. Mol. Catal. A: Chem., 2001, 173, 135-184.

6. Gallucci F., Fernandez E., Corengia P., van Sint Annaland M., Chemical Engineering Science, 2013, 92, 40-66.

7. He X. and Hägg M.B., Membranes 2012, 2, 706-726.

8. Tosti S., Basile A., Chiappetta G., Rizzello C. and Violante V., Chem Eng J. 2003, 93, 23-30.

9. Flytzani-Stephanopoulos M., Qi X., Kronewitter S., Water-gas Shift with Integrated Hydrogen Separation Process, Final Report 2004, DEFG2600-NT40819.

10. Brunetti A., Drioli E., Barbieri G., RSC Adv., 2012, 2 (1), 226-233.

11. Boutikos P., Nikolakis V., Journal of Membrane Science, 2010, 350, 378-386.

12. Adrover M. E., López E., Borio D. O., Pedernera M. N,. AIChE J., 2009, 55 (Dec.), 3206-3213.

13. Gosiewski K., Warmuzinski K., Tanczyk M., Catal. Today, 2010, 156 (Oct.), 229-236.

14. Zou J., Huang J., Ho W.S.W., Industrial and Engineering Chemistry Research, 2007, 46, 2272.

15. Huang J., El-Azzami L., Ho W.S.W., Journal of Membrane Science, 2005, 261, 67.

16. Barbieri G.; Scura F.; Brunetti A.; Series "Membrane Science and Technology", Vol.13; Chapter 9 - "Mathematical modelling of Pd-alloy membrane reactors", pag. 325-400, 2008 – Elsevier B.V., Amsterdam, The Netherlands, Edited by R. Mallada and M. Menendez.

17. Lattner J.R., Harold M.P., Int. J.Hydrogen Energy, 2004, 29, 393-417.

18. Hermann Ch., Quicker P., Dittmeyer R., J. Membr. Sci., 1997, 136, 161-172.

19. Itoh N., Wu T.-H., J. Membr. Sci., 1997, 124, 213-222.

20. Gobina E., Hou K., Hughes R., J. Membr. Sci., 1995, 105, 163-176.

21. Tiemersma T.P., Patil C.S., van Sint Annaland M., Kuipers J.A.M., Chem. Eng. Sci., 2006, 61, 1602-1616.

22. Barbieri G. and Di Maio F. P., Ind. Eng. Chem. Res., 1997, 36, 2121-2127.

23. Gallucci F., Paturzo L., and Basile A., Int. J. Hydrogen Energy, 2004, 29, 611-617.

24. Harold M. P., Nair B. and Kolios G., Chem. Eng. Sci., 2003, 58, 2551-2571.

25. Dittmeyer R., Hollein and Daub K., J. Mol. Catal. A: Chem., 2001, 173, 135-184.

26. DEMCAMER, DEsign and Manufacturing of CAtalitic MEmbranes Reactors by developing new nano-architectured catalytic and selective membrane materials (Ref.: 262840), http://www.demcamer.org/

27. Ullman's Encyclopedia of Industrial Chemistry, 5th Completely Revised Edition. Edited by Barbara Elvers, Stephen Hawkins, and William Russey. VCH: New York, 1995. ISBN 3-527-20126-2.

28. Basile A., Paturzo L., Gallucci F., Catalysis Today, 2003, 82,275.

29. Marigliano G., Barbieri G., Drioli E., Chem. Eng. and Processing, 2003, 42, 231-236.

30. Barbieri G., Marigliano G., Perri G., Drioli E., Ind. Eng. Chem. Res., 2001, 40, 2017.

31. Fogler H. S., "Element of chemical reaction engineering", Prentice-Hall Intenrational, Inc. (3th Ed.)

32. J.C. Amphlett, L. M. Kearns, R. F. Mann, B. A. Peppley and J. P. Salvador, "The Simulation of a Membrane Reactor for Generating Hydrogen from Methanol for a PEM Fuel Cell Power System," Proc. Of the 12th World Hydrogen Energy Conference, Vol. 3, p. 1977, 21-26 June 1998.

33. Brunetti A., Caravella A., Barbieri G., Drioli E., Journal of Membrane Science, 2007, 306, 329-340.

34. Caravella A., Di Maio FP., Di Renzo A., Journal of Membrane Science, 2008, 321, 209-221.

35. Li C. H. and Finlayson B. A., Chem. Eng. Sci., 1977, 32, 1055.

36. D. Q. Kern (Ed.), Process Heat Transfer, McGraw Hill, New York, 1997.

37. Barbieri G., Scura F., Lentini F., De Luca G., Drioli E., Sep. Purif. Technol., 2008, 61, 217-224.

38. Caravella A., Scura F., Barbieri G. and Drioli E., J. Phys. Chem. B 2010, 114, 12264–12276.

39. Caravella A., Barbieri G., Drioli E., Chemical Engineering Science, 2008, 63 Issue 8, 2149-2160.

40. Caravella A., Scura F., Barbieri G. and Drioli E., J. Phys. Chem. B, 2010, 114, 12264-12276.

41. Zhang J., Liu D., He M., Xu H., Li W., Journal of Membrane Science, 2006, 274, Issues 1-2, 83-91.

42. Caravella A., Barbieri G., Drioli E., Separation and Purification Technology, 2009, 66 Issue 3, 613-624.

43. Hla S. S., Park D., Duffy G.J., Edwards J.H., Roberts D.G., Ilyushechkin A., Morpeth L.D., Nguyen T., Chemical Engineering Journal, 2009, 146, 148-154.

44. Byron Smith R J, Muruganandam Loganathany, Murthy Shekhar Shanthaz, Int. J. of Chemical reactor engineering, 2010, vol 8, Review R4.

Chapter 2

Integration of WGS-MR in small scale hydrogen generator: process plant simulation

Introduction

The hydrogen, as a potential energy carrier, will play a very important role in future energy systems. Considering, for instance, the actual concerns over greenhouse gas emissions and air quality, the hydrogen is the future transportation fuel to look at. For this reason many companies and academic institutions are focusing their efforts in trying to increase the hydrogen production and its efficiency [1, 2, 3]. At early stages of a hydrogen economy, the demand for hydrogen is foreseen for small volumes and geographically decentralised. Small production units can be modular, scalable and can provide hydrogen where needed, answering to the market requirements. On the other hand, large-scale plants using fossil feedstock are considered the most economic hydrogen production method [4, 5], but the major barriers are the costs of building the distribution infrastructures. Distributed production at refuelling stations, using the already present natural gas infrastructures, is therefore viewed as an attractive near to medium-term option. In the medium term (2030) a significant fraction of H_2 is expected to be produced in compact and containerized plants by on-site reforming of natural gas (NG) and other hydrocarbons.

Small-scale reformers are commercially available from several suppliers. Most of them are derived from the well established large scale steam-reforming processes. Only a few number of small scale reformers currently uses novel technologies as alternatives to steam-reforming.

Steam-reforming seems to be more amenable to down-scaling than the other two major large scale technologies for converting hydrocarbons into H_2 which

are partial oxidation, and autothermal reforming [3]. The reforming process is somewhat flexible with respect to feedstock, but the reformers usually operate on NG, LPG and methanol, which are the feedstock with more widespread distribution infrastructure. Other fossil fuels like naphtha and kerosene have been commercially used and renewable fuels, like biogas and ethanol, are also looked at.

About 30 H_2-filling stations using reforming techniques are currently operated worldwide, essentially for demonstration purposes. Major demonstration testing has been done in Japan, Germany and in the USA.

H_2 produced by commercially available technologies for on-site reforming of natural gas costs between 0.35 and 0.70 €/Nm^3, depending on H_2 capacity, number of units produced, utilization rate, natural gas cost, investment cost and depreciation period. For the future this target cost has to be reduced, in a way to be competitive with the traditional fuels. A capital cost reduction is therefore a key challenge for the on-site plant. Generally, as outlined by the process intensification strategy, a possible approach to enhance a production process is providing a better exploitation of raw materials, reducing the reaction/separation/purification stages as well as the auxiliary devices and energetic loads. In the hydrogen production field a promising approach is the integration of membrane reactors (MRs). The use of MRs has been suggested as a possible strategy to produce hydrogen in a more *intensified* way, reducing the process complexity, the equipment size and number and, potentially, the production cost [6, 7, 8, 9]. As previously introduced in chapter 1, there are several studies in the literature [10, 11, 12, 13] indicating the feasibility of the Pd-based water-gas shift membrane reactor to produce high purity hydrogen from syngas.

In the following analysis, starting from the results obtained in pilot scale membrane reactor (see chapter 1), the design of a new process, integrated with the WGS-MR developed within the DEMCAMER project, has been investigated. In particular, the application of the WGS-MR has been associated to a small scale NG reforming system for H_2 production.

The reforming process consists in transforming hydrocarbons into hydrogen and it takes place in three main stages (see Figure 21):

➢ Reforming

➢ Gas conversion

➢ Purification
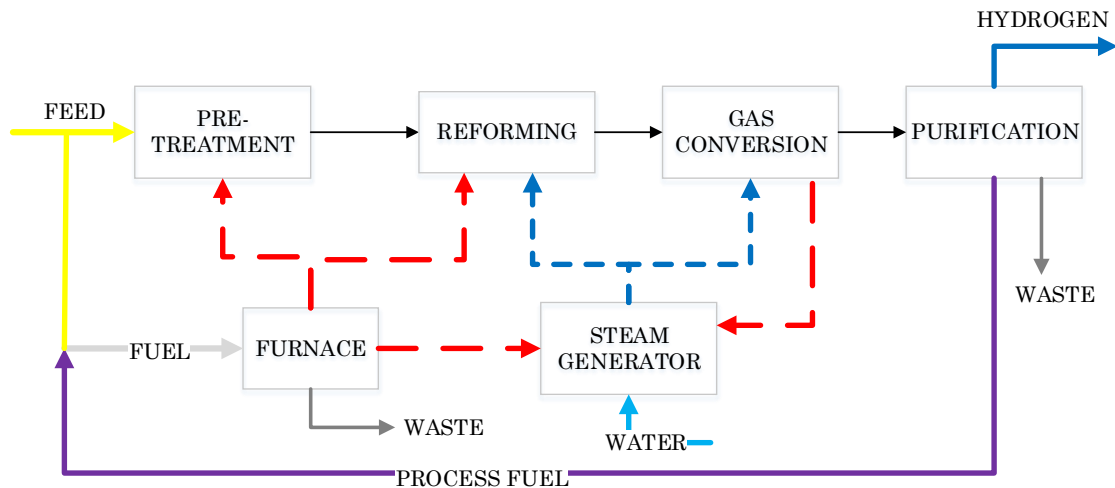
Figure 21 Scheme of steam reforming process showing material and heat integration.

In the first step, feedstock (NG) reacts with steam to produce a synthesis gas (syngas) that is mostly composed of H_2 and CO. A pre-treatment of the feedstock is usually required being the reforming a catalytic process sensitive to impurities in the feed as, for instance, sulphur compound. To increase the amount of hydrogen in the second step, the product gas passes through a shift conversion unit, where the water gas shift reaction occurs. This reaction takes place at lower temperatures than the reforming reaction and uses catalysts. The shift process, as previously described (see Chapter 1, introduction) is usually accomplished in two reactors – typically a high temperature and a low temperature reactor – used to decrease CO content to 1% or less. However, in small-scale reforming systems only a medium temperature shift-reactor (MTS) is used. The produced gas is rich in H_2 (40-60%); the rest is composed of CO_2, CH_4, H_2O and a few percentage of CO. In the last step, after water removal, the dry reformate is sent to a purification unit. Pressure-Swing Adsorption (PSA) is the technology commonly used for H_2 production

capacities in the range 50-1,000 Nm^3/h [14]. The process described above represents the conventional technology reference. When the traditional WGS reactor is substituted with the membrane reactor the process configuration changes. In fact, the membrane reactor influences both the upstream and downstream processing. For instance, the two different streams of the membrane reactor require different separation paths and, also the load of these separations is very different from the one of a conventional process. Aiming to recover more than 90% of the total hydrogen directly from the MR unit, the further H_2 separation step is no more required. This means that the PSA unit can be avoided, reducing the unit number. Thus, designing the new process all the aspects and peculiarity of the membrane reactor, as higher conversion, different operating conditions and downstream processing, have to be considered.

In the performed analysis, the WGS-MR integrated process has been investigated by process simulations, as a function of the main variables affecting the membrane reactor performance and the downstream treatment of MR streams. The carbon dioxide recovery has been also analysed for the innovative integrated process. The design and simulation results obtained for the pilot scale WGS membrane reactor, (described in Chapter 1), represented the base of the design of the integrated MR.

The commercial simulation tool Aspen Plus®, suitable for chemical industrial process, has been used as process simulator.

2.1. On site H_2 generator: size definition

Following a report of the international energy agency (IEA-HIA) [15], the production range of small scale reformers for H_2 filling stations should be between 100 and 300 Nm^3 H_2/h. In the DOE program [16], a capacity of 690 kg/day (7500 Nm^3/day) is considered to be suitable for an H_2 filling station that will satisfy the needs of 140 fuel cell vehicles per day. Many experts agree this production capacity is a foreseeable value that would fit the needs in the short and medium term of the H_2 economy. On the basis of these indications, the size of the on site - H_2 generator considered in the analysis has been fixed to 100 H_2 Nm^3/h. The purity target of 99.99%, as defined in the project, has been assumed. The reformer unit has been assumed operating at 7 bar_a, which is the pressure value fixed for the design of the pilot scale WGS-MR. The membrane reactor integration has been analysed in fact for the scenarios and case studies defined for the pilot scale. In addition, the outlet pressure of produced hydrogen was set to 6 bar_a, in order to match the same output conditions of the conventional technology reference (steam reforming with pressure swing adsorption).

2.2. Definition process up-stream WGS-MR: NG steam reformer

The integration of the WGS-MR has been associated to an NG steam reforming unit. Reforming process, as catalytic operation, requires a minimum quality for the feed composition. Hence, usually, the natural gas is pre-treated in order to remove any catalyst poisoning compounds. For simplicity, the hydro-desulfurization (HDS) has been not included in our design, assuming the absence of sulphur compounds. Table 14 provides the natural gas composition chosen for this analysis. This composition represents the typical composition of natural gas from Groningen region (The Netherland), with an higher N_2 content respect to other NG feedstock, for instance from Russia or Algeria [17].

Table 14 Design natural gas molar composition

Species	CH_4	N_2	C_2H_6	C_3H_8	C_4H_{10}	C_5H_{12}	CO_2
%	81.30	14.34	2.87	0.39	0.16	0.05	0.89

The steam methane reforming reaction (Eq. 57) is an endothermic reaction, equilibrium limited. The conversion is favoured by high temperature, low pressure and high steam to carbon ratio. The reaction generally takes place at temperatures of 700-900°C and pressures of 10-30 bar, in the presence of a catalyst [18].

$$CH_4 + H_2O \leftrightarrow CO + 3\,H_2 \qquad \Delta H_{RX,\ 298\ K} = +\ 206\ kJ/mol$$

Eq. 57
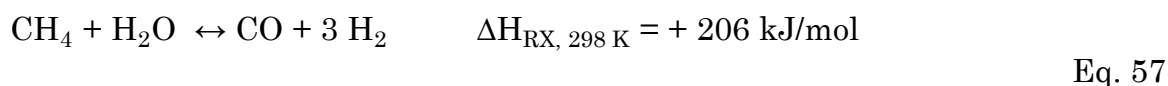
The reaction is supported by external heat from a reformer furnace. The heat supplied can be provided through the combustion of a fraction of the incoming natural gas, eventually supplemented by the combustion of process fuels. The steam-to-carbon ratio is adjusted to avoid the formation of carbon on the surface of the catalyst that leads to its deactivation. Natural gas, distributed by the utility at just slightly above atmospheric pressure, must be compressed to achieve a more favourable combination of equilibrium, reaction rates, and equipment sizing.

A schematic representation of the simulated reforming process is presented in the flow diagram section of Figure 22. It is includes the natural gas compressor, the reformer reactor and the reformer furnace. Table 15 summarizes the main input data and assumption for the reformer reactor. As defined above, we chose to operate the reformer at the same pressure of the pilot scale shift membrane reactor. The idea was, in fact, to analyse the integration of the WGS-MR on the basis of the case studies defined for the pilot scale reactor.

The natural gas feedstock has to be therefore compressed to 7 bar_a. A multistage intercooled compressor has been considered to perform the compression; Table 16 summarizes the design and operating parameters.
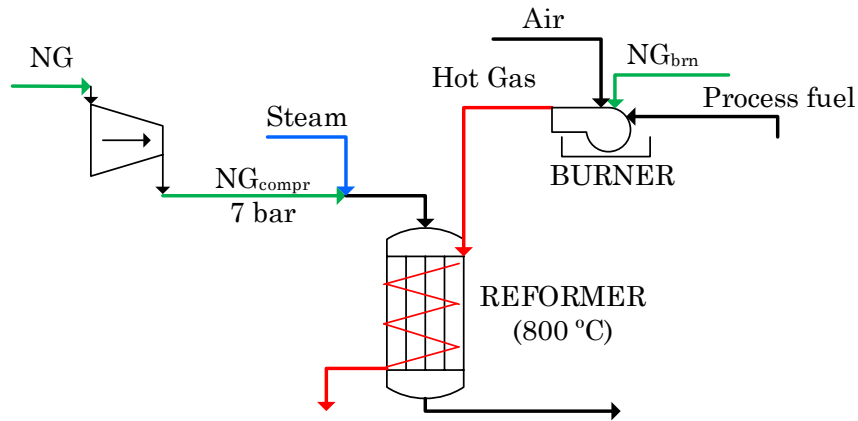
Figure 22 Process flow diagram of reforming section.

Table 15 Input data and model assumption for the reformer

Input	
Pressure	7 bar$_a$
Temperature	800 °C
Steam/carbon ratio	3
Assumption and specification	
CH$_4$ conversion	Equilibrium temperature approach
Higher hydrocarbon conversion	Complete conversion
Heat from the furnace is transferred to the reformer by heat exchange with the furnace hot flue gas	

Table 16 Natural gas compressor parameters

	Unit	Value
Inlet pressure	bar	1.2
Outlet pressure	bar	7
Number of stages	-	2
Overall efficiency	-	0.82 [19]
Maximum temperature after intercooling	°C	60

A steam stream at 7 bar$_a$ has to be also produced; the water required as a feedstock for the reformer is firstly pumped to the reformer pressure and then vaporized. Natural gas from the compressor is pre-heated and, then, mixed with the steam at an appropriate temperature, with a design steam to carbon molar ratio equal to 3 [20]. Before entering the reformer, the feed stream is heated up to the reactor temperature of 800 °C. Table 17 summarizes the set of reactions assumed in the reformer simulation.

Table 17 Reactions taking place in the reforming reactor

R1.	$CH_4 + H_2O \leftrightarrow CO + 3\ H_2$	R2.	$C_2H_6 + 2\ H_2O \leftrightarrow 2\ CO + 5H_2$
R3.	$C_3H_8 + 3\ H_2O \leftrightarrow 3\ CO + 7\ H_2$	R4.	$C_4H_{10} + 4\ H_2O \leftrightarrow 4\ CO + 9H_2$
R5.	$C_5H_{12} + 5\ H_2O \leftrightarrow 5\ CO + 11\ H_2$	R6.	$CO + H_2O \leftrightarrow CO_2 + H_2$

Two reactors, the RStoic and REquil Aspen Plus® reactor, have been used in series to model the reformer reactor. In the first, a conversion reactor, the complete conversion of higher hydrocarbons is modelled. The second is an equilibrium reactor and accomplishes most of the methane reforming. The products composition at the exit of reformer reactor (H_2, CO, CH_4, H_2O, CO_2 and N_2) has been selected in such a way to obtain the feed gas composition fixed for the WGS-MR pilot scale. The equilibrium reactor, REquil, has been defined by means of a temperature approach. For temperature approach

specifications, REquil evaluates the chemical equilibrium constant at a temperature T^* being

$T^* = T_R + \Delta T$

where T_R is the specified reactor temperature and ΔT is the temperature approach. The temperature approach value has been iteratively modified in order to obtain at the reactor outlet the design specified CH_4 and CO molar concentration for the WGS reactor inlet. In the carbon balance no coke formation has been assumed. Two separate reactors have been used for the ASPEN model to manipulate separately the higher hydrocarbons conversion and methane reforming. In the actual plant configuration, the steam reforming reactions occur in one single reactor. A conservative reactor sizing and catalyst loading assure a close approach to equilibrium at the designed operating temperature.

We simulated to supply the heat required to sustain the reforming reactions by heat exchange with the hot gas coming from a furnace, which combines air, natural gas fuel and process fuel. The fuel fed to the furnace has been calculated on the basis of the heat required to support the reformer. A 40% of excess air for combustion has been assumed.

After SR, the produced syngas contains around 9% of CO and goes through the WGS step for further H_2 production. The process gas leaving the reformer before going to the shift reactor has to be cooled to 360 °C.

2.3. Integration of WGS-MR unit in process flow diagram

The syngas from the reformer is rich in H_2 (44.8%, molar composition) with a 9% ca. of CO. The shift reaction (see Table 17, R6) is used to increase the hydrogen content. The membrane reactor, shifting the equilibrium through the hydrogen removal, allows achieving higher conversion, with respect a traditional reactor, recovering a high purity H_2 stream, directly. The further hydrogen separation process is no more required when high H_2 recovery is obtained.

The WGS-MR was modelled in ASPEN using the combination of an adiabatic conversion reactor (RStoic) and a separation unit (Sep) where the H_2 extraction is performed. Downstream of the separation unit, a pressure valve is used to manage the pressure of the permeate stream. In an actual system, reaction and separation take place in one single unit, the membrane reactor, reducing, effectively, the unit number with respect the reference technology, where H_2 purification is usually accomplished by pressure swing adsorption (PSA).

The conversion reactor has been modelled setting as input data the CO conversion, as obtained from the WGS-MR simulation. Similarly, the separation unit (Sep) has been designed by specifying the calculated H_2 recovery value as split fraction. The Sep model is useful to represent component separation operations; the unit combines inlet streams and separates the resulting stream into two or more streams, according to split fraction specified for each component. Two fictitious heat exchangers have been used to manage the retentate and permeate stream temperature, respectively. For each unit the design parameters, such as conversion, split fraction, temperatures have been imported from simulation results by mean of a calculator blocks. Calculator blocks in Aspen Plus lets insert Excel spreadsheets into flowsheet computations to perform user-defined tasks.

The WGS-MR for the small scale H_2 generator has been designed on the basis of the modelling defined for the pilot scale. The same scenarios determined for the pilot scale have been considered for the integrated WGS-MR: the vacuum scenario, when vacuum is applied on the permeate side, the sweep scenario when steam is fed in the permeate side. As a consequence, two different process layouts come from the considered scenarios.

The integrated WGS-MR performance has been simulated using as input data the parameters reported in Table 18. The membrane area has been scaled-up on the basis of the H_2 production capacity using the following scaling equation:

$$A_{\text{new scale}}^{\text{Membrane}} = A_{\text{pilot scale}}^{\text{Membrane}} \left(\frac{H_2\text{Production capacity}_{\text{new scale}}}{H_2\text{Production capacity}_{\text{pilot scale}}} \right)$$

Eq. 58

For conventional reactor a useful parameter to scale-up a reactor is the space velocity. Industrially, the most common versions of space velocities in typical units are gas hourly space velocity (GHSV) or weight hourly space velocity (WHSV), defined as the ratio of volumetric feed flow rate to reactor volume and the ratio of mass feed flow rate to catalyst weight, respectively.

In the case of a membrane reactor not only the reactor volume/catalyst weight has to be taken into account but also the membrane area. In particular, when the removal of hydrogen through the Pd-alloy membrane is slower than the catalytic reaction rate, the relevant parameter that affects MR performance is the membrane area or rather the feed to surface ratio (F/S), which is the feed molar flow with respect to the membrane surface [21]. The scale-up of the integrated WGS-MR has been therefore based on the same F/S ratio of the pilot scale reactor. The reactor geometry was not optimized in this analysis, because we want focus mainly on the integration feasibility demonstration.

Operating condition, design parameters and performance are summarized in Table 18. Figure 23 shows the flow diagram section of the WGS membrane reactor, for vacuum and sweep scenario, respectively.

Table 18 Operating condition, design parameters and performance for WGS-MR

Parameter	Unit	Vacuum	Sweep
Retentate pressure	bar	7	
Permeate pressure	bar	0.35	1.2
Feed temperature [a]	°C	360	
Sweep factor	-	N.A.	0.12
Membrane area	m^2	3.6	
Performance			
CO conversion	%	97.5	97.2
H$_2$ recovery yield	%	94.3	93.4

[a] The same value has been considered for the feed sweep temperature.
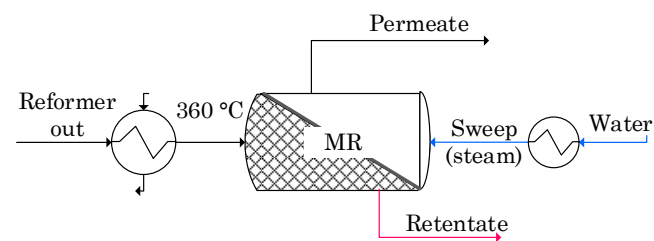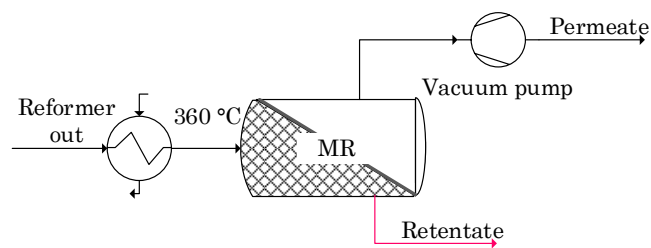
Figure 23 Process flow diagram of WGS-MR section.

A summary of the mass balance and performance on the reaction section, reforming reactor and WGS-MR, is presents in Table 19.

Table 19 Mass balance and performance on the reaction section

	Sweep	Vacuum
Methane conversion, -	0.76	
CO conversion, -	0.972	0.975
H$_2$ recovery yield, -	0.934	0.943
H$_2$ outlet/NG feed	2.58	2.61
Mass balance, kmol/h		
NG feed	1.80	
Water feed reformer	4.85	
Sweep (steam)	1.12	-
Permeate	5.77	4.70
Retentate	4.53	4.48

2.4. Downstream WGS-MR process re-design

The retentate and permeate streams coming out from the membrane reactor have different pressure, temperature and composition. A typical molar composition, for sweep scenario, is reported in Table 20. Moreover, since the hydrogen separation step is no more required, a complete re-design of the downstream WGS-MR process is needed. In particular, the post processing of these streams has to be designed in a different way. Most of the hydrogen produced is recovered in the permeate stream and, depending on the scenario considered, it can be directly obtained at high purity (vacuum scenario) or as a gaseous mixture with steam (sweep scenario). In the latter case, the steam has to be removed to get the required hydrogen purity.

Table 20 Molar composition of permeate and retentate stream for sweep scenario

Species	Permeate	Retentate
CO	0.00	0.01
H_2O	0.19	0.52
CO_2	0.00	0.28
H_2	0.81	0.07
N_2	0.00	0.06
CH_4	0.00	0.08

The retentate, instead, is a hot stream including unrecovered hydrogen, CH_4 and CO unconverted. Also, it is a compressed stream with a CO_2 content, on molar dry basis, higher than 40%. Thus, it can be used as valuable fuel process as well as be sent to a membrane separation unit for the CO_2 capture. Permeate and retentate post processing has been analysed separately. In the following the performed analysis will be presented.

2.4.1.   Permeate post processing

Depending on the scenario, the post processing for the permeate stream is different. With vacuum configuration, the hydrogen is recovered as pure gas stream; four grade purity has been assumed. Due to the operating temperature constrains for the vacuum pump, the permeate stream has to be cooled. Operating parameters and estimated energy required by the vacuum pump are reported in Table 22. Figure 24 shows the process flow diagram of the permeate post processing section for vacuum scenario.
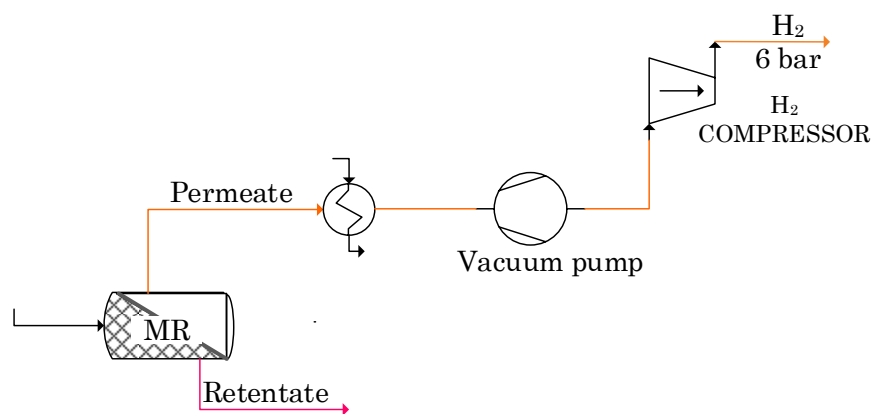
Figure 24 Process flow diagram of permeate post processing section for vacuum scenario.

When steam, acting as a sweep gas, is fed in the permeate side, the hydrogen extracted has to be separated from the steam. To recover the hydrogen at the required purity the separation H_2/H_2O has to be accomplished. This can be easily performed by removing the water by condensation. The hot H_2-rich permeate stream is cooled by heat exchanges to perform the condensation and then fed to a water knock-out tank to remove the liquid water. The tank has been modelled as a flash drum; the design parameters are reported in Table 21. The water separated, expressed as the ratio of water in the liquid stream to the water in the feed stream, is ca. 84% and can be recycled to a closed loop circuit for steam production. A water stream make-up has been included in the circuit to provide the amount of water unrecovered. An additional purification step has to be considered to remove the further trace of water presents in the H_2 rich stream. The dehydration stage can be performed, for

instance, by water adsorption on solid desiccant. This further purification step has been modelled as a simple separation unit, set to achieve design performance goals (100% water removal), since a complete unit design is out of our purposes. The process flow diagram of the permeate post processing section for sweep scenario is presented in Figure 25.

Table 21 Flash drum design parameters

Parameter	Unit	Value
Temperature	°C	35
Pressure	bar	1.2
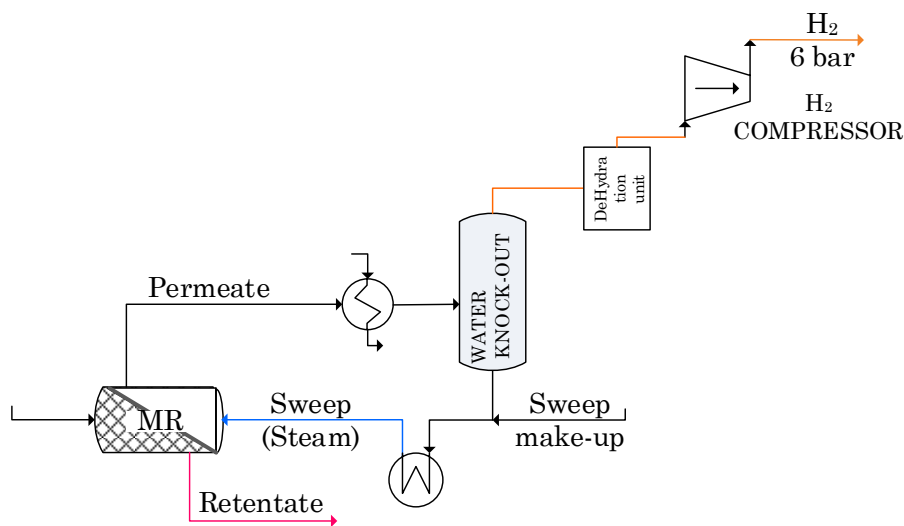
Figure 25 Process flow diagram of permeate post processing section for a sweep scenario.

Since the hydrogen is recovered slightly above the ambient pressure, the last step, for both scenarios, is the hydrogen compression. In fact, as described earlier, the outlet hydrogen pressure target has been set close to the reformer pressure. Actually, this additional compression step has been considered to properly compare the MR integrated process with the conventional technology reference. In the last case, for a reformer operating pressure of 7 bar$_a$, a pure H$_2$ stream at 6 bar$_a$ can be obtained, assuming 1 bar pressure drop across the

PSA. The compressor considered for the hydrogen is a multistage type with intercooling stages, in order to keep discharge temperature below approximately 130 °C. Operating parameters and energy required have been summarized in Table 22.

Table 22 Design data for vacuum pump and H_2 compressor

Parameter	Unit	Vacuum pump	Hydrogen compressor
Inlet pressure	bar	0.35	1.1
Outlet pressure	bar	1.1	6
Overall efficiency	-	0.4	0.78 [19]
Maximum inlet gas temperature	°C	40	60
Energy	kWh/Nm^3 H_2	9.5E-02	8.0E-2

2.4.2. Retentate post-processing

The retentate stream leaves the shift membrane reactor at ca. 7 bar and about 470 °C; the temperature depends on the scenario considered. However, in term of composition, for both configurations almost the same product distribution is obtained. It has to be noticed, in fact, that the achieved CO conversion and H_2 recovery are quit similar. Hence, the retentate post processing has been analysed considering an average composition from both scenarios, as reported in Table 23. Since hydrogen, the main product, is directly recovered in the permeate stream, the destination of the retentate stream depends on its component value. This stream has a high concentration of water and carbon dioxide, including residual methane and small amounts of carbon monoxide, hydrogen and nitrogen. A further reaction step to convert the remaining CO unreacted is not convenient: even assuming to convert all the CO and recover completely the additional H_2 produced, it will increase the total hydrogen output of only 0.5 %.

Table 23 Design retentate stream molar composition on wet and dry basis

Species,	H_2O	CO_2	CH_4	H_2	N_2	CO
Wet basis,%	52.1	27.6	7.7	6.5	5.6	0.5
Dry basis,%	-	57.6	16.1	13.5	11.7	1.1

The possibility to recover the remaining H_2 has been not considered since the H_2 content in retentate stream is a consequence of the fixed H_2 recovery target on the MR, defined on the basis of a trade-off between the membrane area applied (and its cost) and the gain in term of hydrogen recovered.

On dry basis, the CH_4, H_2 and CO constitute almost the 30% of the retentate stream therefore it represents a valuable process fuel. It can be used in the reformer furnace to reduce the overall system fuel requirement. The natural gas required to the burner to thermally support the reformer is equal to 59% of the NG fed, as reactant, to the reformer (NG_{Ref}). If the retentate is sent to the burner (Alternative A) the NG supplied as fuel (NG_{brn}) is two times lower then the previous one; it represents the 25% of the NG_{Ref}. However, as previously discussed, the retentate has an high water content thus the effect of water removal on the overall NG fuel demand has been analysed (Alternative B). Since after water removal the retentate has a higher heating value, the additional NG to the burner is reduced to 17.5% of the NG fed as reactant.

The process flow diagram of the retentate post-processing section is shown in Figure 26; both alternatives are presented.

Recycling the retentate to the burner, the possibility to design a thermally self-sustaining process has been analysed. In particular, the option not including NG fuel stream has been investigated, feeding to the burner a retentate stream richer in H_2 content. The hydrogen retentate fraction can be increased by reducing the H_2 recovery, acting on the WGS-MR area.
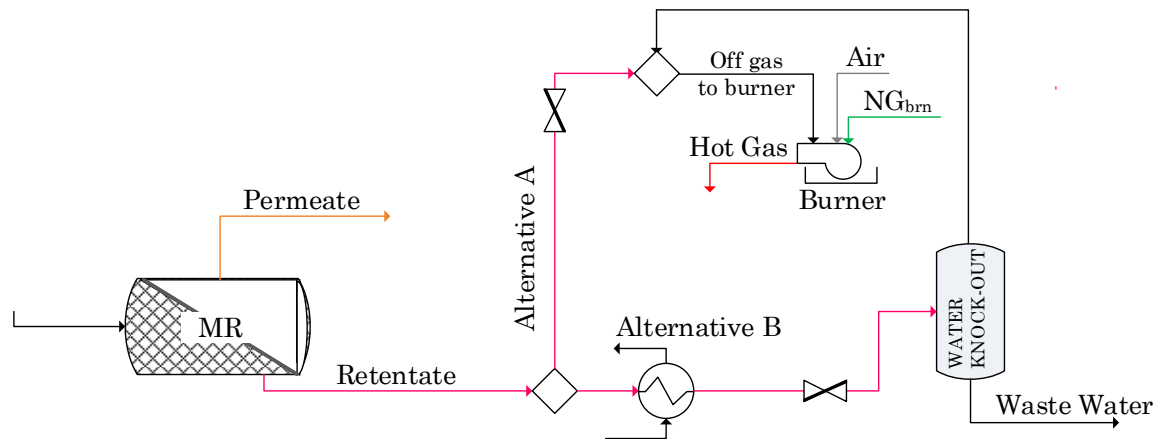
Figure 26 Process flow diagram of the retentate post-processing section: Alternative A and Alternative B.

The calculated performance for both scenario are slightly higher than the target value, thus we can consider to reduce the hydrogen recovery even guaranteeing the 100 Nm³/h of H_2 production. The results show as the H_2 recovery yield has to be reduced to 76% to get a "thermal self-sufficient" reforming. Since the total natural gas is reduced by 15% but the hydrogen recovery is reduced by 18% compared to the reference value, this strategy is entirely not effective, from an economical and productive point of view. In Table 24 are summarized the results for the different alternatives considered.

Table 24 NG fuel demand for the different retentate post processing alternatives

Alternative	H_2 recovery yield, -	NG_{brn}, kmol/h	NG_{tot}, kmol/h	$NG_{brn}/^aNG_{Ref}$, %
Without retentate	0.934	1.06	2.860	59
Alternative A	0.934	0.45	2.250	25
Alternative B	0.934	0.315	2.115	17.5
Alternative B removing NG_{brn}	0.869	0.095	1.895	5.3
	0.763	0	1.800	0

[a] NG_{Ref} = 1.8 kmol/h

Another retentate post processing alternative has been studied. As previously described, on dry basis, the carbon dioxide is the most present component in the retentate stream (see Table 23). In addition, it is a pressurized stream meaning that it has the energy required, in term of pressure, to drive for instance a membrane gas separation process. As a consequence, the possibility to capture the CO_2 by means of a membrane separation unit has been also analysed. The simulation has been performed considering the property of a commercial membrane for CO_2 separation. A separate chapter (see Chapter 3) has been dedicated to describe the performed analysis. Here only some results are presented, since our focus is the integration in the process plant.

The CO_2 membrane separator has been modelled in Aspen by a separation unit (Sep). The unit has been designed specifying each component split fraction as calculated by simulations. In particular, several operating condition, in term of membrane area, pressure ratio and configuration, have been simulated and the results used as design input data.

With a one stage configuration, assuming to use all the pressure driving force available, which means a permeate pressure of ca.1.1 bar, 40% of CO_2 can be recovered with a purity of 70%. The calculated composition of retentate and permeate streams are summarized in Table 25.

Table 25 Calculated molar composition [%], on dry basis, of retenate and permeate stream.

Species	Permeate (Concentrated CO_2 stream)	Retentate (Off gas to burner)
CO_2	71.28	46.14
H_2	25.75	16.67
CH_4	1.61	20.15
N_2	1.19	14.76
CO	0.17	2.23

The results are promising even if for the CO_2 capture the purity target is 95%.

Basically hydrogen affects the achievable purity, since it is the second species more present in the retentate. Thus, the main issues are related to the retentate H_2 content and to the low selectivity of commercial membrane toward this gas. The processing of retentate stream with lower H_2 fraction has been analyzed, for the same previously considered membrane selectivity value, in order to evaluate the effect on CO_2 separation of the retentate H_2 content. To get a retentate stream with lower hydrogen fraction, a WGS-MR with larger membrane area, and thus greater H_2 recovery, has been simulated. A CO_2 purity around 90% has been obtained by feeding a retentate stream with H_2 content, on dry basis, less than 6%.

It has to be noticed that for small scale H_2 generator the on-site CO_2 capture is generally considered to be costly, adding also complexity to the process design. However, also for the small scale generator the future increasing constrains on CO_2 emission are expected to be an issue to face. As a consequence, development of cost effective technologies for CO_2 handling in small-scale reforming is regarded as a long term necessity [14]. In this field the application of membrane technology, as membrane reactor and membrane gas separation unit, can play a crucial role. The retentate post-processing with CO_2 capture has been further investigated and presented as separated case study in the next chapter.

The process flow diagram of retentate post-processing integrated with CO_2 separation unit is shown in Figure 27. The retentate stream coming out from the CO_2 membrane separation unit can be further exploited as process fuel. For this scenario the NG demand to the burner, depending on the process fuel composition, is related to the CO_2 membrane separation performance. For an off gas composition as reported in Table 25 the NG molar flow rate required to the burner is 0.37 kmol/h. This value is slightly higher than that one without CO_2 capture unit (see Table 24, Alternative B). This is due to the fact that only the 35% of the hydrogen present in the WGS-MR retentate stream

and fed to the CO_2 membrane separation unit is then recovered in the off gas. Thus, the off gas recovered after CO_2 separation has a lower heating value.
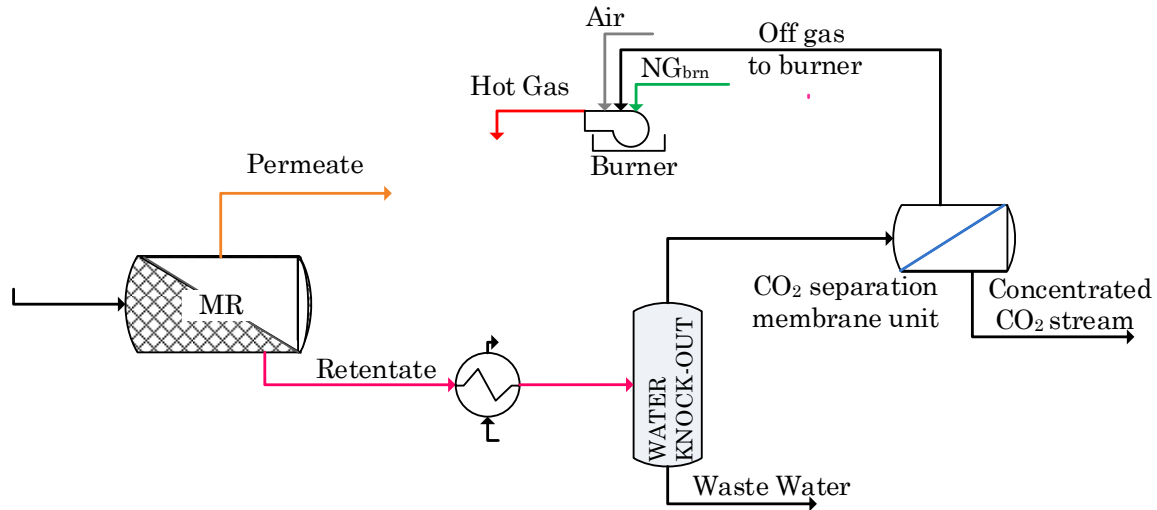
Figure 27 Process flow diagram of the retentate post-processing section with CO_2 membrane separation unit integration.

Finally, the analysis of the heat exchange requirement for the MR integrated process has been performed. The heat exchange network has been defined for both scenarios, considering the simplest retentate post processing alternative which does not include the CO_2 capture. The process flow diagrams of the whole process, for vacuum and sweep scenario respectively, are shown in Figure 28 and Figure 32. The composition of principal streams is reported in the appendix. Table 37 presents the stream summary for vacuum scenario, referring to the process flowsheet of Figure 28. Similarly, Table 38 presents the stream summary for sweep scenario, referring to the process flowsheet of Figure 32.

2.5. Heat exchange network definition

In industrial experience, the calculation of the minimum heating and cooling requirements reveals significant energy savings. Energy integration design procedure is a very important tool for pursuing the energy saving strategy. However, a completed design of the heat exchanger network is not necessary to assess the energy integration design. Targets can be set for the heat exchanger network to assess the performance of the complete process design without actually having to carry out the network design. These targets allow both energy and capital cost for the heat exchanger network to be assessed. The starting point for an energy integration analysis is the calculation of the minimum heating and cooling requirements for a heat-exchanger network. First sources of heat (termed hot streams) and sinks (termed cold streams) from the material and energy balance has to be identified. In any process flow sheet, there are several streams that need to be heated and other that need to be cooled. The heat associated with each stream can be calculated by using the following equation:

$$Q_i = F_i c_{P_i} \Delta T_i$$

<div align="right">Eq. 59</div>

There are two laws for heat integration analysis. The first law states that the difference between the heat available in the hot streams and the heat required for the cold streams, is the net amount of heat that must be removed or supplied. This first law does not take into account the restriction on temperature driving force. In fact, heat transfer from a hot stream to a cold stream is possible only if the temperature of hot stream exceeds that of cold stream, as the second law states. Hence, to estimate in consistent way the duties required, a positive driving force between the hot and cold stream must exist, satisfying also the second law. Hohmann, and Linhoff [22, 23, 24] have presented a simple way of incorporating second-law constrain into the energy integration analysis. A brief description of their analysis is presented. A series of temperature intervals can be obtained if the heat stream data are represented on two temperature scales, one for the hot stream and another for the cold ones, shifted by a chosen minimum temperature driving force (or

temperature approach, ΔT_{min}). In each temperature intervals heat can be transferred from the hot streams to the cold streams because it is guaranteed that the temperature driving force is enough. The heat transfer in each interval can be expressed by following equation:

$$Q_i = \left[\sum (Fc_P)_{hot,\,i} - \sum (Fc_P)_{cold,\,i} \right] \Delta T_i$$

<div align="right">Eq. 60</div>

The sum of the heat available in all the intervals corresponds to the net difference between the heat available in the hot streams and that in the cold streams, as calculated by first law.

To satisfy the net heating and cooling requirement in each temperature interval the simplest way could be to supply any heat requirement from hot utility and to discharge any excess heat to a cold utility. Clearly this strategy corresponds to a very poor engineering design, incurring excessive energy cost and also incompatible with the goals of sustainable industrial activity, which claim for use of the minimum energy consumption. Instead, it is preferable to use the heat available at high temperature to cover some heat requirement at lower temperature. The idea is therefore to transfer the heat available at higher temperature to satisfy the heat demand at lower temperature intervals, until there is sufficient heat load. When all the heat available at higher temperature has been exploited then the hot utility can be used. Appling for each temperature intervals this heat transfer strategy a so called cascade diagram is obtained, showing how heat cascades through the temperatures intervals. By means of the cascade diagram the minimum utility loads can be defined; it depends actually on the minimum temperature driving force chosen. If the minimum approach temperature changes, heat intervals also change and so the minimum heating and cooling loads. The temperature interval where no heat transfer is possible represents pinch point.

To define the heat exchanger network for the identified process flowsheet, a pinch analysis tool has been used. The pinch analysis is a technique for evaluating the heat flows in any heat exchanger network. The process

streams are first divided into hot and cold streams. Then, the enthalpy temperature diagram is drawn for both hot and cold streams. The curves obtained, called hot composite curve and cold composite curve, respectively, include the effect of all the streams. In particular, the composite hot stream is a single stream that is equivalent to the individual hot streams in terms of temperature and enthalpy. Similarly, occurs for the composite cold stream. These curves can be created by calculating the cumulative enthalpy of all streams of the same kind (hot or cold) within each temperature interval for each stream. The hot and cold composite curves provide a comprehensive picture of the heat supply and heat demand for the process over the entire temperature range. When the two curves are drawn together, the combined composite curve is obtained; the relative position of the two curves is determined by the minimum approach temperature chosen. The point at which the two curves come closest is the pinch point, and the corresponding temperature is the pinch temperature. The pinch point divides the process into two thermodynamically separate regions. According to Linnhoff and Hindmarsh, the appropriate procedure to design the overall networks of heat exchangers is separately defining the network for the region above the pinch and the network for the region below the pinch. Below the pinch, there is a heat excess thus any heating utility supplied to the process below the pinch temperature cannot be absorbed and will be rejected by the process to the cooling utility, increasing the amount of cooling utility required. Similarly, above the pinch only utility heating are required. Hence, the following rules of thumb associated with the use of utilities have been developed:

➢ Do not transfer heat across the pinch.
➢ Add heat only above the pinch.
➢ Cool only below the pinch.

There is also a heuristic design for feasible matches at the pinch condition that assures no violation of the minimum temperature approach:

➢ Above the pinch: $F_H c_{P_H} \leq F_C c_{P_C}$

➢ Below the pinch: $F_H c_{P_H} \geq F_C c_{P_C}$

When the stream match is performed, the most constrained hot stream (the one with the lowest temperature) is considered for heat exchange with the most constrained cold stream (the one with the highest temperature).

If heat exchange is thermodynamically possible between these two streams, it is counted as a match. If heat exchange is not possible, the next most constrained stream is chosen for consideration. This process is continued until a match is found and the process is repeated for all the streams. The heat exchanger network configuration is therefore created, based on the matches made. Following the rules and strategy reported above a complete heat exchanger network design is accomplished, ensuring that the minimum energy requirement is satisfied. Nevertheless, it has to be noticed that the design depends on the minimum temperature approach initially selected. Actually, an optimum value of the ΔT_{min} exists resulting from a trade-off between amount of energy recovery and capital cost. As earlier discussed, when the values of ΔT_{min} changes, the relative position of the composite curves also changes. In particular, as the ΔT_{min} between the curves is increased, the capital cost decreases, resulting from lower heat transfer area required. On the other hand, the energy cost increases as ΔT_{min} increases.

In the next section the heat exchange network definition for the vacuum and sweep scenario are presented. A Pinch Analysis Tool [25] has been used; the tool takes as input the stream process data and applies the basic concepts of pinch analysis, as described above, to design the heat exchanger network. The stream matching is done by user, on the basis of the calculated possible match.

2.5.1 Vacuum scenario

The process flow diagram for the whole process is shown in Figure 28. The heat exchanger network has been defined for the process without the CO_2 capture unit. The heat required to sustain the reformer has been not considered in the integration, because we assumed to supply it by the furnace, designed a part. For the vacuum scenario there are nine representative streams, four to be heated up and five streams to be cooled. Table 26 reports the process stream data.

Figure 28 Process flow diagram for vacuum scenario.

From the first law, the net amount of heat that must be removed or supplied to the process can be calculated. If no restrictions on temperature-driving forces are present, 62.5 kW has to be discharge to a cold utility. A minimum temperature approach value of 30 °C has been selected and the relative hot and cold cumulative curves have been evaluated. The ΔT_{min} has selected on the basis of typical value for chemical process.

Figure 29 and Figure 30 show the combined composite curves and the grand composite curve, respectively. The pinch temperature can be thus calculated; actually the problem obtained has no pinch point. In fact, the composite curves are in alignment at the hot end, indicating that there is no longer a demand for hot utility. The only utility to be used is a cold utility, as cooling water. The pinch temperature corresponds to 830 °C, and there are not cold or hot streams above the pinch.

Table 26 Process stream data for vacuum scenario

Stream name	Phase	Source temperature T_{IN}	Target temperature T_{OUT}	Heat Load Q	Thermal Capacity $F_i c_{P_i}$
-	°C			kW	kW/°C
W1	Liquid	25	164	14.2	1.02E-01
W1$_{P.C}$	two-phase	164	165	50.2	5.02E+01
NG$_{COMPR}$	gas	144	400	6.2	2.42E-02
REF$_{FEED}$	gas	240	800	46.6	8.31E-02
REF$_{OUT}$	gas	800	360	40.22	9.14E-02
R1	gas	453	141	15.59	4.99E-02
R1$_{P.C}$	two-phase	141	45	31.55	3.30E-01
P1	gas	450	30	16.04	3.82E-02
EXH	gas	830	120	76.40	1.08E-01

The match between the streams has been performed following the rules described above.

The evaporation of water stream for the reformer steam has been accomplished in two stages, since the heat load required for the overall steam production was not available at the required temperature level, from one single hot stream. Thus, we assumed to vaporized most of the water (4/5 of the whole load) in a first evaporator sending the remaining liquid water (1/5) into a second heat exchanger where the residual needed steam amount is generated. For the first evaporator, the exhaust gas has been used as hot stream, while for the second exchanger the stream match has been performed with the hot retentate stream. It has to be noticed that we assumed to feed a water stream previously treated (e.g. by a revers osmosis unit) in order to remove the water impurity.
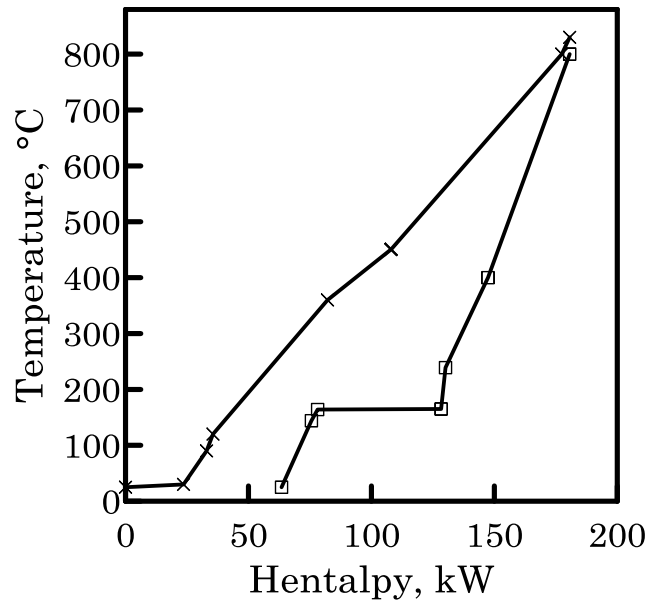
Figure 29 Combined composite curve for vacuum scenario.
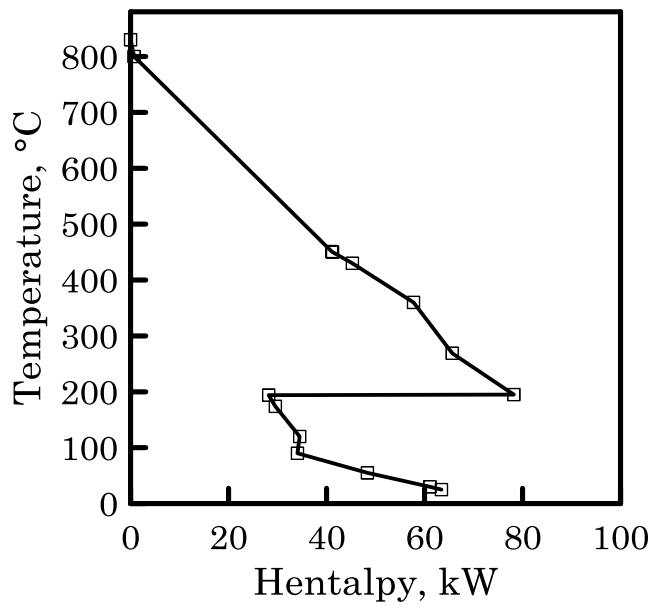
Figure 30 Grand composite curve for vacuum scenario.

The results of the stream match performed are summarized in Table 33 while Table 34 reports the heat load for each hot stream to be cooled by cold utility (see Appendix). The total cooling utility requirement is equal to 62.5 kW. An external cold utility, as cooling water, is required to remove the remaining heat excess of the retentate stream. Regarding the heat excess of exhaust gas streams, it could be also used to pre-heater the air stream fed to the burner. The final layout including the heat exchanger network is shown in Figure 31.

Figure 31 Process flow diagram for vacuum configuration including heat exchanger network.

2.5.2 Sweep scenario

The heat exchange network definition for the sweep scenario has been accomplished in analogy with that one above described for the vacuum scenario. The process flow diagram for sweep scenario process is shown in Figure 32. The representative process stream data are reported in Table 27; the stream number for the sweep scenario is higher then the vacuum one, since the sweep gas stream has to be also taken into account. In particular, there are seven to be heated up and six stream to be cooled.

Figure 32 Process flow diagram for sweep scenario.

The net amount of heat that must be removed form the process, assuming no restrictions on temperature-driving forces, is 60.7 kW. The same minimum temperature approach value of vacuum scenario has been selected.

The relative hot and cold cumulative curves are shown in Figure 33 and Figure 34.

Table 27 Process stream data for sweep scenario

Stream name	Phase	Source temperature T_{IN}	Target temperature T_{OUT}	Heat Load Q	Thermal Capacity $F_i c_{P_i}$
	-	°C		kW	kW/°C
W1	liquid	25	164	14.2	1.02E-01
W1$_{P.C}$	two-phase	164	165	50.2	5.02E+01
W2	liquid	25	106	1.89	2.34E-02
W2$_{P.C}$	two-phase	106	107	12.53	1.25E+01
W2$_{Sur}$	gas	107	360	2.83	1.12E-02
NG$_{COMPR}$	gas	144	400	6.2	2.42E-02
REF$_{FEED}$	gas	240	800	46.6	8.31E-02
REF$_{OUT}$	gas	800	360	40.22	9.14E-02
R1	gas	478	141	17.03	5.05E-02
R1$_{P.C}$	two-phase	141	45	31.60	3.31E-01
P1	gas	404	67	18.76	5.57E-02
P1$_{P.C}$	two-phase	67	35	12.89	4.05E-01
EXH	gas	830	120	74.61	1.05E-01
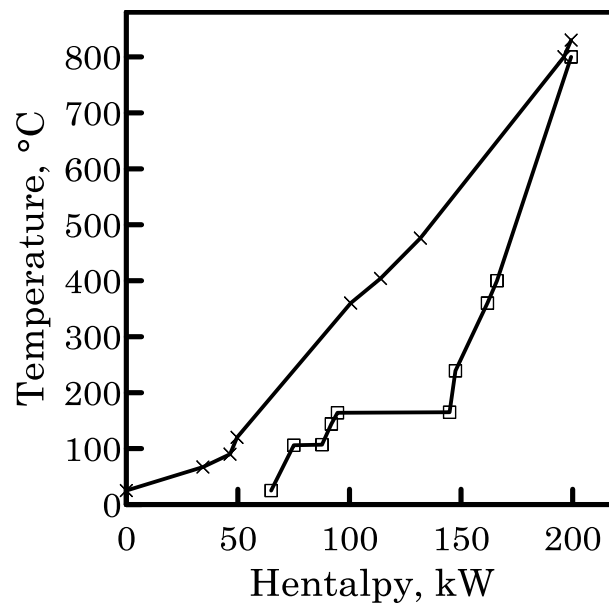
Figure 33 Combined composite curve for sweep scenario.
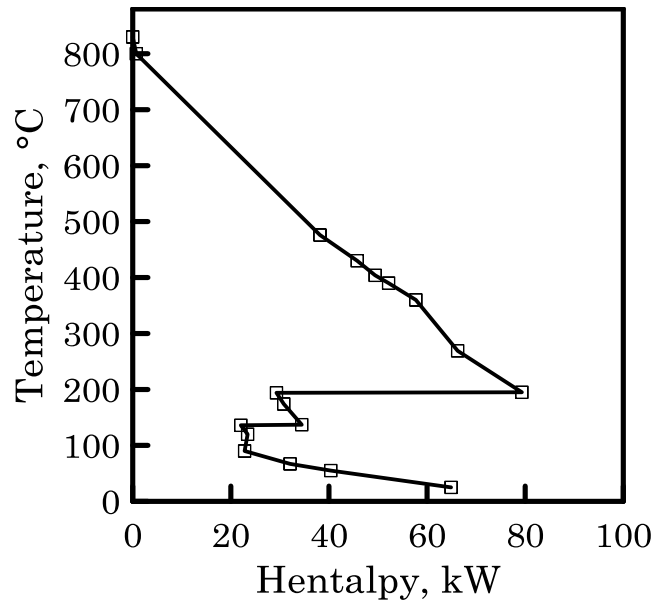
Figure 34 Grand composite curve for sweep scenario.

The pinch temperature can be thus calculated. As expected, also for the sweep scenario a problem without pinch is obtained. No cold or hot streams above 830 °C, pinch temperature, are present.

The match between the streams has been performed following the rules described above. For the sweep scenario, with respect to the vacuum one, an additional steam stream is required. In fact, we assumed to use steam as sweep gas. This steam can be then recovered, by condensation, and recycled to the sweep steam generator.

The results of the stream match performed and the cooling utility requirements are summarized in Table 35 and Table 36 (see Appendix).

An external cold utility, as cooling water, is required to remove the remaining heat excess of retentate and permeate stream, and to condense the water. Figure 35 shows the final layout including the heat exchanger network.

Figure 35 Process flow diagram for sweep configuration including heat exchanger network.

2.6 Comparison of scenario performance

A comparison between sweep and vacuum scenario has been performed, focusing on some factors as raw material exploitation, electricity consumption, heat requirement.

Table 28 and Table 29 report a summary of the production features for the vacuum and sweep scenario.

The quantity of NG treated per year is the same for both scenario. It actually depends on the reforming unit that is not effected by the MR itself.

In terms of annual production, the hydrogen production for the vacuum scenario is slightly higher than the sweep one. The vacuum scenario shows, as a consequence, a better exploitation of the raw material per H_2 produced. This is only due to a small gain in H_2 recovery achieved in the MR operating with vacuum pump with respect to the sweep configuration (see Table 19). The other terms, such as the natural gas fed to the burner to sustain the reformer (Heat – Natural Gas), the water process and the waste water, are quite similar for both scenarios. In the vacuum scenario a little more natural gas (an additional 10% with respect to the value of sweep scenario) has to be

fed to the burner. As previously described, part of the fuel required to sustain thermally the reformer is provided recycling to the burner the retentate stream. The burner is, therefore, fed with natural gas and the retentate stream coming from the WGS-MR. Since the retentate stream of vacuum scenario has a lower heat value, being less rich in hydrogen, more natural gas is required.

Regarding the CO_2 emission, the value reported is related to the overall CO_2 produced by NG reforming and NG combustion in the burner. The option with CO_2 removal by membrane gas separation technology has been not included.

A significant difference between the scenarios regards the electricity consumption. The electricity from grid value takes into account the main electricity consumption terms. These are related to the natural gas compression, the H_2 compression and, for the vacuum scenario, to the vacuum pump operation. A summary of the specific electricity consumption values and their percentage with respect to the total consumption are reported in Table 30 and Table 31 for both scenarios. As expected, the electricity consumption for the vacuum scenario is larger due to the energy required for the vacuum pump. In particular, a two times higher electricity consumption is obtained and the specific electricity for the vacuum pump accounts for 48% of the overall electricity from grid demand. It has to be noticed that a low efficiency (ca. 40%) has been assumed for the vacuum pump; this actually affects the estimated energy consumption value. The assumed efficiency value was based on data from suppliers and on heuristic criteria. Considering a vacuum pump efficiency value of 70%, the electricity demand for the vacuum pump decreases from 9.54E-05 up to 5.45E-05 MWh/Nm^3 H_2, reducing the overall electricity from grid of 20%.

On the other hand, for the sweep configuration, only a steam stream, at a low pressure, has to be provided. This steam can be produced by means of the hot streams available in the plant, as shown in the heat integration (see Heat exchange network definition: Sweep scenario). Finally a comparison with the reference technology has been done.

Table 28 Production features for vacuum scenario

H_2 production	Unit	Value
Processing/treatment capacity (quantity of NG treated per year)	tonnes/year	269
Annual H_2 production	Nm^3/year	8.42E+05
Raw materials/feedstock		
NG (81% CH_4, 14% N_2)	kg/Nm^3 H_2	0.32
Others (steam)	kg/Nm^3 H_2	0.83
Ancillary inputs		
Electricity from the grid	MWh/Nm^3 H_2	2.09E-04
Heat - Natural Gas	GJ/Nm^3 H_2	2.25E-03
Water (process)	m^3/Nm^3 H_2	8.29E-04
Wastes and residues		
Liquid effluents (waste water)	m^3/Nm^3 H_2	3.94E-04
CO_2 Direct process emissions	kg/Nm^3 H_2	0.79

Table 29 Production features for sweep scenario

H_2 production	Unit	Value
Processing/treatment capacity (quantity of NG treated per year)	tonnes/year	269
Annual H_2 production	Nm^3/year	8.34E+05
Raw materials/feedstock		
NG (81% CH_4, 14% N_2)	kg/Nm^3 H_2	0.33
Others (steam)	kg/Nm^3 H_2	0.84
Ancillary inputs		
Electricity from the grid	MWh/Nm^3 H_2	1.14E-04
Heat - Natural Gas	GJ/Nm^3 H_2	2.04E-03
Water (process)	m^3/Nm^3 H_2	8.37E-04
Wastes and residues		
Liquid effluents (waste water)	m^3/Nm^3 H_2	3.98E-04
CO_2 Direct process emissions	kg/Nm^3 H_2	0.78

Table 30 Specific electricity consumption values for vacuum scenario

	Electricity from grid, MWh/Nm^3 H$_2$	Percentage of total electricity consumption, %
NG compression	3.33E-05	16
H$_2$ compression	8.00E-05	38
Vacuum pump operation	9.54E-05	48
Total	2.09E-04	

Table 31 Specific electricity consumption values for sweep scenario

	Electricity from grid, MWh/Nm^3 H$_2$	Percentage of total electricity consumption, %
NG compression	3.36E-05	30
H$_2$ compression	8.00E-05	70
Total	1.14E-04	

For the reference technology a modern hydrogen plant, as defined in the introduction, has been considered: steam methane reformer followed by high temperature WGS reactor and pressure swing adsorption (PSA).

Referring to the steam methane reformer there are no difference in term of performance with respect to the one considered in the WGS-MR integrated system. For the high temperature WGS reactor a traditional adiabatic reactor, operating at the same pressure of reformer in the temperature range 320-400°C, has been taken into account. A CO conversion equal to the 95% of the equilibrium conversion value has been considered. An H$_2$ recovery and H$_2$ purity of 80% and 99.99%, respectively, have been assumed for the PSA. The summary of the production features for the reference technology is reported in Table 32. In this case a lower raw material exploitation is obtained since a higher feedstock amount is required (0.39 kg NG/Nm^3 H$_2$) to get the same hydrogen production volume of the membrane reactor. On the other hand, since the H$_2$ recovered from the PSA unit does not require a compression stage, less electricity from grid is needed for the conventional technology.

Moreover, by recycling the off gas as valuable process fuel in the reformer furnace an additional fuel NG stream has not to be fed. The off gas stream coming out from the PSA unit, being richer in unrecovered H_2 and unconverted CO, fulfils the overall process fuel requirement to the burner. It has to be highlighted, however, that this is not an advantage. Actually, from an economic point of view, it is better to recover more hydrogen, which has a higher economic value, and use an additional NG stream as fuel.

Table 32 Production features for reference technology

H_2 production	Unit	Value
Processing/treatment capacity (quantity of NG treated per year)	tonnes/year	269
Annual H_2 production	Nm^3/year	6.85E+05
Raw materials/feedstock		
NG (81% CH_4, 14% N_2)	kg/Nm^3 H_2	0.39
Others (steam)	kg/Nm^3 H_2	1.02
Ancillary inputs		
Electricity from the grid	MWh/Nm^3 H_2	4.09E-05
Heat - Natural Gas	GJ/Nm^3 H_2	0
Water (process)	m^3/Nm^3 H_2	1.02E-03
Wastes and residues		
Liquid effluents (waste water)	m^3/Nm^3 H_2	5.31E-04
CO_2 Direct process emissions	kg/Nm^3 H_2	0.76

2.7 Conclusion

A new process, integrated with WGS-MR for the production of 100 Nm^3/h of H_2 by natural gas steam reforming, has been designed for two MR operating scenarios (vacuum and sweep scenarios, as described in Chapter 1). By integrating the WGS membrane reactor, the traditional HT shift reactor and pressure swing adsorption have been substituted with a single unit, the membrane reactor indeed. More than 90% of produced H_2 can be directly recovered in the permeate stream thus the hydrogen separation unit is no more required. Moreover, the MR integration implies a re-design of the process downstream the WGS reactor. The two distinct permeate and retentate streams, coming out from the MR, have to be processes in a different way. The permeate post processing depends on the scenario: a pure H_2 stream is recovered in the vacuum scenario whereas, for the sweep scenario, the steam, used as sweep gas, has to be removed by water condensation and phase separation to get the purity target. The last step, for both scenarios, is the H_2 compression up to 6 bar, to match the same pressure condition of the reference technology.

The retentate can be used, instead, as valuable process fuel in the reformer furnace or it can be sent to a CO_2 membrane separation unit to recover a concentrated CO_2 stream. Applying a commercial membrane by means of a one stage unit, the 40% of CO_2 can be recovered with a purity of 70%. The application of enhanced H_2 selectivity membrane, as will be shown in chapter 3, allows higher CO_2 purity and recovery.

The heat exchange network definition for the MR integrated process has been also performed. No external hot utility is required, for both scenario. Furthermore, for the sweep scenario, the required steam can be produced by heat exchange with hot streams of plant that have to be cooled.

Finally, the comparison between both scenarios showed a slight difference in term of H_2 productivity and raw material exploitation but significant difference in the electricity consumption. In particular, due to the energy required by vacuum pump, the electricity from grid for the vacuum scenario

is almost two times higher then the one for sweep scenario. Consequentially a higher H_2 production cost is expected.

The performed analysis clearly shows, for both scenarios, the technical feasibility of WGS-MR integration into a small scale H_2 generator. However, to define the best solution, an H_2 production cost estimation, for both sweep and vacuum scenario, is required. In fact, the final hydrogen production cost is one of the key factor to choose between the possible scenarios.

With respect to the conventional system, the one integrated with WGS-MR results in a more "intensified" process since higher H_2 productivity and enhanced exploitation of raw materials are attained.

In addition, as highlighted above, the MR technology allows the reduction of the separation load and stage number after the reaction. In particular, the possibility to remove the PSA unit is a significant advantage, implying a volume reduction of separation unit, leading to a more compact system. Furthermore, a gain in term of production cost is expected. On the other hand, the cost related to the membrane reactor (membrane tubes and module) and the cost related to the hydrogen compression have to be considered, actually reducing the gain coming from the removal of PSA unit.

 An economic evaluation is therefore needed to compare both technologies and find in which conditions the MR integrated system is more cost-effective than the traditional one.

Together with an economic assessment, pursuing the logic of process intensification, other factors, such as productivity/foot print, waste production, energy consumption, equipment size, process flexibility, should be taken into account to evaluate the validity of a technology.

In this logic, WGS-MR integration in H_2 generator unit appears to be more competitive, with better exploitation of materials and higher efficiency, leading to a smaller plant (less and smaller equipment), delivering a high purity hydrogen stream and a high-pressure CO_2-rich stream. The latter can be more easily recovered, for instance, as proposed by membrane gas separation technology application.

Appendix

Table 33 Heat exchanger network for vacuum scenario

Heat Exchanger. E1	Heat Load, Q	ΔT_{LMTD}		
	6.2 kW	88.7 °C		
			Cold Stream	Hot Stream
	Stream name		NG_{COMPR}	P1
	Inlet Temperature, °C		144	450
	Outlet Temperature, °C		400	288
	Thermal Capacity, kW/°C		2.42E-02	3.82E-02

Heat Exchanger. E2	Heat Load, Q	ΔT_{LMTD}		
	46.6 kW	76.6 °C		
			Cold Stream	Hot Stream
	Stream name		REF_{FEED}	EXH
	Inlet Temperature, °C		240	830
	Outlet Temperature, °C		800	398
	Thermal Capacity, kW/°C		8.31E-02	1.08E-01

Heat Exchanger. E3	Heat Load, Q	ΔT_{LMTD}		
	40.22 kW	373.5 °C		
			Cold Stream	Hot Stream
	Stream name		$W1_{P.C.}/1$	REF_{OUT}
	Inlet Temperature, °C		164	800
	Outlet Temperature, °C		165	360
	Thermal Capacity, kW/°C		40.22	9.14E-02

Heat Exchanger. E4	Heat Load, Q	ΔT_{LMTD}		
	9.98 kW	163 °C		
			Cold Stream	Hot Stream
	Stream name		$W1_{P.C.}/2$	R1
	Inlet Temperature, °C		164	453
	Outlet Temperature, °C		165	252
	Thermal Capacity, kW/°C		9.98	4.99E-02

Heat Exchanger. E5	Heat Load, Q 14.19 kW		ΔT_{LMTD} 235 °C	
			Cold Stream	Hot Stream
	Stream name		$W1_{P.C.}$	EXH
	Inlet Temperature, °C		25	398
	Outlet Temperature, °C		164	266
	Thermal Capacity, kW/°C		1.02E-01	1.08E-01

Table 34 Cooling utility requirement for vacuum scenario

Stream name	Inlet Temperature, °C	Outlet Temperature, °C	Thermal Capacity kW/°C	Heat Load, kW
EXH	266	120	1.08E-01	15.77
P1	288	30	3.82E-02	9.85
R1/ R1 $_{P.C}$	252	45	-	36.88
			Total cooling utility required	62.5

Table 35 Heat exchanger network for sweep scenario

Heat Exchanger. E1	Heat Load, Q 6.2 kW	ΔT_{LMTD} 130.5 °C		
			Cold Stream	Hot Stream
	Stream name		NG_{COMPR}	R1
	Inlet Temperature, °C		144	478
	Outlet Temperature, °C		400	355
	Thermal Capacity, kW/°C		0.02	5.05-02

Heat Exchanger. E2	Heat Load, Q 46.6 kW	ΔT_{LMTD} 76.5 °C		
			Cold Stream	Hot Stream
	Stream name		REF_{FEED}	EXH
	Inlet Temperature, °C		240	830
	Outlet Temperature, °C		800	386
	Thermal Capacity, kW/°C		8.31E-02	1.05E-01

Heat Exchanger. E3	Heat Load, Q 40.2 kW	ΔT_{LMTD} 373.4 °C		
			Cold Stream	Hot Stream
	Stream name		$W1_{P.C.}/1$	REF_{OUT}
	Inlet Temperature, °C		164	800
	Outlet Temperature, °C		165	360
	Thermal Capacity, kW/°C		40.22	9.14

Heat Exchanger. E4	Heat Load, Q 2.8 kW	ΔT_{LMTD} 117.4 °C		
			Cold Stream	Hot Stream
	Stream name		$W2_{Sur}$	P1
	Inlet Temperature, °C		107	404
	Outlet Temperature, °C		360	353
	Thermal Capacity, kW/°C		1.12E-2	5.57E-2

Heat Exchanger. E5	Heat Load, Q 12.5 kW	ΔT_{LMTD} 128.8 °C		
			Cold Stream	Hot Stream
	Stream name		$W2_{P.C.}$	EXH
	Inlet Temperature, °C		106	290.5
	Outlet Temperature, °C		107	171
	Thermal Capacity, kW/°C		12.53	1.05E-1

Heat Exchanger. E6	Heat Load, Q 1.9 kW	ΔT_{LMTD} 265.0 °C		
			Cold Stream	Hot Stream
	Stream name		W2	R1
	Inlet Temperature, °C		25	355
	Outlet Temperature, °C		106	317
	Thermal Capacity, kW/°C		2.34E-2	5.05E-2

Heat Exchanger. E7	Heat Load, Q 14.2 kW	ΔT_{LMTD} 122.2 °C		
			Cold Stream	Hot Stream
	Stream name		W1	P1
	Inlet Temperature, °C		25	353
	Outlet Temperature, °C		164	98
	Thermal Capacity, kW/°C		1.02E-1	5.57E-2

Heat Exchanger. E8	Heat Load, Q 10.0 kW	ΔT_{LMTD} 180.5 °C		
			Cold Stream	Hot Stream
	Stream name		$W1_{P.C.}/2$	EXH
	Inlet Temperature, °C		164	386
	Outlet Temperature, °C		165	290.5
	Thermal Capacity, kW/°C		9.98	1.05E-1

Table 36 Cooling utility requirement for sweep scenario

Stream name	Inlet Temperature, °C	Outlet Temperature, °C	Thermal Capacity kW/°C	Heat Load, kW
P1	98	35	-	14.35
R1/ R1 $_{P.C}$	317	45	-	41.0
EXH	171	120	1.05E-1	5.35
			Total cooling utility required	60.7

Table 37 Composition of principal streams for the vacuum scenario (1/2)

	NG	NG$_{IN}$	NG$_{brn}$	Air	Water	Steam	REF$_{FEED}$	REF$_{IN}$	REF$_{OUT}$
Molar fraction,-									
CO	0.000	0.000	0.000	0.000	0.000	0.000	0.000	0.000	0.092
H$_2$O	0.000	0.000	0.000	0.000	1.000	1.000	0.729	0.729	0.347
CO$_2$	0.009	0.009	0.009	0.000	0.000	0.000	0.002	0.002	0.047
H$_2$	0.000	0.000	0.000	0.000	0.000	0.000	0.000	0.000	0.448
N$_2$	0.142	0.142	0.142	0.790	0.000	0.000	0.039	0.039	0.028
CH$_4$	0.813	0.813	0.813	0.000	0.000	0.000	0.220	0.220	0.038
C$_2$H$_6$	0.029	0.029	0.029	0.000	0.000	0.000	0.008	0.008	0.000
C$_3$H$_8$	0.004	0.004	0.004	0.000	0.000	0.000	0.001	0.001	0.000
C$_4$H$_{10}$	0.002	0.002	0.002	0.000	0.000	0.000	0.001	0.001	0.000
C$_5$H$_{12}$	0.001	0.001	0.001	0.000	0.000	0.000	0.000	0.000	0.000
O$_2$	0.000	0.000	0.000	0.210	0.000	0.000	0.000	0.000	0.000
Total molar flow, kmol/h	1.80	1.80	0.32	8.49	4.85	4.85	6.65	6.65	9.19
Total flow, kg/h	33.6	33.6	5.88	245	87.3	87.3	121	121	121
Temperature, °C	25	400	25	25	25	165	240	800	800
Pressure, bar	1.20	7.00	1.20	1.20	1.00	7.00	7.00	7.00	7.00
Vapour fraction, -	1.0	1.0	1.0	1.0	0.0	1.0	1.0	1.0	1.0

Table 37 Composition of principal streams for the vacuum scenario (2/2)

	MR_{FEED}	P1	H_2COMP_{IN}	H_2OUT	R1	WW1	$OFFGAS_{BRN}$	EXH
Molar fraction,-								
CO	0.092	0.000	0.000	0.000	0.005	0.000	0.010	0.000
H_2O	0.347	0.000	0.000	0.000	0.520	1.000	0.036	0.146
CO_2	0.047	0.000	0.000	0.000	0.282	0.000	0.566	0.176
H_2	0.448	1.000	1.000	1.000	0.059	0.000	0.119	0.000
N_2	0.028	0.000	0.000	0.000	0.057	0.000	0.115	0.643
CH_4	0.038	0.000	0.000	0.000	0.078	0.000	0.156	0.000
C_2H_6	0.000	0.000	0.000	0.000	0.000	0.000	0.000	0.000
C_3H_8	0.000	0.000	0.000	0.000	0.000	0.000	0.000	0.000
C_4H_{10}	0.000	0.000	0.000	0.000	0.000	0.000	0.000	0.000
C_5H_{12}	0.000	0.000	0.000	0.000	0.000	0.000	0.000	0.000
O_2	0.000	0.000	0.000	0.000	0.000	0.000	0.000	0.036
Total molar flow, kmol/h	9.19	4.70	4.70	4.70	4.48	2.25	2.23	10.90
Total flow, kg/h	121	9.48	9.48	9.48	111.5	40.50	70.89	321.8
Temperature, °C	360	450	30	117	453	35	35	830
Pressure, bar	7.00	0.35	1.20	6.00	7.00	1.20	1.20	1.20
Vapour fraction, -	1.0	1.0	1.0	1.0	1.0	0.0	1.0	1.0

Table 38 Composition of principal streams for the sweep scenario (1/2)

	NG	NG_{IN}	NG_{brn}	Air	W1	Steam	$W2_{MakeUp}$	REF_{FEED}	REF_{IN}	REF_{OUT}
Molar fraction,-										
CO	0.000	0.000	0.000	0.000	0.000	0.000	0.000	0.000	0.000	0.092
H_2O	0.000	0.000	0.000	0.000	1.000	1.000	1.000	0.729	0.729	0.347
CO_2	0.009	0.009	0.009	0.000	0.000	0.000	0.000	0.002	0.002	0.047
H_2	0.000	0.000	0.000	0.000	0.000	0.000	0.000	0.000	0.000	0.448
N_2	0.142	0.142	0.142	0.790	0.000	0.000	0.000	0.039	0.039	0.028
AIR	0.000	0.000	0.000	0.000	0.000	0.000	0.000	0.000	0.000	0.000
CH_4	0.813	0.813	0.813	0.000	0.000	0.000	0.000	0.220	0.220	0.038
C_2H_6	0.029	0.029	0.029	0.000	0.000	0.000	0.000	0.008	0.008	0.000
C_3H_8	0.004	0.004	0.004	0.000	0.000	0.000	0.000	0.001	0.001	0.000
C_4H_{10}	0.002	0.002	0.002	0.000	0.000	0.000	0.000	0.001	0.001	0.000
C_5H_{12}	0.001	0.001	0.001	0.000	0.000	0.000	0.000	0.000	0.000	0.000
O_2	0.000	0.000	0.000	0.210	0.000	0.000	0.000	0.000	0.000	0.000
Total molar flow, kmol/h	1.80	1.80	0.29	8.22	4.85	4.85	0.175	6.65	6.65	9.19
Total flow, kg/h	33.6	33.6	5.41	237	87.3	87.3	3.15	121	121	121
Temperature, °C	25	144	25	25	25	165	25	240	800	800
Pressure, bar	1.20	7.00	1.20	1.20	1.00	7.00	1.2	7.00	7.00	7.00
Vapour fraction, -	1.0	1.0	1.0	1.0	0.0	1.0	0.0	1.0	1.0	1.0

Table 38 Composition of principal streams for the sweep scenario (2/2)

	MR_{FEED}	P1	H_2COMP_{IN}	H_2OUT	R1	SWP	WW1	$OFFGAS_{BRN}$	EXH
Molar fraction,-									
CO	0.092	0.000	0.000	0.000	0.005	0.000	0.000	0.010	0.000
H_2O	0.347	0.193	0.000	0.000	0.516	1.000	1.000	0.037	0.150
CO_2	0.047	0.000	0.000	0.000	0.278	0.000	0.000	0.554	0.178
H_2	0.448	0.807	1.000	1.000	0.067	0.000	0.000	0.134	0.000
N_2	0.028	0.000	0.000	0.000	0.057	0.000	0.000	0.112	0.639
AIR	0.000	0.000	0.000	0.000	0.000	0.000	0.000	0.000	0.000
CH_4	0.038	0.000	0.000	0.000	0.077	0.000	0.000	0.153	0.000
C_2H_6	0.000	0.000	0.000	0.000	0.000	0.000	0.000	0.000	0.000
C_3H_8	0.000	0.000	0.000	0.000	0.000	0.000	0.000	0.000	0.000
C_4H_{10}	0.000	0.000	0.000	0.000	0.000	0.000	0.000	0.000	0.000
C_5H_{12}	0.000	0.000	0.000	0.000	0.000	0.000	0.000	0.000	0.000
O_2	0.000	0.000	0.000	0.000	0.000	0.000	0.000	0.000	0.033
Total molar flow, kmol/h	9.19	5.77	4.66	4.66	4.53	1.12	2.25	2.27	10.63
Total flow, kg/h	121	29.5	9.39	9.39	111.5	20.1	40.5	80.0	313.5
Temperature, °C	360	404	30	117	478	360	35	35	830
Pressure, bar	7.00	1.20	1.20	6.00	7.00	1.20	1.20	1.20	1.20
Vapour fraction, -	1.0	1.0	1.0	1.0	1.0	1.0	0.0	1.0	1.0

References

1. Holladay J.D., Hu J.,. King D.L, Wang Y., Catalysis Today, 2009, 139, 244-260.

2. Lui K., Song C., Subramani V., Hydrogen and syngas production and purification technologies, Wiley, 2010.

3. "On-site Hydrogen Generators from Hydrocarbons", Roads2HyCom, 11 July 2009 (link).

4. Simbeck DR, Chang E. Hydrogen supply: cost estimate for hydrogen pathways-scoping analysis. Report no. NREL/SR-540- 32525. Mountain View, CA: NREL; 2002.

5. Ogden JM. Hydrogen energy systems studies. Report no. NREL/CP-570-26938. Golden, CO: NREL; 1999.

6. Stankiewicz A., Moulijn, J. A., Ind. Eng. Chem., Res. 2002, 41(8), 1920-1924.

7. Drioli E., Brunetti A., Di Profio G., Barbieri G., Green Chem., 2012, 14, 1561-1572.

8. Criscuoli A., Basile A., Drioli E., Loiacono O, J. Membr. Sci., 2001, 181, 21-27.

9. Roses L., Manzolini G., Campanari S., De Wit E. and Walter M., Energy fuels, 2013, 27 (8), 4423-4431.

10. Catalano J, Guazzone F., P. Mardilovich I., Kazantzis N. K and Yi Hua Ma, Ind. Eng. Chem. Res., 2013, 52, 1042-1055.

11. Brunetti A., Drioli E., Barbieri G., RSC Adv., 2012, 2 (1), 226-233.

12. Augustine A. S, Ma Yi Hua, Kazantzis N. K., Int. J. Hydrogen energy, 2011, 36, 5350-5360.

13. Pinacci, P.; Broglia, M.; Valli, C.; Capannelli, G.; Comite, A., Catal. Today 2010, 156, 165–172.

14. PHYRENEES Association – Ecole des Mines d'Albi-Carmaux, "Small-scale reforming systems for hydrogen refuelling stations" Technology Watch Report, 2010

    (http://www.isq.pt/EN/HttpHandlers/FileHandler.ashx?id=108&menuid=843).

15. Hansen A.M., "Small-scale Reformers for Stationary Hydrogen Production with Minimum CO_2 emissions", IEA-HIA Task 16 Hydrogen from Carbon Containing Materials – Subtask C report, July 2005 (ieahia.org/pdfs/rapperswil/Task16CFinal.pdf).

16. "Hydrogen production roadmap – Technology pathways to the future", FreedomCAR & Fuel Partnership Hydrogen Production Technical Team, January 2009 (link)

17. Gas in focus, gasinfocus.com/en/category/environment/

18. Ullman's Encyclopedia of Industrial Chemistry, 5th Completely Revised Edition. Edited by Barbara Elvers, Stephen Hawkins, and William Russey. VCH: New York, 1995. ISBN 3-527-20126-2.

19. Branan CR. Rules of thumb for chemical engineers. Oxford: Butterworth-Heineman, 2002.

20. Appl M., Modern production technologies, ammonia, methanol, hydrogen, carbon monoxide. CRU Publishing Ltd.; 1997.

21. Sjardin M., Damen K.J., Faaij A.P.C., Energy 31, 2006, 2523-2555.

22. Douglas M.J., "Conceptual design of chemical processes", Mc.Graw-Hill, New York, 1988.

23. Hohmann E.C., "Optimum Networks for Heat Exchanger", Ph.D. Thesis, University of Southern California, 1971.

24. Linnhoff B., "The Pinch Design Method for Heat Exchanger Networks", Chemical Engineering Science, vol 38, No. 5, 745 Great Britain.

25. Umbach J.S, "Online Pinch Analysis Tool", 2010 http://www.uic-che.org/pich/

CO₂ recovery by membrane gas separation: retentate stream post-processing case study

Introduction

There is clear evidence that the concentration of carbon dioxide (CO_2) in the atmosphere has been increasing significantly and the power and industry sector account for about 60% of the total emission this increment [1, 2]. According to the IEA findings, to achieve a global reduction in CO_2 emissions various efforts are require [3]. Industry has to reduce its direct emission, by means of new technologies such as carbon capture and storage (CCS), but also energy efficient measures, like implementation of Best Available Technologies (BAT, http://eippcb.jrc.es/reference/), has to be applied. Thus, the combination of using more energy efficient processes together with CO_2 capture technologies will decrease the whole emissions.

Although CO_2 capture is a global issue, there is not a simple/unique solution that can be applied in a global scale. In particular, it has to be evaluated how current and/or novel technology, such as membrane separation technology, can be adapted to the existing process.

Currently, the main strategies for the carbon dioxide capture which aim at maximizing the concentration of CO_2 in the gas stream are [4, 19, 27144] i) post-combustion capture; ii) pre-combustion capture; iii) oxyfuel combustion; and iv) electrochemical separation.

Post-combustion capture is the simplest to be implemented and can be considered as a retrofit strategy since the separation process can be easily adapted to the existing plant. However, in this case, the CO_2 has to be separated from a flue gas stream that is at atmospheric pressure and with a

low CO_2 concentration, making the separation more difficult and energy demanding.

Oxy-combustion is an alternative when the CO_2 is produced from combustion process. In this case, performing the combustion with nearly pure oxygen, a stream consisting mainly of CO_2 and water is generated, ready for sequestration after water removal.

In the pre-combustion capture, a CO_2 has to be separated from the H_2 and the separation is different since it could happen at very high pressures (up to 80 bar of pressure difference) and high temperatures (300–700 °C) [5].

The conventional separation technology by absorption with amines (e.g., monoethylamine, MEA) has been widely used due to the high selectivity of amines towards CO_2 and it is the most developed technology nowadays [6, 7, 8]. However, this technology presents operating limitations such as the interdependence of the two fluid phases to be contacted, the toxicity of amines and their susceptibility to degradation (specifically in presence of oxygen). Furthermore, this technology is costly and energy intensive, requiring significant amount of energy in the regeneration step [9]. A relatively novel technology is based on cryogenic removal of CO_2 [10, 11]. This operation has been used in the last years for the removal of CO_2 from natural gas and its introduction for flue gas treatment is relatively new. No chemical absorbents are required, resulting in an advantages with respect to absorption; however operative constrains as water trace removal and low operating temperature require several costly steps.

For the pre-combustion capture approach, due to the high concentration of CO_2 in the high pressure gas, existing capture processes, such as Rectisol and Selexol, can capture CO_2 effectively [12]. These processes use physical solvents and the high pressure of the gas stream but they are energy intensive due to the heat transfer requirements, since it is necessary to cool the syngas before carbon capture. Also pressure swing adsorption is applied in pre-combustion capture. In this case porous solids with high adsorbing properties, such as zeolite, metal oxide or active carbon [12, 13, 14] are used to remove the CO_2 and obtain a purified H_2.

Membrane-based technology is today considered as a promising separation method for both pre-combustion and post-combustion capture. It represents a valid alternative to the conventional technology, overcoming the disadvantages of gas absorption, being less energy intensive and easy to operate [2]. In addition, it offers the opportunity of replacing energy-inefficient separation processes and the modular design is also very attractive from the point of view of process intensification [15, 16].

As above described, the conventional technology for CO_2 capture, can be usually applied for great flue gas volume. In case of low volume of carbon dioxide emission, from source like small scale H_2 generator, no CO_2 capture is performed. The CO_2 capture on this scale is generally considered to be costly, adding also complexity to the process design. However, it is necessary to look at the development of technologies for CO_2 handling in small-scale reforming as a long term necessity. In fact, the future increasing constrains on CO_2 emission will make the CO_2 capture a critical issue also for on-site H_2 generator [17, 18]. The application, in this filed, of gas separation membrane technology can be regarded as a sustainable solution, since membrane systems offer important design quality as high operating flexibility, easy of expansion (modular design), low control requirement [19].

On the basis of the above considerations, the possibility to recover the CO_2 in the WGS-MR integrated process for hydrogen production, as described in chapter 2, has been investigated in this chapter. In particular, the potentialities of membrane gas separation (GS) application have been explored, giving general guidelines on some design parameters to take into account. Two configuration schemes, single e multiple stages, have been analysed, considering two types of membranes with different separation property.

3.1. Membrane gas separation technology for CO_2 capture

Membrane technology holds great potential for both CO_2 and H_2 separation. The simplicity of the approach, the removal of gas through a selective film, ensures it has high-energy efficiencies, small equipment footprint and therefore low capital cost compared to conventional separation processes [20, 21, 33]. Gas separation membranes have been commercially proven in the sweetening of natural gas (removal of CO_2 and H_2S) and for H_2 recovery in refineries. Membrane gas separation (GS) is most often indicated as potential candidate for CO_2 capture in pre-combustion as well as in post-combustion scenario. Membrane-based technology shows great potentiality to overcome the intrinsic difficulties related to the CO_2 capture, like high energy demand, meeting the objectives of process intensification strategy [22]. Both pre-combustion and post-combustion involve the separation of CO_2 from a gas mixture, composed of CO_2 and H_2 in the first approach and CO_2 diluted in air and other combustion product gasses in the second one. In post combustion capture, the membrane GS technology shows fundamental engineering and economic advantages over other competing separation systems. However, the main problem limiting the application is the low CO_2 concentration and pressure of the flue gas which requires the use of high selective membranes to fit the targets of recovery and purity delivered by the International Energy Agency (i.e. CO_2 recovery of 80% with a purity, of at least 90%) [23]. The purity target is related to the fact that the cost of CO_2 sequestration and in general the cost of all the further physical processes downstream to the CO_2 capture system will negatively affect the final electricity cost. To be useful for the CO_2 capture a membrane should have high carbon dioxide permeability and high carbon dioxide/nitrogen selectivity; moreover thermal, chemical and plasticisation resistance are required [24]. Cost effectiveness and ability to be cheaply manufactured are additional desired properties. Amongst the most important polymer materials currently present in the literature only few membrane materials show selectivities close to 100 and often these high selectivities correspond to low permeability. Interesting properties in terms of

CO_2 selectivity and/or permeability have been shown mainly by the following categories of membranes: polyimides (PI), polypropylene oxide (PPO), poly-ether ether ketone (PEEK), poly-ether block amide (PEBA), facilitated transport, mixed matrix [17, 4]. Polyimides are the class of polymer most investigate due to their excellent thermal and chemical stability with a wide range of CO_2 permeabilities [24]. In facilitates transport membranes a carrier agent, with a specific affinity toward the target gas molecule, is incorporated into the membrane. They have received a lot of attention in gas separation because they shown promising results, improving the selectivity at larger flux [25]. The incorporation of micro- or nano-particles of inorganic material into the polymer matrix (Mixed matrix membrane) is another well know strategy to enhance the properties of polymeric membrane. From a more applicative point of view and for real world system designs, together with the development of advanced membrane materials, an engineering approach on how to use the membrane currently on the market has to be pursued. In fact, designing a specific membrane gas separation process, the selectivity or permeance can be the key/limiting factor depending on the composition, pressure and flow rate of the stream to be treated and the aimed target (recovery and purity).

Regarding the pre-combustion capture where the main component to separate are CO_2 and H_2, the development of a membrane that retains the small H_2 molecules but permeates the larger CO_2 is a significant challenge. For polymeric membranes to be CO_2-selective it is important that the solubility selectivity strongly favours CO_2 and that diffusivity selectivity (which favours H_2) be minimized [26, 27]. Rubbery polymeric membranes typically have these capabilities. The high mobility of the polymer chains increases the diffusivity of all gases through the polymer matrix. Solubility selectivity favours condensable gases such as CO_2. Rubbery polymers such as polydimethylsiloxane (PDMS) and poly(amide-b-ethyleneoxide) (PEBAX) are often cited in this regard [28]. To achieve CO_2 selectivity for the IGCC process, for instance, polymeric membranes would appear to be the best

option, nevertheless they need to operate at low temperatures, which forces a cooling liability on the process.

For the application considered in this analysis, as previously described, there are few membranes studied for this specific separation. In particular, the stream to be processed is rich in CO_2, but still contained a fraction of H_2 unrecovered, CO and CH_4 unconverted and N_2. Unlike pre-combustion CO_2 separation, most of the H_2 in this case has been already recovered in the permeate stream of MR. On the other hand, the retentate stream is still different from a flue gas. As a consequence, the definition of new CO_2 capture strategy arises from the integration of WGS-MR reactor in H_2 production process. In the following analysis, the application of membrane GS technology has been investigated considering to apply in one case, a membrane for CO_2 post-combustion capture (cellulose acetate) and, in another case, a membrane for pre-combustion capture (PEBAX). The properties of two types of CO_2 selective-membranes have been taken from the literature [29].

A short overview on membrane fundamentals and on a simple tool used to evaluate the performance of GS membrane unit is firstly reported.

3.2.   Membrane fundamentals

In gas permeation, the membrane is responsible for the separation since it determines the permeability and selectivity of the process. The flux of gas transport through the membranes is generally governed by Eq. 61, obtained using Fick's first law:

$$J_i = Permeability_i \frac{\left(p_i^{Feed} - p_i^{Permeate}\right)}{\delta}$$

Eq. 61

where J_i is the flux of species i, δ is the membrane thickness, p_i^{Feed} and $p_i^{Permeate}$ are the partial pressure of species i on the feed side, and on the permeate side, respectively. The membrane permeability represents a measure of the ability of the membrane material to permeate gas. In gas

phase membrane applications permeability and permeance are usually used as measures of gas transport rate. The permeance is defined as the flux per unit pressure difference between the two sides of the membrane. The permeability is a property of the material whereas the permeance is a property of the membrane, depending on the separation layer thickness. If solution-diffusion is assumed as transport mechanism (typical of dense membranes) of the species through the membrane, the permeability of a single gas can be described as the product of its solubility (S_i) and diffusivity (D_i) through the material [30, 31]:

$$\text{Permeability}_i = D_i S_i$$

Eq. 62

where Di reflects the mobility of the individual molecules in the membrane material and the solubility reflects the number of molecules dissolved in the membrane material.

In polymer materials, the diffusion coefficients decrease with increasing molecular size hence the permeation of small molecules, such as hydrogen, are favoured with respect to the larger ones, such as carbon dioxide. The solubility of the gas permeating in the polymer generally increases with increasing condensability.

The relative magnitude of both properties, diffusion and solubility, depends on whether the polymer used is above or below its glass transition temperature. Below the glass transition temperature, the polymer chains are essentially fixed with very limited motion. Consequently, the effect of permeating gas size is larger compared to solubility difference, allowing small molecules to permeate preferentially. Vice versa, if the polymer is above its glass transition temperature, the polymer chain motion is increased. Hence, for these polymers, the effect of molecular size on the mobility of permeants is reduced, becoming dominant the selectivity based on sorption coefficient [32]. The ratio of the permeability of the more permeable gas (i) to that of the less permeable species (j) is called ideal permselectivity or selectivity ($\alpha_{i/j}$) and it represents a measurement of the ability of a membrane to separate two gases. The selectivity is expressed as:

$$\alpha_{i/j} = \frac{\text{Permeability}_i}{\text{Permeability}_j} = \frac{S_i \, D_i}{S_j \, D_j}$$

<div align="right">Eq. 63</div>

The selectivity term for a carbon dioxide-selective membrane with respect to the hydrogen, α_{CO_2/H_2} , for instance, can be written as:

$$\alpha_{CO_2/H_2} = \frac{\text{Permeability}_{CO_2}}{\text{Permeability}_{H_2}} = \frac{S_{CO_2} \, D_{CO_2}}{S_{H_2} \, D_{H_2}}$$

The separation properties of polymer membranes for the most important binary gas separations have been summarized by Robeson [34]. In particular, the plot of membrane selectivity versus membrane permeability has been applied by Robeson as useful tool to rationalize the properties of different membrane materials. By means of this tool a so called upper bound has been identified: it is the line, linking the properties of these most promising membrane materials, beyond which no better material exists. The upper bond is considered as a target in order to improve existing membranes. A wide range of selectivity/permeability combinations are provided by different polymers; however there is a strong inverse relationship between permeability and selectivity since in general the higher the permeability the lower the selectivity. That is the challenge to face in synthesis of new membrane for gas separation. Together with the development of better materials, once the application of the available membrane material is considered, matter of debate is the convenience to apply a membrane with high permeance and low selectivity or vice versa. Generally, a high permeance minimizes the membrane area required, while high selectivity improves the permeate concentration of the target species. Moreover, it has to be taken into account that the ratio of pure gas permeabilities gives the ideal membrane selectivity that is the selectivity value obtained when the membrane is exposed only to single gas. In actual gas separation processes, gas mixtures have to be treated, and in that case the selectivity measured with a gas mixture may then be one-half or less of the selectivity calculated from pure gas measurements [27]. In particular, if one of the components is so sorbed by the membrane to affect the permeability of the other component,

such occurs for instance in carbon dioxide/methane separation, quite different gas mixture selectivity value are obtained. Otherwise, if the gases in the mixture do not interact with the membrane material, the ideal and mixed gas selectivities could be equal or close. In the literature, since they are easier to measure, pure gas selectivities are more commonly reported. Furthermore, the temperature effect on selectivity should be also considered, acting on membrane material and permeating species properties. From the above considerations, it appears clear that permeance and selectivity are key parameters for the evaluation of the performance of a membrane gas separation process. However, beyond this parameter, mainly related to material and membrane properties, for the performance analysis of a GS membrane unit there are other variables to be taken into account. They are related to the system design (e.g. membrane area, flow configuration) and the operating condition. A simple tool, described in the next paragraph, has been used to study the influence of the most important parameters affecting the whole membrane system performance.

3.3.   Tools for performance analysis of GS membrane unit

A simple tool to analyse the performance of a membrane separation unit for CO_2 capture has been applied. This tool consists of a 1D mathematical model, already reported in the literature for a binary mixtures [17, 35], for the steady-state permeation in no sweep mode and co-current configuration. The model, modified and applied for a multi-species system, consists of a system of N ordinary differential equations for the retentate side and N algebraic equations for the permeate side, being N the number of gaseous species. The equation, for retentate and permeate side respectively, are the following:

$$-\frac{dF_i^{Retentate}}{dz} = Permeance_i \frac{A^{Membrane}}{L}\left(p_i^{Retentate} - p_i^{Permeate}\right)$$

Eq. 64

$$F_i^{Permeate}(z) = F_i^{Feed} - F_i^{Retentate}(z)$$

Eq. 65

For a CO_2 membrane separation unit, where the carbon dioxide is the target species to be removed, the previous equations can be written as a function of

122

CO_2 permeance and selectivity; the following equation, written in dimensionless form, are obtained:

Feed/Retantate side

$$-\frac{d\overline{F_{CO_2}^{Retentate}}}{d\zeta} = \frac{1}{\phi}\Theta_{CO_2}\left(\phi\, x_{CO_2}^{Retentate} - x_{CO_2}^{Permeate}\right)$$

Eq. 66

$$-\frac{d\overline{F_i^{Retentate}}}{d\zeta} = \frac{x_{CO_2}^{Feed}}{x_i^{Feed}}\frac{1}{\alpha_{CO_2/i}}\Theta_{CO_2}\frac{1}{\phi}\left(\phi\, x_i^{Retentate} - x_i^{Permeate}\right)$$

Eq. 67

Permeate side

$$\overline{F_i^{Permeate}}(\zeta) = F_i^{Feed} - F_i^{Retentate}(\zeta)$$

Eq. 68

In the equations $\overline{F_i}$ is the dimensionless molar flow rate and ζ is the dimensionless module length.

$$\overline{F_i} = \frac{F_i}{F_i^{Feed}}$$

Eq. 69

$$\zeta = \frac{z}{L}$$

Eq. 70

Θ_{CO_2} and ϕ are two dimensionless parameters, defined as permeation number (Eq. 71) [17] and feed to permeate pressures ratio (Eq. 72), respectively, that affect the performance of the stage membrane unit.

$$\Theta_{CO_2} = \frac{Permeance_{CO_2}A^{Membrane}P^{Feed}}{x_{CO_2}^{Feed}\,F^{Feed}}$$

Eq. 71

$$\phi = \frac{p^{Feed}}{p^{Permeate}}$$

Eq. 72

In the permeation number is indirectly expressed a comparison between the permeation through the membrane and the total flux along the module. Basically, a great permeation number corresponds to a high permeate flow rate, due to large membrane area and/or high permeance. The pressure ratio, expressing the driving force for the permeation, represents one of the most important and determinant operating parameters. The calculations of the

flow rate profiles and composition, for both membrane sides, can be performed integrating the equations along the module length when the feed composition, membrane properties (species permeance and selectivity), module geometry (total installed membrane area and module length) and operating conditions (flow rate and pressures) are known. The performance, in terms of final species purity and total recovery in the permeate stream can be easily calculated considering the species composition at the module exit.

The potentiality of the tool here utilized is its possibility for use in a preliminary design of a membrane unit for gas separation. In particular, the same solution for the membrane system are obtained for any combination of membrane properties, membrane area and operating conditions that gives the same value of permeation number and pressure ratio.

3.4. Process design background

In this chapter, various membrane process designs for capturing CO_2 from the outlet retentate stream of a WGS-MR have been analysed. Owing to the necessity to cool the stream and condense the water contained in, the membrane gas separation unit operates around 35-50 °C with a feed pressure of 7 bar. The feed pressure actually depends on the operating pressure of the WGS-MR. The membrane selectivities used in the following calculations have been chosen referring on membrane materials properties commercial available. The impact on process performance of enhanced membrane properties, especially in term of selectivity, is discussed later. As previously described, it has to be pointed out that most of the membrane properties reported in the open literature are related to specific separation such as CO_2/N_2, CO_2/CH_4 or CO_2/H_2 [7, 24, 27, 36]. The stream that has to be treated in our case is rich in carbon dioxide but also contains hydrogen, nitrogen, carbon monoxide and methane. As first approach the properties of a commercial CO_2 selective-membrane for post-combustion capture has been chosen. In particular, a cellulose acetate membrane has been considered; the related properties are reported in Table 39. For the CO selectivity the same value of the N_2 selectivity has been assumed. For the H_2 instead, because of

its small molecular size a selectivity value of 1 has been assumed, as suggested from the literature [7].

Table 39 Membrane selectivity value used in the process design calculations

CO_2/H_2	CO_2/N_2	CO_2/CO	CO_2/CH_4
1	20	20	20

Two different feed compositions have been considered in the following analysis. The feed composition named A corresponds to a retentate stream coming out from the WGS-MR, as described in chapter 2, with a CO conversion equal to 95% and a hydrogen recovery yield of 90%. The feed composition B is representative of a retentate outlet stream from a WGS-MR achieving higher CO conversion and H_2 recovery yield. Essentially, the two feed compositions differ for the hydrogen content. As will be further shown, the hydrogen content strongly affect the final CO_2 purity that can be obtained in the permeate stream of gas separation membrane unit. Table 40 summarizes both stream compositions, whereas details of the WGS-MR condition are given in Table 41.

Table 40 Feed composition, on molar dry basis, used in the calculations

Molar composition, %	Feed A	Feed B
CO_2	53.21	60.08
N_2	10.94	12.21
H_2	19.22	9.94
CH_4	14.94	16.67
CO	1.65	1.06

Table 41 WGS-MR process conditions

	Feed A	Feed B
CO conversion, %	95	97
H_2 recovery yield, %	90	95

The design proposed in this study assumes to operate at low temperature, since the stream coming from the WGS membrane reactor has been cooled in order to condensate and remove the water. The water molar fraction in the WGS-MR retenate stream is in fact more than 50%. The pressure ratio and permeation number, used in the calculation, are reported in the following paragraph, where the potentialities of the application of one stage gas separation membrane unit has been described.

3.5.   Single stage membrane process design

For CO_2 post-combustion capture one of the challenge that has to be faced by membrane technology implementation in the industry is the scale of the process due to the high volume of gas stream to be treated and the low concentration (i.e., low driving force) of CO_2 (e.g., around 15 vol. % CO_2), leading to the requirement of large membrane areas to perform the separation. The driving force for the gas permeation is the CO_2 partial pressure difference between the feed and the permeate side. It can be increased following different strategies [2, 32,]: increasing the feed side pressure (using a compressor), increasing the carbon dioxide concentration in the feed (recirculating an enriched CO_2 stream), decreasing the permeate side pressure (using a vacuum pump) and decreasing the CO_2 concentration in the permeate (using a sweep gas). However, all these actions involve a penalty in term of extra energetic demand and the energy cost of generating the required pressure difference across the membrane is a key issue. For one-stage separations, compression of the flue gas or use of vacuum pumps on the permeate side are usually needed.

In our case study a stream already compressed, at ca. 7 bar, and rich in CO_2, more than 50%, is available. Actually, the retentate stream coming from the WGS-MR can not be considered as a flue gas stream, since it still has hydrogen, methane and carbon monoxide. On the other hand, it is neither comparable with a shifted syngas stream because the H_2 has been already recovered in the membrane reactor permeate side. As first approach, the performance of a single stage membrane system has been analysed, assuming to exploit all the driving force available (see Figure 36, scheme on the left). In particular, a pressure of 1.2 bar has been considered on the permeate side, giving a pressure ratio ca. 6. In addition, the performance has been calculated also for higher pressure ratio value, to evaluate the possible improvement given by pressure ratio increment. The pressure ratio effect has been investigated since it represents a measurement of the enrichment achieved in the permeate relative to feed. In principle, a membrane module with set membrane properties (permeance and selectivity) operated at high pressure ratio, owing to the promoted permeation driving force, involves achieving higher recovery of the desired product, but does not imply a higher permeate concentration [35]. In practical separation applications, the pressure ratio across the membrane is usually between 5 and 15 [31].To achieve higher pressure ratios we assumed to apply on the permeate side a vacuum pump (see Figure 36, scheme on the right). Pressure ratios of 10 and 14 have been considered, which correspond to a permeate pressure of 0.7 bar and 0.5 bar, respectively. The possibility to compress the feed stream was not taken into account since the integration of a CO_2 membrane separation unit downstream a WGS-MR has been here analysed. Therefore, compression of the feed stream would be not reasonable, because if higher pressure is required in the separation section of the process this means that all the upstream units have to operate at higher pressure, reducing the unit volume. As a consequence, a re-design of the upstream units would be required. Moreover, the vacuum application seems a more convenient strategy from the energy point of view because the vacuum pump has to process the permeate flow rate, which is smaller than the feed one.
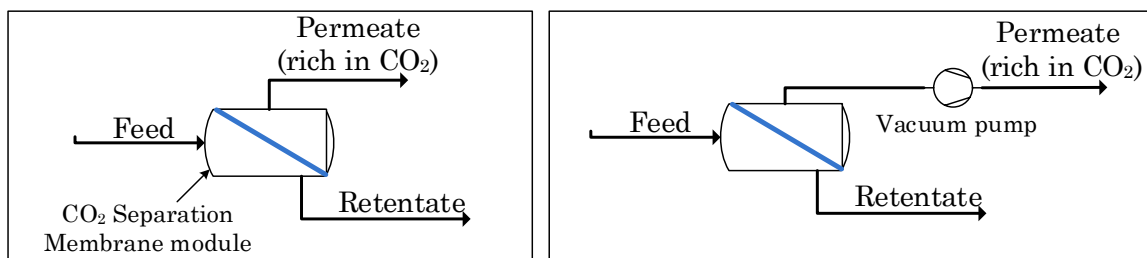
Figure 36 One stage configuration scheme

By means of the model above introduced, the performance of a one-stage membrane system has been calculated, on the basis of membrane properties and operating condition as reported in Table 42. Regarding the permeation number, two values have been considered, 1 and 10 respectively. As afore mentioned, the permeation number influences the final permeation concentration once the pressure ratio and selectivity are set.

Increasing the permeation number the permeation of the most permeable species (desired product) is initially promoted. However, also the flux of less permeable component increases, so depleting the final permeate concentration.

Table 42 Membrane properties and operating condition used in single stage membrane calculation

	Case study 1A	Case study 1B
Feed composition	A	B
Scheme	I stage	
Pressure ratio	5.8; 10; 14	
Permeation number	1; 10	
α_{CO_2/H_2}	1	
$\alpha_{CO_2/i}$ with i = N_2, CH_4, CO	20	

3.5.1. Single stage results

In the first approach, the performance of a single stage membrane unit has been calculated. The CO_2 permeate purity reachable in one stage is shown in Figure 37 as a function of pressure ratio. For the feed composition A (CO_2 = 53%), operating at low permeation number (Θ = 1) and without vacuum (pressure ratio 6) a CO_2 permeate concentration of 71 % can be obtained. In the range investigated, increasing the pressure ratio the CO_2 permeate concentration remains almost constant, showing as the pressure ratio is not limiting factor for the CO_2 purity achievable in one stage. As previous described, higher pressure ratio, promoting the permeation driving force, mainly affects the recovery, but does not imply a higher permeate concentration. Similar trends are observed for feed composition B (Figure 37, left side) where a CO_2 purity higher than 80% is achieved by means of single stage, feeding a stream with 60% of CO_2. Regarding the permeation number effect, as expected, an increment leads to a reduction of CO_2 permeate concentration. Basically, for a permeation number equal to 10 no separation has accomplished: CO_2 permeate concentrations close to the feed concentration values are obtained.
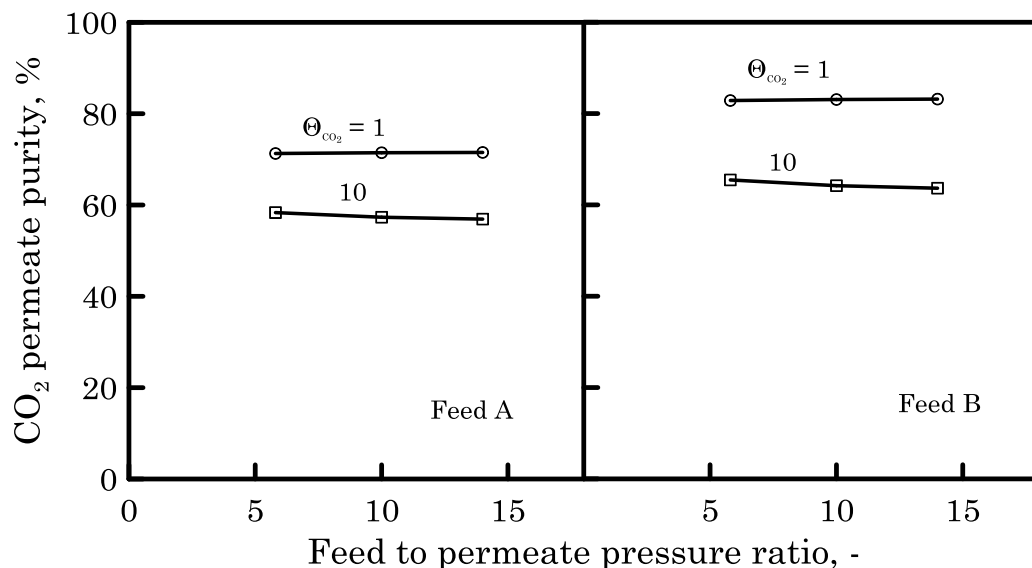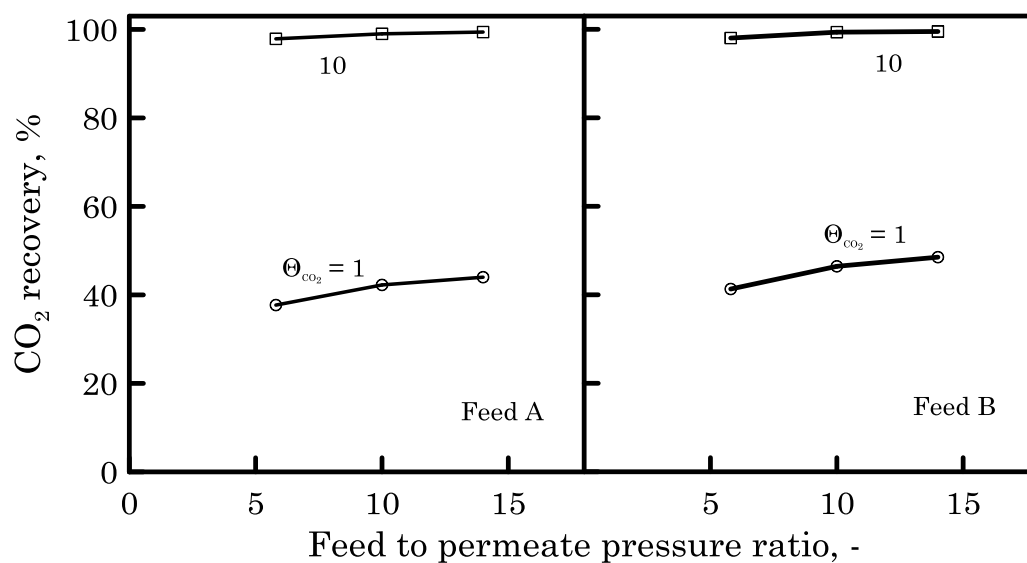

Figure 37 CO_2 permeate purity as a function of feed to permeate pressure ratio, for two different permeation number and feed composition (case study 1A and 1B).

Higher pressure ratio and permeation number promote the CO_2 recovery, as shown in Figure 38. Increasing the pressure ratio from 5 to 14 a CO_2 recovery increment of 15% is obtained at the lower permeation number. Nevertheless, even the highest recovery value achieved, ca. 50% for feed B at pressure ratio 14, is quit far from the target requirement, 90% [37, 38]. Recovery value fitting the target can be attained at greater permeation number. However, higher Θ value implies a penalty in term of CO_2 purity.
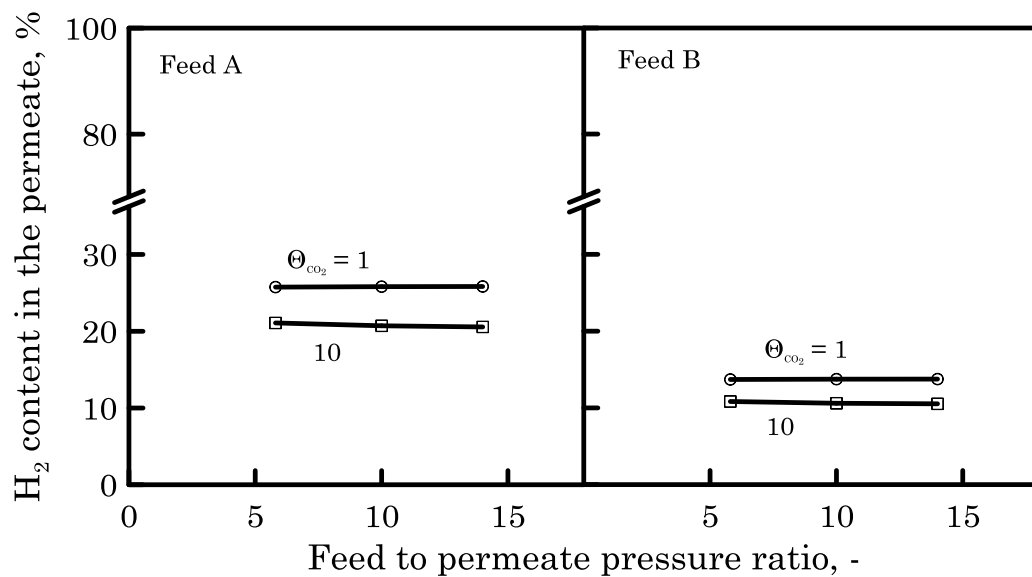

Figure 38 CO_2 recovery as a function of feed to permeate pressure ratio, for two different permeation number and feed composition (case study 1A and 1B).

To understand how to act to improve the CO_2 permeate purity it is necessary to look at the whole permeate stream composition. In particular, the most present component beyond the CO_2 is, as expected, the hydrogen (see Figure 39). This is mainly due to the fact that the membrane considered has the same permeance for CO_2 and H_2 ($\alpha_{CO_2/H_2} = 1$), meaning that the hydrogen molecules permeate trough the membrane as well as the CO_2 ones, without difference. This selectivity value has been assumed since the applied membrane, designed to separate mainly CO_2 and N_2, does not have selectivity with respect the small H_2 molecules. A higher CO_2 permeate concentration, ca. 80%, can be obtained by feeding a stream with a lower hydrogen content

(Feed B, hydrogen molar fraction minor then 0.1); however, the hydrogen permeate concentration, although reduced, is still around 15% (see Figure 39 right side). It has to be noticed that feed compositions A and B have also different CO_2 content, 53% and 60% respectively, but the main difference is in term of H_2 concentration.

From the single stage configuration analysis results as the purity target for CO_2 capture cannot be met, principally because of limitation related to the property of selected membrane. Nevertheless, on the basis of the results obtained, some general guideline can be drown, helping the design of a two stages membrane system. In particular, a permeation number minor than 10 has to be considered on the first stage. Moreover, to operate at pressure ratio higher than 5 is not suitable both in term of CO_2 purity and recovery.

Figure 39 H_2 permeate content as a function of feed to permeate pressure ratio, for two different permeation number and feed composition (case study 1A and 1B).

3.6.   Multi stage membrane process design

The previous simulation results demonstrated that, by means of a single stage membrane process a high-purity CO_2 permeate stream cannot be obtained, on the basis of the considered membrane selectivities, regardless of the pressure ratio and permeation number investigated. A double stage process has been then analysed to evaluate the possible improvements (Figure 40). The permeate stream coming out from the first unit is fed to a second membrane unit, with a serial configuration, also defined as enricher [2]. Since we assumed to use all the pressure energy in the first stage, on the second stage the driving force has been promoted applying a vacuum pump. A pressure ratio equal to 4.8 has been considered, corresponding at 0.25 bar of permeate side pressure.

Two scheme of operation have been used:

1) I stage and II stage membrane units with cellulose acetate membrane, so called M1.

2) I stage and II stage membrane units with Pebax®/PEG membrane, so called M2.

The choice 2) has been done considering that the key issue limiting the performance of the CO_2 separation, mainly in term of CO_2 purity, was related to the low selectivities of the membrane used in the single stage configuration. In particular, Pebax®/PEG membrane has been considered since the H_2 ideal selectivity value reported on literature for this membrane is ca. 11 [29]. Table 43 summarizes the membrane selectivity values.
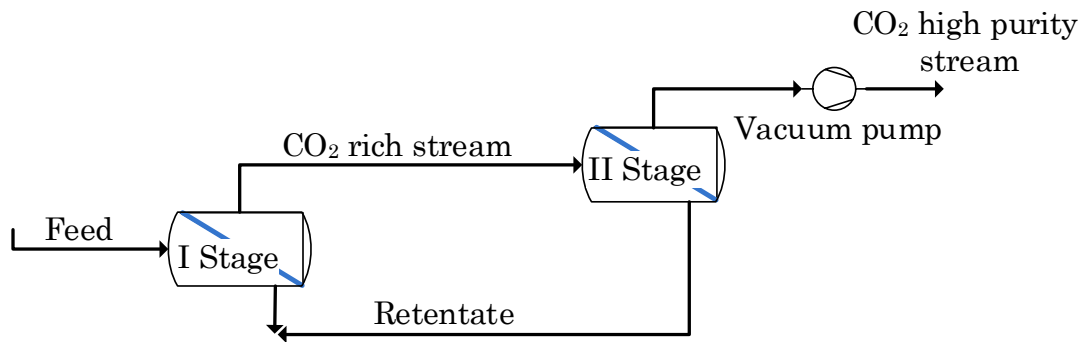
Figure 40 Two stages configuration with vacuum on the second stage

Table 43 Membrane properties used in the two stages calculation

Membrane type	α_{CO_2/H_2}	α_{CO_2/N_2}	α_{CO_2/CH_4}	$\alpha_{CO_2/CO}$
M1 (cellulose acetate)	1		20	
M2 (Pebax®/PEG)	9	40	15	40[a]

[a] The selectivity to CO was not reported in [29]; the same value of the N_2 one has been assumed.

Concerning the permeation number value, in the first stage a permeation number equal to 5 was assumed, mean value between the ones considered in single stage analysis. This value has been chosen aiming to balance the higher purity get for low permeation number and the higher recovery achieved with larger one. On the second stage a low permeation number (equal to 1) has been considered pursuing a further CO_2 purity increment.

A summary of the case studies considered for the two stages configuration and the related operating condition are reported in Table 44.

Table 44 Operating condition used in two stages membrane calculation

	Case study 2		Case study 3	
Feed composition	A and B		A and B	
Stage	I	II	I	II
Pressure ratio	5.8	4.8	5.8	4.8
Permeation number	5	1	5	1
Membrane property	M1		M2	

3.6.1 Multi stage results

The simulation results for the double stage configuration are summarized in Table 45 - Table 48. For each case study the design parameters, CO_2 recovery and permeate compositions are reported, for feed A and B respectively. The CO_2 recovery is defined as the total CO_2 recovered in the permeate outlet stream from the second stage (Permeate 2) with respect the CO_2 fed in the first stage. With the M1 membrane, operating at a permeation number of 5 on the first stage a CO_2 permeate concentration equal to 66% and 75% are achieved for feed composition A and B respectively. As expected, these values are in the range identified in the single stage analysis ($\Theta = 1$ and $\Theta = 10$). By means of a second stage a further enrichment in CO_2 purity are obtained, although under the target value yet.

The results for the M2 membrane (case study 3, Table 47 and Table 48), with higher α_{CO_2/H_2}, are the most interesting. The enhanced selectivity of the M2 membrane allows the required CO_2 purity target to be achieved with a two membrane stage configuration, for both analysed feed compositions. The comparison between membrane system M1 and M2 in term of CO_2 purity and CO_2 recovery is shown in Figure 41 - Figure 43. In particular, for feed composition A, results show as the CO_2 permeate concentration reached in the first stage with M2 membrane is 20% greater than the one with M1 membrane (see Figure 41). Moreover, by means of a second stage is finally

possible to reach the CO_2 purity target value, since the second stage allows a further appreciable enrichment in CO_2 content. For the membrane system M1, instead, the addition of a second stage is not a convenient option. In fact, since the low selectivity of the membrane toward the H_2 a further separation between CO_2 and H_2 cannot be obtained in the second stage. Similar results are attained for the feed composition B. In this case, because of the lower hydrogen feed content, a CO_2 permeate concentration about 85% is achieved with the M1 membrane. This value is still under the target whereas the performance of M2 membrane overcomes the target, reaching a CO_2 purity of 96%. The results comparison confirms that the key issue is related to the hydrogen content and CO_2/H_2 selectivity.

Table 45 Summary of design parameter and result for case study 2, feed composition A
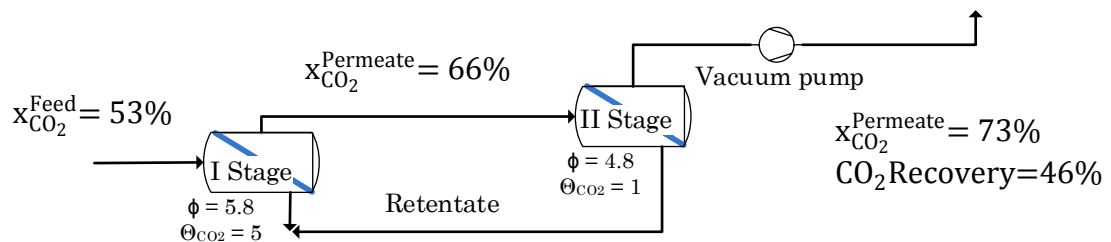
	Stage I	Stage II
Pressure ratio	5.8	4.8
Permeation number, -	5	1
Stage cut, -	0.758	0.443
CO_2 recovery, %	94.2	45.9

Composition, %	Permeate 1	Permeate 2
CO	0.56	0.051
CO_2	66.11	72.76
H_2	23.88	26.28
N_2	3.99	0.38
CH_4	5.44	0.52

Table 46 Summary of design parameter and result for case study 2, feed composition B
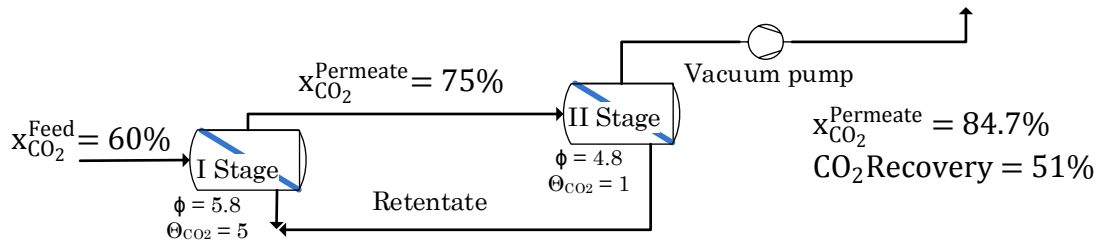
	Stage I	Stage II
Pressure ratio	5.8	4.8
Permeation number, -	5	1
Stage cut, -	0.75	0.481
CO_2 recovery, %	94.1	50.9

Composition, %	Permeate 1	Permeate 2
CO	0.41	0.04
CO_2	75.37	84.72
H_2	12.47	14.03
N_2	4.97	0.51
CH_4	6.78	0.7

Table 47 Summary of design parameter and result for case study 3, feed composition A
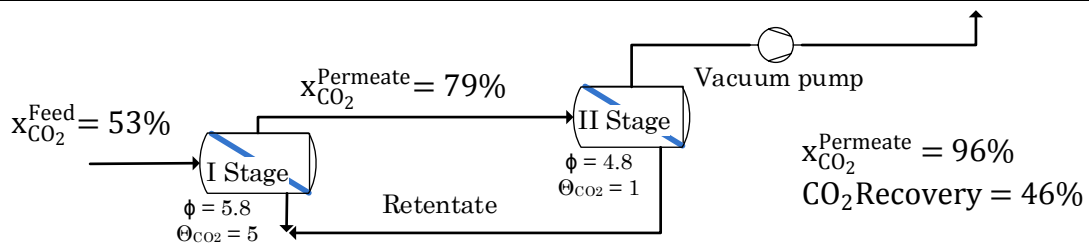
	Stage I	Stage II
Pressure ratio	5.8	4.8
Permeation number, -	5	1
Stage cut, -	0.584	0.437
CO_2 recovery, %	86.7	46.1

Composition, %	Permeate 1	Permeate 2
CO	0.28	0.016
CO_2	78.95	95.89
H_2	12.36	3.0
N_2	1.97	0.1
CH_4	6.43	0.97

Table 48 Summary of design parameter and result for case study 3, feed composition B

$x_{CO_2}^{Feed} = 60\%$ $x_{CO_2}^{Permeate} = 82\%$ Vacuum pump   I Stage $\phi = 5.8$ $\Theta_{CO2} = 5$ II Stage $\phi = 4.8$ $\Theta_{CO2} = 1$ Retentate $x_{CO_2}^{Permeate} = 97\%$ CO_2 Recovery = 51%

	Stage I	Stage II
Pressure ratio	5.8	4.8
Permeation number, -	5	1
Stage cut, -	0.664	0.478
CO_2 recovery, %	90.9	51.2

Composition, %	Permeate 1	Permeate 2
CO	0.22	0.02
CO_2	82.28	96.97
H_2	6.97	1.67
N_2	2.51	0.14
CH_4	8.02	1.20
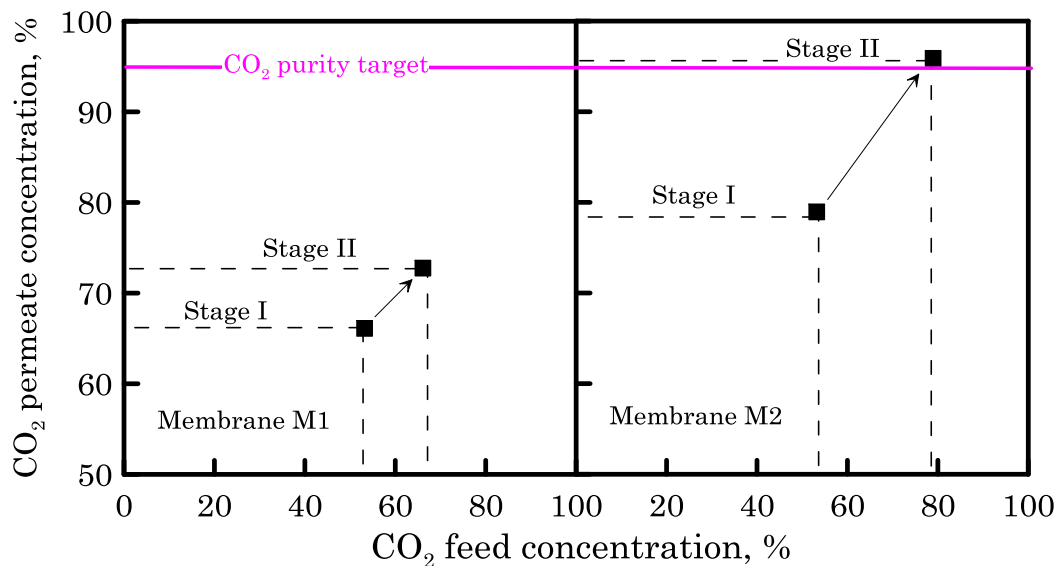
Figure 41 CO_2 permeate concentration as a function of CO_2 feed concentration for two stages configuration with different membrane (M1 left side, M2 right side). Feed composition: Feed A.
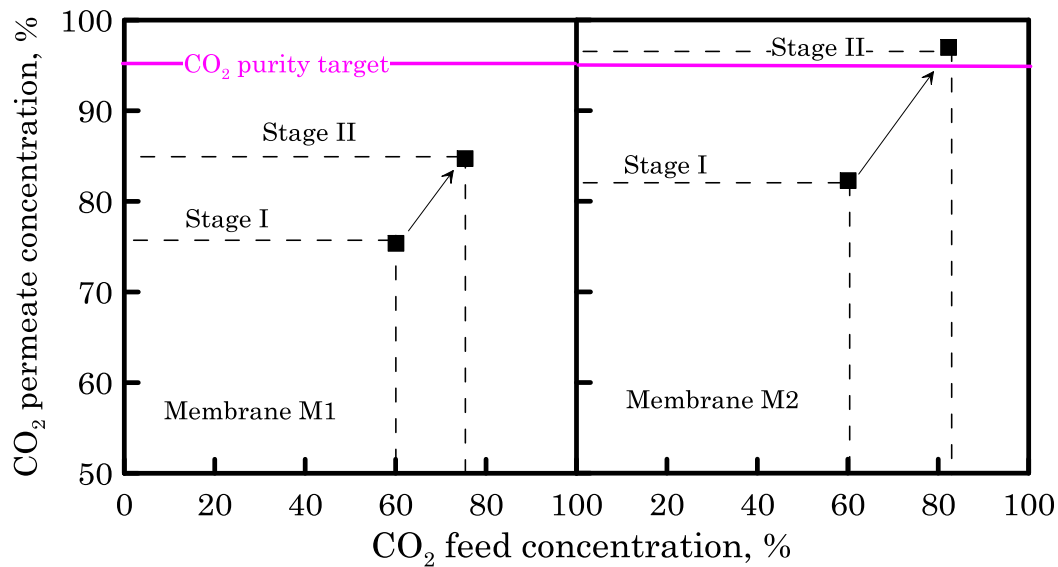
Figure 42 CO_2 permeate concentration as a function of CO_2 feed concentration for two stages configuration with different membrane (M1 left side, M2 right side).Feed composition: Feed B.

The other performance index to be taken into account is the CO_2 recovery. Figure 43 and Figure 44 show the CO_2 recovery for membrane system M1 and M2 for the two feed composition, feed A and feed B, respectively. In this case similar results are obtained for both membranes. This is due to the fact that the same design parameters have been considered. In fact, as previously discussed, the CO_2 recovery is mainly affected by permeation number and pressure ratio. In the first stage more than 90% of CO_2 is recovered; anyway, since a series configuration scheme has been considered, from first to second stage the total recovery necessarily decreases. After the second stage, for the feed composition B for instance, the overall CO_2 recovery decreases up to 50%. The large reduction is mainly due to the low permeation number considered on the second stage. As described in the second stage process design, a low permeation number has been selected pursuing higher purity rather than higher recovery. However, if the highest reachable recovery is pursued, regardless the purity target, the possibility to operate with a single membrane stage can be explored, getting also a good enhancement in CO_2

concentration. For the feed composition B, using the M2 membrane, 90% of CO_2 can be recovered with a CO_2 concentration of 82%.
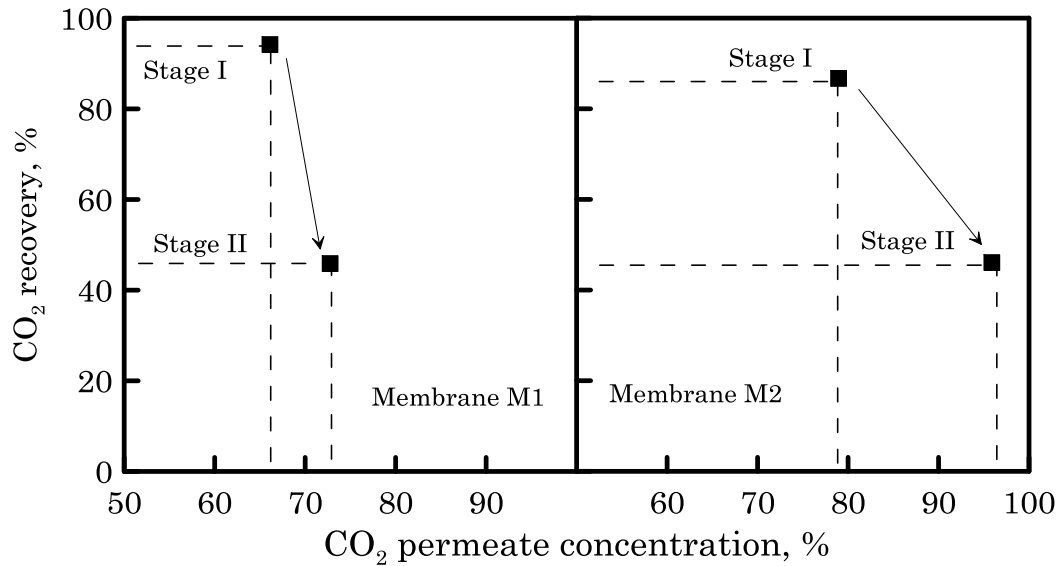

Figure 43 CO_2 permeate concentration as a function of CO_2 recovery for two stages configuration with different membrane (M1 left side, M2 right side).Feed composition: Feed A.
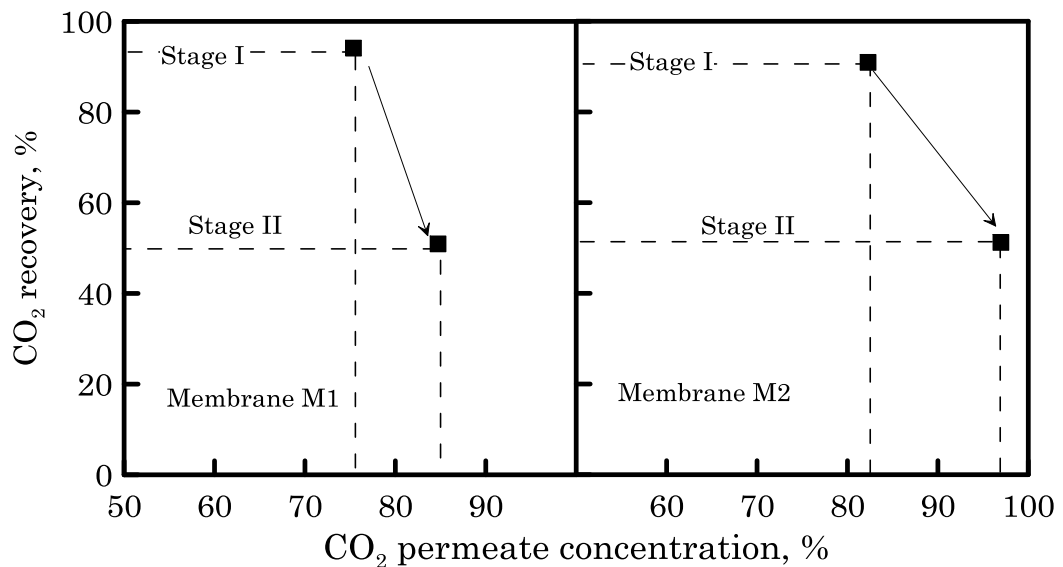

Figure 44 CO_2 permeate concentration as a function of CO_2 recovery for two stages configuration with different membrane (M1 left side, M2 right side). Feed composition: Feed B.

3.7.   Conclusion

The application of membrane gas separation system to CO_2 capture as a possible alternative in the post processing of WGS-MR retentate stream has been investigated. The CO_2 capture on small scale H_2 generator, as the production scale considered in our analysis (100 Nm^3/h H_2), is generally considered to be costly. However, due to the increasing constrains on carbon dioxide emission, the CO_2 handling is a long term issue also for this production scale.

As described in chapter 2, the integration of a WGS-MR downstream to a reforming unit allows the CO shifting, recovering in the permeate side the produced H_2 directly. A retentate stream, mainly containing water and CO_2, with remains of unconverted methane and CO, and unrecovered H_2, is obtained. The possibility to capture the CO_2 from this stream has been proposed since it is a pressurised stream rich in CO_2 (CO_2 > 50%, on dry basis). These two aspects enable the application of membrane gas separation technology.

Two membranes, with different selectivity properties, have been considered. As first approach, since no membrane specifically designed for this separation exists, the performance of a typical commercial pre-combustion membrane, cellulose acetate, have been investigated. The results show as this kind of membrane are not suitable if the CO_2 purity target (CO_2 > 95%) is pursued. This is due to the low membrane selectivity toward the H_2, that mainly affect the CO_2 permeate concentration achievable, regardless of the used operating condition. Even if a feed stream with a lower H_2 content (as feed B) is processed, the highest purity achievable with two stages of cellulose acetate membrane unit is about 85%. In alternative, the application of a PEBAX/PEG membrane that exhibits higher CO_2/H_2 selectivity has been investigated. Better performance is attained, recovering about 50% of CO_2 with purity above the target value. The results for the PEBAX/PEG membrane thus confirm the CO_2 capture feasibility, processing the retentate stream coming

out from the WGS-MR in a two stages membrane gas separation unit. Although these results are promising, some aspects have to be highlighted.

In particular, it has to be noticed that to get a high purity a penalty in term of recovery is paid. The highest CO_2 recovery achievable is ca. 50%, whereas the target value is in the range of 80- 90%. However, the purity target, since it is related to specific issue on pipeline transport and storage, is stricter than the one on CO_2 recovery. In addition, it has to be observed that in this analysis a membrane-only process has been considered. This approach is a useful starting point, however, in many industrial membrane applications, membrane are used joined with other separation techniques to take advantages of the benefit of each technology. As a consequence, if high recovery is pursued the possibility to operate with a single membrane stage can be explored, assuming to get the required CO_2 purity by extra permeate treatment.

Once the carbon dioxide is obtained as a concentrated/high purity gas stream, a further issue to be addressed is what to do with this captured CO_2. One recent solution consists of transportation of captured CO_2 to a storage location and storing it in such a way that avoids its release in atmosphere. Hence, for small-scale CO_2 capture, a distribution infrastructure is required to transport the CO_2 to sequestration sites.

The overall costs, including CO_2 separation, compression and sequestration should be estimated to evaluate the economic feasibility of the proposed system. However, the analysis performed shows the technological feasibility, also highlighting a new challenge on membrane development. In particular, to recover the CO_2 from the retentate stream, obtained by MR integration in H_2 production process, membrane specifically designed to perform this separation are needed. The retentate stream is in fact different with respect to a typical flue gas stream, where basically a CO_2-N_2 mixture has to be treated. Analogously, the retentate processing differs from the CO_2 pre-combustion capture process, since the most H_2/CO_2 separation has been already accomplished in the MR. Therefore, membrane with tuned selectivity

toward H_2, N_2, CH_4 (depending on retentate composition) and large CO_2 permeance value should be developed for this novel application.

Nomenclature

List of symbols

A	membrane area
D_i	diffusivity
F	molar flow rate
J_i	permeating flux
L	membrane module length
p	Pressure
Permeance	species permeance
S_i	solubility
x	molar fraction
z	axial coordinate along reactor length

Greek symbol

α	selectivity
δ	thickness
Θ_{CO_2}	permeation number
ϕ	pressure ratio
ζ	dimensionless module length

Subscripts and superscripts

Feed	membrane module inlet stream referred to
i	ith species referred to
Membrane	membrane referred to
Permeation	membrane module permeation stream referred to

References

1. Solomon S., Qin D., Manning M., Chen Z., Marquis M., Averyt KB., et al. Contribution of working group I to the fourth assessment report of the intergovernmental panel on climate change. Cambridge, United Kingdom and New York, USA: Cambridge University Press; 2007.

2. Zhao L., Riensche E., Blum L., Stolten D., Journal of Membrane Science, 2010, 359, 160–172.

3. IEA. Energy technology transitions for industry e strategies for the next industrial revolution. Paris, France: International Energy Agency; 2009.

4. Luis P., Van Gerven T., Van der Bruggen B., Progress in Energy and Combustion Science, 2012, 38, 419-448.

5. Davidson O., Metz B., Special Report on Carbon Dioxide Capture and Storage, International Panel on Climate Change, Geneva, Switzerland, 2005. www.ipcc.ch.

6. Aaron D., Tsouris C., Separation of CO_2 from flue gas: a review. Sep. Sci. Technol., 2005, 40, 321-348.

7. Ebner AD, Ritter JA., Sep. Sci. Technol., 2009, 44, 1273-1421.

8. Olajire AA., CO_2 capture and separation technologies for end-of-pipe applications: a review, Energy, 2010, 35, 2610-2628.

9. Rao AB, Rubin ES., Environ Sci. Technol. 2002, 36, 4467-4475.

10. Tuinier M.J., van Sint Annaland M., Kramer G.J., Kuipers J.A.M., Chemical Engineering Science, 2010, 65, 114.

11. Eide L.I., Anheden M., Lyngfelt A., Abanades C., Younes M., Clodic D., Bill A.A., Feron P.H.M., Rojey A., Giroudière F., Novel capture processes, Oil & Gas Science & Technology, 2005, 60,497.

12. Figueroa JD., Fout T., Plasynski S., McIlvried H., Srivastava RD., Int. J Greenhouse Gas Control, 2008, 2, 9-20.

13. Yong Z., Mata V., Rodrigues AE., Sep. Purif. Technol. 2002, 26, 195-205.

14. Thiruvenkatachari R., Su S., An H., Yu X., Prog. Energy Combust., 2009, 35, 438-455.

15. Criscuoli A., Drioli E., Ind. Eng. Chem. Res., 2007, 46, 2268-2271.

16. Van Gerven T., Stankiewicz A., Ind. Eng. Chem. Res., 2009, 48, 2465-2474.

17. Hansen A.M., "Small-scale Reformers for Stationary Hydrogen Production with Minimum CO_2 emissions", IEA-HIA Task 16 Hydrogen from Carbon Containing Materials – Subtask C report, July 2005 (ieahia.org/pdfs/rapperswil/Task16CFinal.pdf).

18. PHYRENEES Association – Ecole des Mines d'Albi-Carmaux, "Small-scale reforming systems for hydrogen refuelling stations" Technology Watch Report, 2010 (http://www.isq.pt/EN/HttpHandlers/FileHandler.ashx?id=108&menuid=843)

19. Brunetti A., Scura F., Barbieri G., Drioli E., J. Membr. Sci., 2010, 359, 115-125.

20. Bracht M., Alderliesten P.T., Kloster R., Pruschek R., Haupt G., Xue E., Ross J.R.H., Koukou M.K., Papayannakos N., Energy Convers. Mgmt. 38,S159–S164.

21. Shelly S., Chem. Eng. Prog., 2009, 105, 42–47.

22. Favre E., Bounaceur R., Roizard D., J.Membr.Sci., 2009, 328, 11-14.

23. Bounaceur R., Lape N., Roizard D., Vallieres C., Favre E., Energy, 2006, 31, 2556.

24. Powell C.E., Qiao, G.G., Journal of Membrane Science, 2006, 279, 1.

25. Yang H., Xu Z., Fan M., Gupta R., Slimane RB., Bland AE, et al., J. Environ. Sci 2008, 20, 14-27.

26. Perry J.D., Nagai K., Koros W.J., Polymer membranes for hydrogen separations, MRS Bull. 2006, 31, 745–749.

27. Scholes Colin A, Smith K. H., Kentish S. E, Stevens G. W., Int. J. of Greenhouse Gas Control, 2010, 4, 739-755.

28. Kim J.H., Ha S.Y., Lee Y.M., J. Membr. Sci., 2001, 190, 179–193.

29. Car A., Stropnik C., Yave W., Peinemann KV., J. Membr. Sci., 2008, 307, 88-95.

30. Mulder M., Basic Principles of Membrane Technology, Kluwer Academic Publishers, Dordrecht, the Netherlands, 1996.

31. Baker R.W., Membrane Technology and Applications, 2nd ed., John Wiley &Sons Ltd, Chichester, England, 2004.

32. Merkel Tim C., Zhou M., Baker R. W., J. Membr. Sci, 2012, 389, 441-450.

33. Follmann P.M, Bayer C., Wessling M. and Melin T., Membrane Engineering for the Treatment of Gases: Gas-Separation Problems with Membranes. Eds. Enrico Drioli, Giuseppe Barbieri. Vol. 1. Royal Society of Chemistry, 2011.

34. Robeson L.M., J. Membr. Sci., 1991, 62, 165.

35. Brunetti A., Drioli E., Lee Y.M, Barbieri G., J. Membr. Sci., 2014, 454, 305-315.

36. Zhanga Y., Sunarso J., Liu S., Wang R., International Journal of Greenhouse Gas Control, 2013, 12, 84-107.

37. de Visser E., Hendriks C., Barrio M., Molnvik M., de Koijer G., Liljemark S. and Le Gallo Y., 2008, International journal of greenhouse gas control, 2008, 2, 478-484.

38. Mikunda T. and de Coninck H., "CO2ReMoVe: Possible impacts of captured CO_2 stream impurities on transport infrastructure and geological storage formations. Current understanding and implications for EU legislation" Deliverable 4.1.4 of the CO2ReMoVe project, 2011, ECN (Energy Research Centre of the Netherlands) http://www.ecn.nl/docs/library/report/2011/o11040.pdf

Chapter 4

Integration of novel water gas shift catalyst in membrane reactor: reaction investigations

Introduction

During the last decades, due to increased hydrogen demand, renewed interest has been addressed to the gas shift process, looking for innovative catalyst and reactor handling. In particular, several studies [1, 2, 3, 4, 5, 6] and research projects [7, 8, 9, 10, 11] have been attempted to develop novel catalysts, able to provide a better exploitation of raw material, and to design advanced reactor and separation units, able to improve the reaction/separation stages.

The water gas shift is a moderately exothermic reaction and characterized by no variation in the number of moles. Thus, low temperatures favour the CO equilibrium conversion, which is independent of the reaction pressure. Since the reaction rate is low, a catalyst is required to carry on the reaction. The most used catalysts are usually distinct depending on the reaction temperature, since the WGS is a staged process and the reaction temperature depends on the stage [12, 13]. Currently, there are two main classes of materials being used in industry as CO-shift catalysts: Fe-based and Cu-based catalysts [14]. Industrially, the Fe-based catalysts are some of the earliest catalysts that have been used; they are commonly called High Temperature (HT) shift catalysts because of the operating reaction temperature range, around 320–450 °C. Most industrial HT shift catalysts contain Cr oxide (Cr_2O_3) as well as Fe oxide, being generally believed that Cr_2O_3 is a structural promoter [15]. The Cu-based catalysts allowed enhancement in the process conversions and yields in the production of H_2. Several Cu formulations have been employed in the low temperature (LT) WGS stage [16]. However, the thermal stability of this catalyst is still lower

to the HT ones. Therefore, operating temperatures should be restricted, usually to below 300 °C [16, 17].

In recent times, as mentioned above, the renewed interest in the WGS reaction pursued the development of very efficient catalysts able to reduce the CO content at very low concentrations (i.e. ~2 ppm). Co-based catalyst brought some interest being more active, sulphur tolerant and preserving their catalytic activity, with respect to the conventional HT and LT catalyst systems [13]. Other materials that have gained much attention are Au and Pt, as based catalysts, and ceria among the oxide supports [18].

However, beyond the catalyst improvement, many research efforts have been addressed to develop new H_2 purification technology, being the hydrogen production the final goal of reformate shifting process.

Amongst the technologies for purifying hydrogen Pd-based membranes have received increased interest due to their unique hydrogen separation properties. In particular, many studies have been focused on the use of H_2-selective Pd membrane integrated into the WGS reactor [19, 20, 21, 22]. As already described in chapter 1 and 2, the integrated membrane-reactor system, a membrane reactor (MR) indeed, allows achieving higher conversions with respect to a conventional fixed bed reactor and, in addition, producing a pure hydrogen stream that required no further purification step. In this way, the WGS reaction and the hydrogen separation steps required in the conventional process can be replaced by a single WGS membrane reactor, pursuing the logic of the Process Intensification Strategy [23]. Moreover, due to H_2 extraction from the reaction volume, it is possible exceeds the thermodynamic equilibrium limitation and carries out the reaction at high temperature and high pressure, useful both for reaction kinetic and membrane permeation. Additionally, by the MR, the catalyst amount necessary for a given conversion can be significantly reduced as well [24]. Several studies on WGS reaction in Pd membrane reactors were usually conducted using commercial catalysts. However, the present WGS commercial catalysts have been designed for traditional reactor.

Consequently, a new challenge is presented in developing very effective catalysts suitable for MR applications.

It is known that the WGS reaction products inhibit the reaction and lower the reaction rate over WGS catalysts. The inhibition effect depends on the nature of the catalyst and temperature range. In the case of MRs, this inhibition effect depends also on the properties of the membrane. For H_2 selective membrane, the higher CO_2 concentration in the reaction volume will affect the reaction rate. Some studies [25] showed that inhibition of ferrochrome catalysts by CO_2 has a strong effect on the overall performance of membrane reactors. The commercial low temperature $Cu/ZnO/Al_2O_3$ catalysts, used in some membrane reactor studies [20, 26], seem to be low suitable for MR, as well. In fact, since the CO more inhibits H_2 transport through Pd and Pd alloy membranes below 320 °C [27, 28], in Pd-MR it appears more efficient to carry out the WGS reaction at higher temperatures.

The recent noble metal catalysts (Pt-based) supported on CeO_2 have been intensely investigated as promising next-generation WGS catalysts. These catalysts exhibit much faster high-temperature kinetics [29, 30, 31] and generally reveal a lower inhibition by CO_2 [32], showing good potentiality also for application in MR. Hence, the integration of these catalysts in membrane reactor required to be more deeply studied.

The objective of this study was to investigate the performance, in terms of conversion enhancement and H_2 recovery, of a Pd membrane reactor packed with a novel $Pt/CeTiO_2$ catalyst, developed in the framework of DEMCAMER project, using simulated reformate gas mixture. In particular, the effect of the reaction temperature, reaction pressure and gas hourly space velocity on the integrated MR-catalyst system was studied. The conversions attained were compared with the ones achieved in a conventional packed-bed reactor and with the maximum reachable conversion, calculated on the basis of thermodynamic equilibrium. The results were compared, whenever possible, with literature data, too.

4.1. Materials and methods

4.1.1.　　　Experimental apparatus

The experiments were carried on in a tube in tube MR. It consists of two concentric tubes (Figure 45): the outer tube is a stainless steel shell, the inner tube is the Pd-alloy self-supported membrane. The membrane is blind and has only one exit. The membrane characteristics are reported in Table 49. A self supported commercial membrane (Goodfellow) has been used. This membrane has a quite high thickness, 100 micron, implying lower permeance value with respect to novel very thin metallic alloy membranes. However, this commercial membrane has the advantage to be very stable, from both chemical and mechanical point of view, thus it is more suitable to study the performance of the novel catalyst integration in the MR.
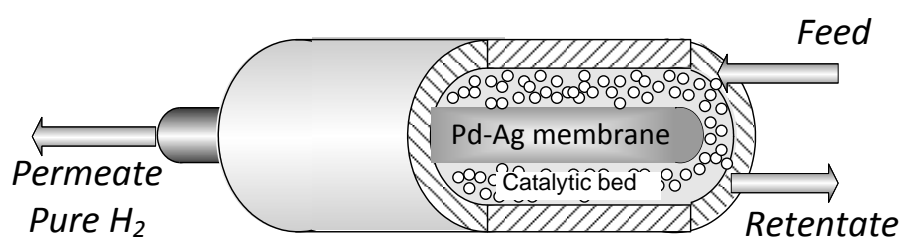
Figure 45 Membrane reactor scheme [33].

A novel WGS reaction catalyst has been used to perform the reaction measure. This catalyst has been developed in the framework of the DEMCAMER project at the Institute of Catalysis and Petrochemistry (ICP-CSIC, Madrid). The catalyst delivered by project partner has been tested in ITM-CNR lab. It based on $Pt/Ce/TiO_2$ and it has been designed for a low-middle temperature shift reaction; its characteristics are described in Table 50. The catalyst has been packed into the shell side, since this configuration was demonstrated to be more efficient for the heat exchange between the reaction volume and the furnace [34], allowing a better catalyst exploitation. The reaction occurs in the shell side while the permeated stream is recovered in the core of the membrane. The catalyst was diluted with quartz of the same particle size before loaded into the annulus.

Table 49 Membrane characteristics

Membrane	Pd-Ag - Commercial (Goodfellow) Self-supported
Thickness	100 micron
Superficial Area	1.63 cm^2
Outer Diameter	1 mm
Length	52 mm

Table 50 Catalyst characteristics

Composition	Pt/CeTiO$_2$
Particle size	1 mm
Catalyst amount loaded in the reactor	1.3 g

The experimental apparatus used in permeation and reaction tests is shown in Figure 46. The MR was placed in a temperature controlled electric furnace (with PID control). A mass flow controller (Brooks Instrument 5850S) was used for feeding the gaseous mixture, and an HPLC pump (Dionex P680A) was used to feed the water. A heating coil for vaporizing the water was put into the furnace, close to the MR. The flow rates of the outlet streams were measured by means of bubble soap flow-meters.

The retentate and permeate streams compositions were analysed by means of a gas chromatograph (Agilent 6890N) with two parallel analytical lines. Each line is equipped with two columns: an HP-Plot-5A (for separating permanent gases such as H_2, N_2 and CO) and an HP-Poraplot-Q (for other species) and a TCD. This allowed to contemporary analyse the retentate and permeating streams. The reaction temperature was determined by using a thermocouple inserted in the middle of the reactor shell. The reaction side pressure was controlled through a back pressure regulator in the retentate line while the permeate side was maintained at atmospheric pressure. No sweep gas was used in the permeate side.
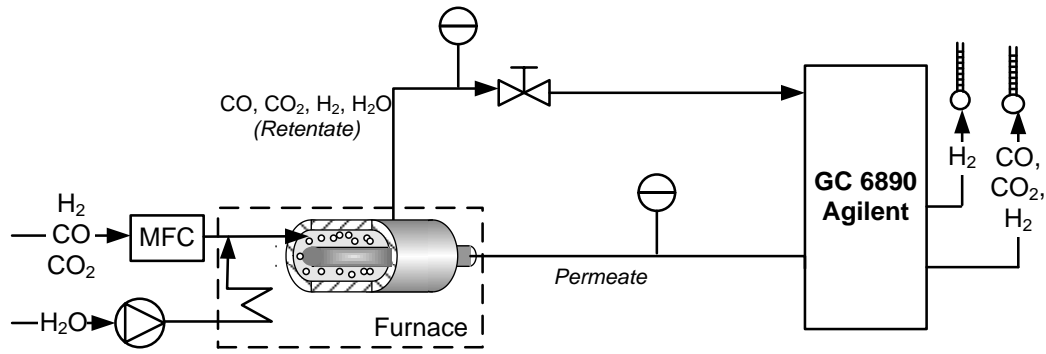
Figure 46 Experimental laboratory-scale plant. MFC: mass flow controller; GC: gas chromatograph [33].

4.1.2. Methodology and operating condition

Pd-alloy membranes are generally utilized in a temperature range where the diffusion in the metal bulk is the rate-determining step. Sieverts law is used worldwide for the mathematical description of H_2-permeating flux in these types of membrane. Also in this study the Sieverts law (Eq. 73) was applied to describe the H_2 permeating flux. In this case, the hydrogen flux is a linear function of the permeability and driving force, which is given by the difference of the square root of the H_2 partial pressure on both membrane sides, and reverse function of the membrane thickness.

$$H_2 \text{ Permeating flux} = \text{Permeance}_{H_2}^{0} \ e^{-Ea/RT} \left(\sqrt{p_{H_2}^{\text{Reaction side}}} - \sqrt{p_{H_2}^{\text{Permeate side}}} \right)$$

Eq. 73

CO conversion for traditional and membrane reactor was calculated taking into account the CO and CO_2 present in the feed and retentate streams, using the Eq. 74. In particular it was calculated as the mean value of CO_2 produced (lower value) and CO present in the retentate (upper value); the difference between them is the carbon balance [35].

$$\text{CO conversion} = \frac{1}{2}\left[\left(\frac{F_{CO_2}^{\text{Retentate}} - F_{CO_2}^{\text{Feed}}}{F_{CO}^{\text{Feed}}} \right) + \left(1 - \frac{F_{CO}^{\text{Retentate}}}{F_{CO}^{\text{Feed}}} \right) \right]$$

Eq. 74

The upper limit of a chemical reaction is given by the thermodynamic equilibrium conversion. To describe the equilibrium of an MR the same concepts valid for the traditional reactor are applied, but the permeative equilibrium has to be considered in addition to the chemical one. Therefore, the MR equilibrium conversion (MREC) is a function of the thermodynamic variables and initial composition on both sides of the Pd-alloy membranes:

$$\text{MREC} = f\left(K_{eq},\ T^{\text{Reaction side}},\ p^{\text{Reaction side}},\ y_i^{\text{Feed}},\ T^{\text{Permeation side}},\ p^{\text{Permeation side}},\ p_{H_2}^{\text{Equilibrium}}\right)$$

MREC is independent of the membrane permeation properties, but the final value depends on the extractive capacity of the system. The MREC represents the maximum conversion achievable with the MR, for set operating conditions. Thus, for the studied reaction system the MR equilibrium conversion has been also evaluated.

A fundamental variable to analyse the MR performance for producing H_2 is the recovery capability of MR, the H_2 recovery index (Eq. 75). It is defined as the H_2 fraction permeated through the membrane with respect to the whole H_2 present in the reaction side, constituted by the one produced by reaction and the one fed to the MR [36].

$$H_2\text{Recovery} = R_{H_2} = \frac{F_{H_2}^{\text{Permeate}}}{F_{H_2}^{\text{Permeate}} + F_{H_2}^{\text{Retentate}}}$$

Eq. 75

The operating conditions used for the experiments are reported in Table 51.

A syngas stream simulating the composition of a stream coming out from a methane steam reformer unit was considered. A stoichiometric steam to carbon ratio was assumed; actually in industrial WGS application this value is higher in order to shift the CO conversion. However, in MR system the conversion shifting is promoted by the H_2 removal, so it is possible to operate at lower steam/CO ratio. The reaction test has been performed at two temperatures, 350 °C and 400° C, respectively.

Table 51 Reaction tests operating conditions

Temperature	350-400°C
Feed Pressure	7.4-9.6 bar
Permeate Pressure	1 bar
H_2O /CO feed molar ratio	1
GHSV (gas hourly space velocity)	7,000; 12,200; 30,500 h^{-1}
Feed molar composition (wet), %	$H_2O:CO:H_2:CO_2:N_2 = 31:31:33:4:1$
Feed molar composition (dry), %	$CO:H_2:CO_2:N_2 = 46:48:5:1$
No sweep gas was used	

For both temperature values, the effects of the GHSV (gas hourly space velocity, Eq. 76) and the feed pressure were analysed. The GHSV is a variable indicating the inverse of the residence time between catalyst and reactants. A low GHSV corresponds to a high residence time and, thus, favours the reactants conversion. On the contrary, a high GHSV implies a reduced contact time and, thus, lower conversion. However, industrially high GHSV value is desired since it means the possibility to treat a huge amount of reactants with a low catalyst amount.

$$\text{Gas Hourly Space Velocity} = \text{GHSV} = \frac{\text{Feed flow rate}}{\text{Reaction volume}}$$

Eq. 76

No sweep gas was used during the experiments and the permeate side was kept constant at atmospheric pressure. The integrity of the membrane and its infinite hydrogen selectivity was verified by feeding nitrogen at 5 bar and confirming the absence of any flux on permeate side.

4.2. Results and Discussion

4.2.1. Permeation measurements

The H_2 permeating flux through the Pd-Ag membrane was measured by feeding pure gas, for evaluating the permeation membrane properties, flux and permeance, as a function of the permeation driving force, before to carry out the reaction experiments.

As expected, a linear dependence of the H_2 flux as a function of the driving force was observed at both investigated temperatures (Figure 47), therefore it was confirmed that hydrogen flux follows the Sieverts law and a constant permeance value can be assumed for each temperature (Table 52).
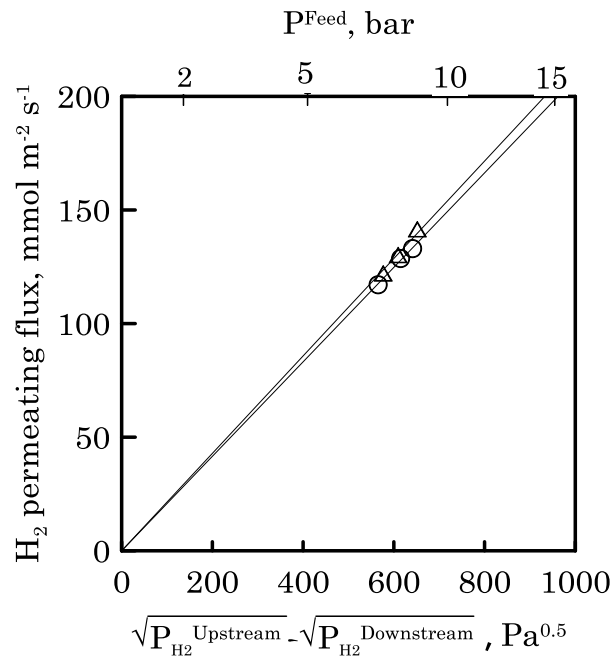
Figure 47 Pd-Ag membrane module permeation tests up to 9 bar. Hydrogen permeating flux as a function of driving force at 350°C. Symbols: measured data (400 °C triangles, 350 °C circles); lines: linear regression through the axes origin.

Table 52 Pd-Ag membrane permeance and permeability as a function of temperature

Temperature, °C	Permeance $\mu mol\ m^{-2}\ s^{-1}\ Pa^{-0.5}$	Permeability $nmol\ m\ m^{-2}\ s^{-1}\ Pa^{-0.5}$
350	208	20.8
400	214	21.4

4.2.2.   Reaction measurements

To verify the performance of a new catalyst for the WGS reaction in a membrane reactor, reaction measurements at different operating conditions were carried out. In particular the influence of three parameters on the reaction was studied: reaction pressure, temperature and feed space velocity. Two temperatures, 350 and 400°C and a wide range of GHSV were chosen. The performances of a Pd-Ag MR are significantly favoured by the pressure driving force between the two membrane sides; keeping the permeate side at atmospheric value and acting on the feed pressure CO conversion and H_2 recovery change. In particular, increasing the feed pressure more hydrogen is produced and recovered in the permeate side. Indeed, even though the feed pressure does not influence the reaction from a thermodynamic point of view, the removal of hydrogen from reaction sides shifts the reaction toward further formation of products. Figure 48 shows the CO conversion measured at 350 and 400°C as a function of the feed pressure, for different GHSV values. As expected, increasing the feed pressure the CO conversion increases. At the highest temperature, 400 °C, and lowest GHSV value, 7000 h^{-1}, a conversion greater than the equilibrium conversion of a traditional reactor has been obtained. As the CO conversion increases the H_2 fraction collected in the permeate side with respect to that totally fed/produced into MR (H_2 Recovery, Eq. 75) increases too (Figure 49). At 350°C for a reaction pressure of 9.3 bar and a GHSV equal to 7,000 h^{-1} it reached the 40%. This value means that the 40% of the hydrogen present in the reaction side was continuously collected as pure stream in the permeate. This value is quite low if compared with the

higher recovery target fixed for the WGS-MR unit. However, the low recovery depends on the high thickness of the membrane and consequentially on the low permeance that affect the H_2 permeating flux.
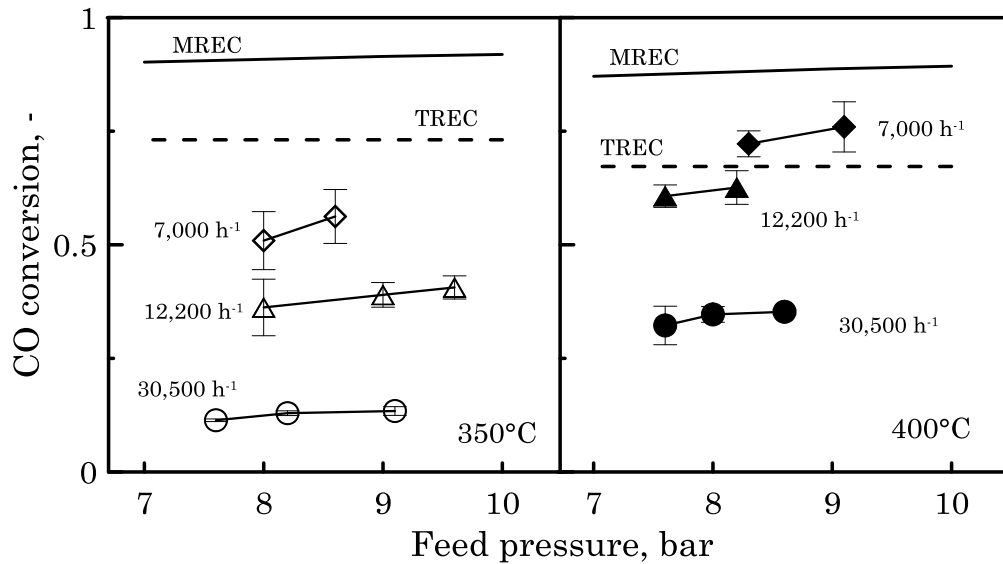

Figure 48 CO conversion as a function of feed pressure for different values of GHSV, measured at 350 and 400°C, respectively.
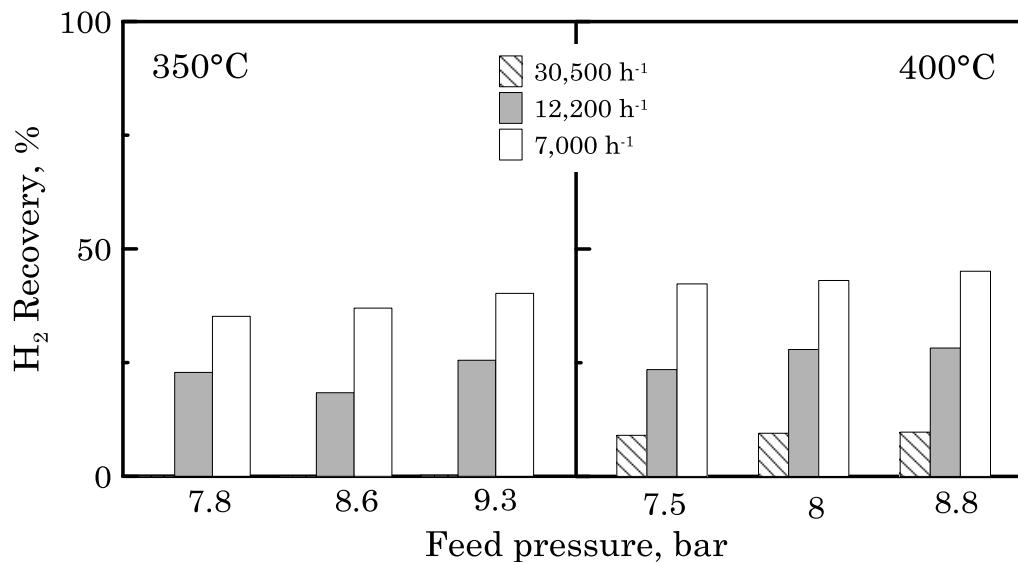

Figure 49 H_2 Recovery as a function of feed pressure for different values of GHSV, measured at 350 and 400°C, respectively.

Both the CO conversion and the H_2 recovery index depend on the GHSV. This latter represents the inverse of the contact time between reactants and catalyst (Eq. 5), therefore the higher the GHSV the lower the CO conversion (Figure 50). Indeed, at 350°C and 8 bar, the CO conversion decreases from 50% to 10% as the GHSV increases, and it happens at 9 bar as well, where the CO conversion drops down from 55% to 14%. Same trends were observed at higher temperature. Moreover, a comparison with the conversions achieved in a traditional reactor is shown in Figure 50. For high GHSV (i.e., 30,500 h^{-1}) the difference between the performance of MR and TR decreases. Since increasing the gas hourly space velocity the contact time between the H_2 in the retentate and the membrane area decreases, the amount of H_2 that can be extracted decreases and the MR behaviour tends to the TR's one. Thus the H_2 percentage removed from reaction side and recovered in the permeate side decreases as the GHSV increases (Figure 51). In addition, lower CO conversion implies smaller hydrogen production or, rather, a depleted H_2 partial pressure on the reaction side. Decreasing the permeation driving force a smaller amount of H_2 can be recovered in the permeate side.
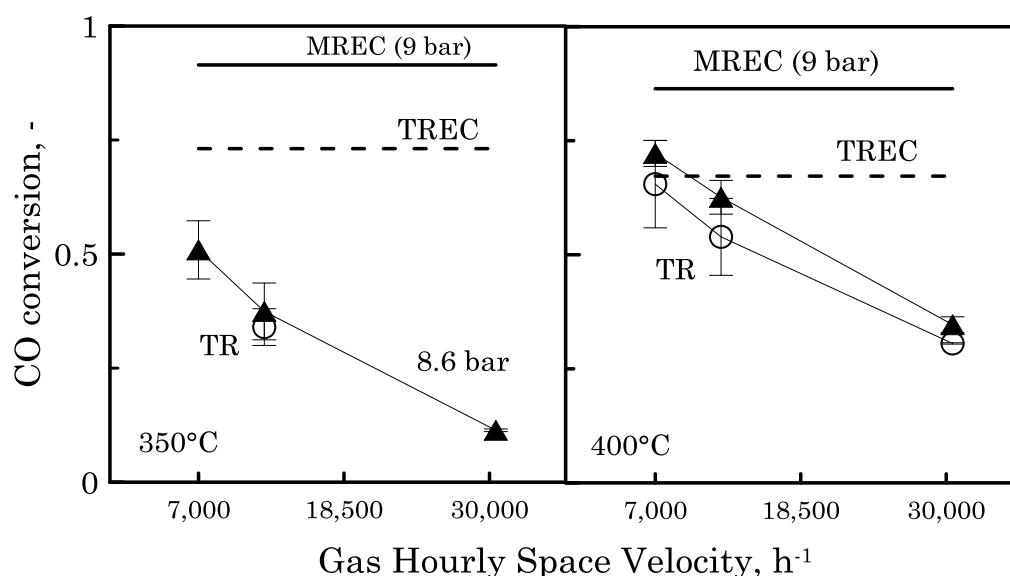

Figure 50 CO conversion as a function of GHSV for traditional and membrane reactors, measured at 350 and 400°C, respectively.
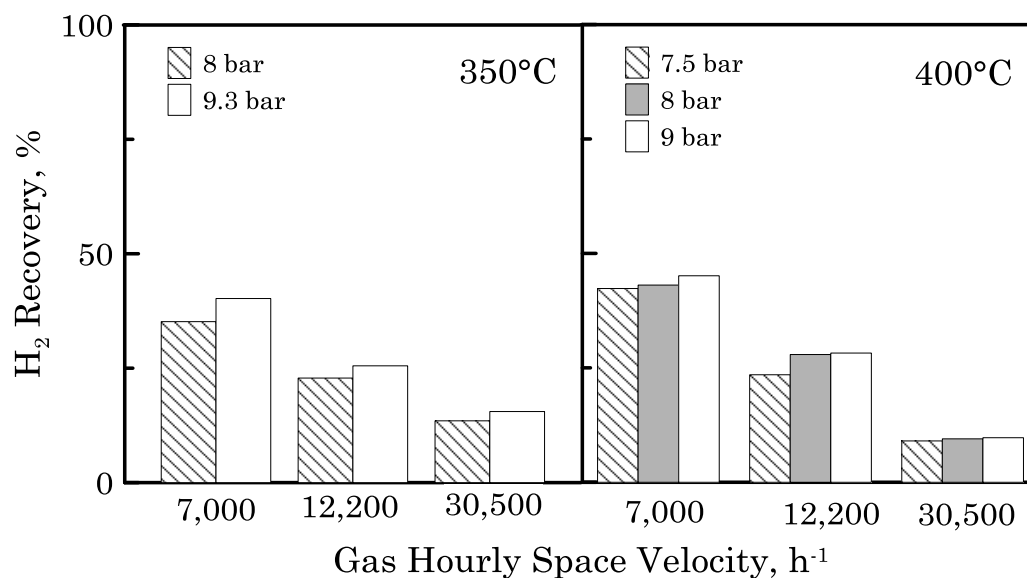
Figure 51 H$_2$ recovery as a function of GHSV at different values of feed pressure, measured at 350 and 400°C, respectively.
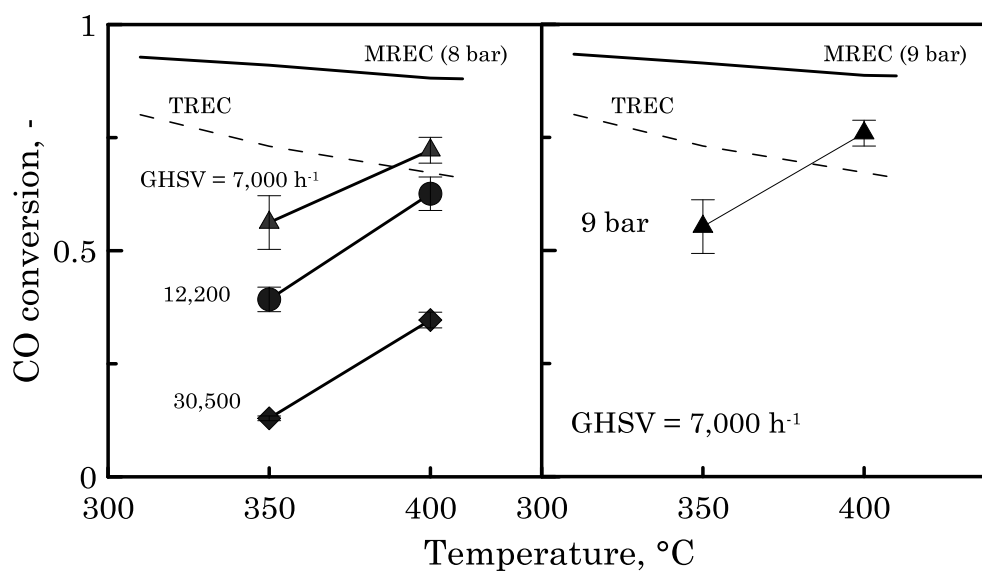

Figure 52 CO conversion as a function of temperature for different values of GHSV and feed pressure (8 bar left side, 9 bar right side).

Figure 52 highlights the effect of the temperature on the CO conversion for different values of feed pressure and GHSV. From a general point of view the high temperature has a dual effect on the reactor performance. Thermodynamically, the high temperature depletes the reaction, as exothermic, nevertheless both the reaction kinetics and the H_2 permeation are favoured, since they follow Arrhenius law. Therefore, as it can be seen in Figure 52, in MR, at a high feed pressure, as the temperature increases, the CO conversion increases as well, the advantages induced on kinetics and H_2 permeation are more significant than the depletion due to the thermodynamics. As a combination of the positive effect supplied by the feed pressure and the high temperature as well, the highest CO conversion (76%) was got at higher pressure (9 bar) and 400°C. Since the H_2 recovery depends on the permeating capacity of the system, the higher the temperature and feed pressure the higher its value (Figure 52). At ca. 9 bar, 7,000 h^{-1} and 400°C, in fact, about 45% of the H_2 fed and produced by reaction was recovered as pure in the permeate side of the MR.

At the end of WGS reaction tests H_2 permeating flux and permeance were measured in a pure hydrogen experiment at temperature of 400 °C. No difference with respect to the value obtained before to perform the reaction tests were found. In addition, it was also investigated the hydrogen permeating flux in reactive condition. In particular, Figure 53 shows the hydrogen permeating flux for pure H_2 feeding stream and during WGS reaction tests. The permeating flux in reaction condition still follows a linear dependence on the Sieverts driving force, however an H_2 permeance reduction is observed. This reduction is due to the CO presence that inhibits the H_2 permeation. In fact, the presence of CO was demonstrated having a negative effect on H_2 permeation [37, 38]. Thus, the present results agree with other experimental result found in the literature [35, 39]. In particular, for a set temperature, the H_2 permeance reduction is higher at a higher space velocity, since, in this case, the CO conversion is lower and CO partial pressure in the retentate side is higher, with consequent higher inhibition effects.
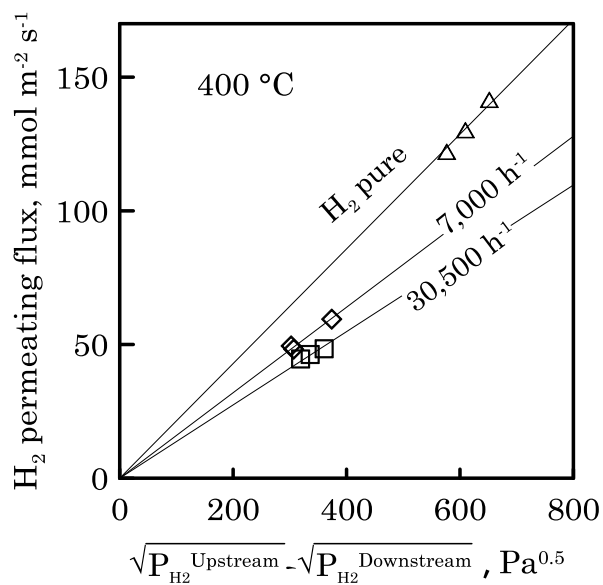
Figure 53 Hydrogen permeating flux as a function of driving force for pure H_2 feeding stream and during WGS reaction tests. Symbols: measured data; lines: linear regression through the axes origin.
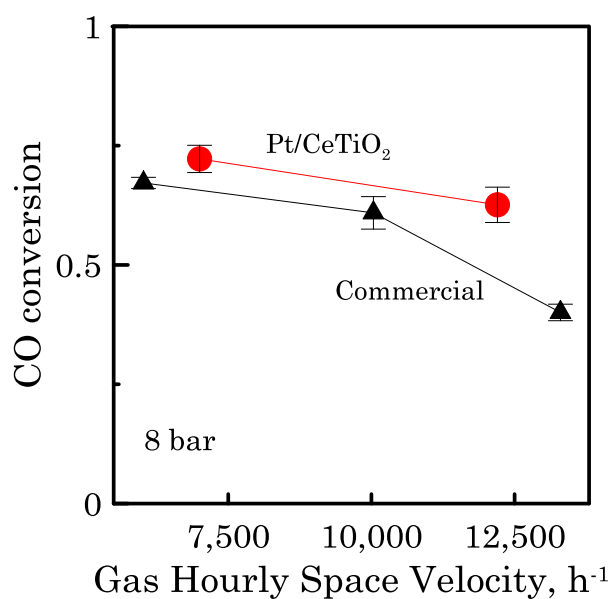

Figure 54 Performance comparison between $Pt/CeTiO_2$ (dots) and commercial catalyst (triangle) [22]. CO conversion as a function of GHSV, measured in MR operating at 8 bar.

A comparison with respect to a commercial catalyst has been also done. In particular, as shown in Figure 54, the results have been compared with experimental literature data, attained applying the same membrane at similar operating condition [22]. The $Pt/CeTiO_2$ catalyst shows better performance, achieving higher CO conversion than the commercial one, also in a range of larger GHSV value, where the commercial catalyst conversion drops.

Finally, after about three months, the reaction tests were also repeated in order to check the stability of membrane and catalyst. In particular, no change in the permeance value at pure hydrogen tests was detected. In terms of MR performance a slight reduction of CO conversion was observed. Figure 55 shows the performance comparison between the first and the second experimental runs.

For a GHSV value of 12,200 h^{-1} and a feed pressure of ca. 8 bar, for instance, the conversion reduction percentage $[(x_{CO}^{old} - x_{CO}^{new})/x_{CO}^{old}, \%]$ is equal to 14%. The conversion decrease could be due to a catalyst deactivation, remaining the membrane property constant.
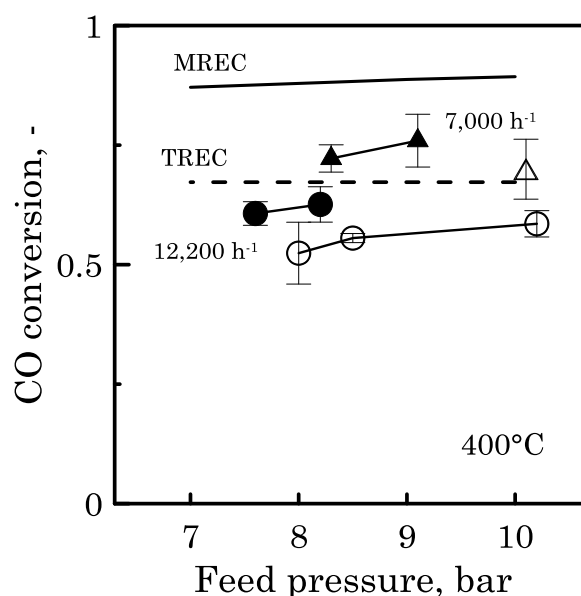

Figure 55 CO conversion as a function of feed pressure for different values of GHSV, at 400°C. Open dots are measured at the first experimental run, filled dots at the second experimental run.

4.3.   Conclusions

The integration of a novel water gas shift reaction catalyst with a palladium membrane was investigated, resulting in a WGS-MR that exhibited good performance.

A syngas mixture was upgraded in one-stage, carrying out the reaction in the high temperature range. A syngas stream simulating the composition of a reformate stream was considered. A commercial 100 micron Pd–Ag membrane, operating at two different reaction temperatures (350 and 400 °C) and up to 10 bar as feed pressure, was used. No sweep gas to promote the permeation was used but only the pressure difference between the two membrane sides.

The performance of the combined system, novel catalyst and Pd-Ag membrane, was evaluated in terms of CO conversion and H_2 recovery, for different feed pressure and a quite wide range of GHSV values.

At the highest temperature, 400 °C, and lowest GHSV value, 7000 h^{-1}, a conversion greater than the traditional reactor equilibrium conversion was obtained. The MR showed satisfactory performance also at higher GHSV, achieving a CO conversion nearby to the equilibrium value. In particular at 12200 h^{-1} and 400 °C, operating condition much closer to actual medium/high temperature WGS industrial application, 63% of CO is converted. The results obtained for the traditional reactor also confirm a good activity of the catalyst, especially at higher temperature. In the MR the fast kinetic together with the H_2 removal allow to exceed the thermodynamic constrain.

A hydrogen production rate of 0.8 Ndm^3/h was found at 9 bar of pressure in the retentate side, 400 °C, and GHSV equal to 7,000 h^{-1}.

The gain in CO conversion and H_2 recovery is more relevant at a higher feed pressure since the latter is responsible for the driving force promoting the H_2 permeation. In the permeate side a pure H_2 stream can be recovered, requiring no further separation step. Operating at 7000 h^{-1} and 9 bar ca. 50% of the H_2 produced by reaction was recovered as pure permeate stream. The recovery index, at each temperature, is a function of the permeation driving

force, permeance in the actual condition and space velocity. In particular, it increases with the permeation driving force and conversion, owing to the higher H_2 production, but decreases with gas space velocity. Moreover, the permeance values in reaction condition were evaluated on the basis of retentate compositions measured during reaction test. The negative impact of the CO inhibition effect on the membrane surface can be the reason of the lower H_2 permeance value obtained.

Finally, the reaction tests repeated after few months confirmed a good stability of the integrated system, membrane and catalyst, showing only a slight reduction of conversion. This is likely due to a less catalytic activity, since the membrane properties remained constant. CO conversion and hydrogen recovery comparable with the ones reported in the literature for the same type of membrane at similar operating condition were achieved. However, further improvement can be obtained if thinner membrane is applied, increasing the H_2 permeation flux and consequently the whole MR performance.

Reference

1. Holladay J.D., Hu J., King D.L., Wang Y., Catalysis Today, 2009,139, 244-260.

2. Babita K., Sridhar S., Raghavan K.V., Int. J. Hydrogen energy, 2011, 36, 6671-6688.

3. Mendes D., Chibante V., Zheng J-M., Tosti S., Borgognoni F., Mendes A., Madeira L. M., Int. J. Hydrogen energy, 2010, 35, 12596-12608.

4. Augustine A. S, Ma Yi Hua, Kazantzis N. K., Int. J. Hydrogen energy, 2011, 36, 5350-5360.

5. Liu Paul KT, Sahimi M. and Tsotsis T. T., Current Opinion in Chemical Engineering, 2012, 1, 1-10.

6. Catalano J, Guazzone F., P. Mardilovich I., Kazantzis N. K and Yi Hua Ma, Ind. Eng. Chem. Res., 2013, 52, 1042-1055.

7. DEMCAMER, DEsign and Manufacturing of CAtalitic MEmbranes Reactors by developing new nano-architectured catalytic and selective membrane materials (Ref.: 262840), http://www.demcamer.org/

8. CACHETII, Carbon dioxide capture and hydrogen production with membranes (Ref.: 241342), http://www.cachet2.eu/

9. COMETHY, Compact Multifuel-Energy To Hydrogen converter (Ref.: 279075), http://www.comethy.enea.it/index.php

10. NEMESIS2+, New Method for Superior Integrated Hydrogen Generation System 2+ (Ref.: 278138), http://www.nemesis-project.eu/home.html

11. NANOWGS, Water-gas shift reaction on metal-oxide nanocatalysts for hydrogen production (Ref.: 303688), http://cordis.europa.eu/project/rcn/102844_en.html

12. Ullman's Encyclopedia of Industrial Chemistry, 5th Completely Revised Edition. Edited by Barbara Elvers, Stephen Hawkins, and William Russey. VCH: New York, 1995. ISBN 3-527-20126-2.

13. Newsome DS. The water–gas shift reaction. Catal Rev Sci Eng, 1980, 21, 275-318.

14. Mendes D., Mendes A., Madeira L. M., Iulianelli A., Sousa J. M. and Basile A., Asia-Pac. J. Chem, 2010, 5, 111-137.

15. H.F. Rase. Handbook of Commercial Catalysts: Heterogeneous Catalysts, CRC Press: 2000, p.520.

16. Twigg M.V., Catalyst Handbook (2nd ed.) Wolfe Publishing Ltd.: London, 1989.

17. Twigg M.V., Spencer M.S., Appl. Catal., 2001, 212(1-2),161-174.

18. Cameron D., Holliday R., Thompson D., J. Power Sources, 2003, 118(1-2), 298-303.

19. Dittmeyer R., Hollein and Daub K., J. Mol. Catal. A: Chem., 2001, 173, 135-184.

20. Tosti S., Basile A., Chiappetta G., Rizzello C. and Violante V., Chem Eng J. 2003, 93, 23-30.

21. Flytzani-Stephanopoulos M., Qi X., Kronewitter S., Water-gas Shift with Integrated Hydrogen Separation Process, Final Report 2004, DEFG2600-NT40819.

22. Brunetti A., Drioli E., Barbieri G., RSC Adv., 2012, 2 (1), 226-233.

23. Stankiewicz A., Moulijn, J. A., Ind. Eng. Chem., Res. 2002, 41(8), 1920-1924.

24. Brunetti A., Caravella A., Barbieri G., Drioli E., Journal of Membrane Science, 2007, 306, 329-340.

25. Ma DH, Lund CRF., Ind Eng Chem Res, 2003, 42, 711.

26. Wang WP, Pan XL, Zhang XL, Xiong GX, Yang WS., Chin J Catal., 2005, 26, 1042-1046.

27. Li H, Goldbach A., Li WZ, Xu HY., J Membr Sci, 2007,299,130-137.

28. Scura F., Barbieri G., De Luca G., Drioli E., Int J. Hydrogen Energy, 2008, 33, 4183-4192.

29. Bi Y., Xu H., Li W., Goldbach A., Int. J. Hydrogen energy, 2009, 34, 2965-2971.

30. Bi YD, Zhang W, Xu HY, Li WZ., Catal Lett., 2007, 119,126-133.

31. Ricote S., Jacobs G., Milling M., Ji YY, Patterson PM., Davis BH., Appl Catal A 2006, 303, 35-47.

32. Phatak AA, Koryabkina N., Rai S., Ratts JL, Ruettinger W., Farrauto RJ, et al., Catal Today, 2007, 123, 224-234.

33. Barbieri G., Brunetti A., Caravella A. and Drioli E., RSC Advances, 2011, 1, 651-661.

34. Marigliano G., Barbieri G., Drioli E., 2001, Catal. Today, 67, 85-99.

35. Barbieri G., Brunetti A., Tricoli G. and Drioli E., J. Power Sources, 2008, 182, 160-167.

36. Barbieri G., Brunetti A., Granato T., Bernardo P., Drioli E., Ind. Eng. Chem. Res.. 2005, 44 (20), 7676-7683.

37. Wadhwani S., Wadhwani A.K., Agarwal R.B., 2002, Clean coal technologies - recent advances. In: First International Conference on Clean Coal Technologies for Our Future, Chia Laguna, Sardinia, Italy, pp.21-23.

38. Barbieri G., Scura F., Lentini F., De Luca G., Drioli E., Sep. Purif. Technol. 61 (2007) 217–224.

39. Brunetti A., Barbieri G., Drioli E., Chemical Engineering Science, 2009, 64, 3448-3454.

Chemical equilibrium analysis of membrane reactor for reaction involving H_2 production: n-butane dehydroisomerization case study

Introduction

Over the years, the focus of the chemical and industrial processes has been addressed towards the development and application of integrated processes, combining the reaction and separation in one single unit, pursuing the logic of Process Intensification [1, 2]. Reduction in equipment number and size, improvement of process efficiency and hence, a better process economy, are some of the expected benefits [3, 4, 5]. As already above presented, the membrane reactor (MR) application, which combines the reaction and separation in the same unit, meets this goal very well. Moreover, in the field of equilibrium limited reactions, the possibility by MR of exceeding the equilibrium constraint of traditional reactors (TRs) has attracted wide attention [6]. In particular, for reversible reactions such as dehydrogenations, the application of MRs, where hydrogen can be removed with high selectivity from the reaction mixture, is an interesting strategy. For such reactions, in fact, the removal of a product can shift the equilibrium, improving the achievable conversion.

In this final chapter, the potentiality of membrane reactor integration in processes involving production of hydrogen, as by-product, has been analysed. In particular, the isobutene production from n-butane by dehydroisomerization reaction has been investigated as case study.

Isobutene is an important intermediate in the petrochemical industry [7] and the forecast is for its worldwide demand to increase; thus the interest in

further improving its production is great. Furthermore, with the ever increasing importance of hydrogen, there is an extra incentive to research especially dehydrogenative-type reactions of light alkanes due to their high H/C molar ratio. Isobutene, owing to the presence of its reactive double bond, can take part in various chemical reactions, such as hydrogenation, oxidation, and other additions, resulting in a great variety of products. One of the most widely used reactions in the industry is the addition of methanol or ethanol to isobutene which leads to two well-known fuel additives: methyl *tert*-butyl ether (MTBE) or ethyl *tert*-butyl ether (ETBE). Besides this important application, isobutene is also used in a variety of polymerization reactions, as a monomer or copolymer for the formation of various products. One of these products is, for instance, butyl rubber, a polymer of isobutene and isoprene. Another promising application of isobutene is the production of antioxidants for food [8].

Currently, isobutene is obtained on a large scale from crude oil, by petrochemical cracking with the butadiene removed, and from butanes, supplied from natural gas reserves and refinery streams [9, 10]. The isobutene production from butanes, used as raw materials, is commonly accomplished by n-butane isomerisation and successive isobutane dehydrogenation [11, 12], with a two-step process.

An interesting alternative is a one-step process, allowing the direct conversion of n-butane to isobutene [13, 14] by the n-butane dehydroisomerization reaction (R3). The latter involves the dehydrogenation of n-butane (R1) and successive isomerisation to isobutene (R2). The main products measured [12] are normal butenes, isobutane and isobutene.

Table 53 Reaction scheme

R1.	n-butane $\leftrightarrow$ n-butene + H_2	$\Delta H_{RX, 298\ K}$ = 130 kJ/mol
R2.	n-butene $\leftrightarrow$ isobutene	$\Delta H_{RX, 298\ K}$ = -17 kJ/mol
R3.	n-butane $\leftrightarrow$ isobutene + H_2	$\Delta H_{RX, 298\ K}$ = 113 kJ/mol

Some bi-functional catalytic systems, usually considering zeolite supported Pt catalysts, have been reported in the literature as successfully catalysts for such direct conversion [15, 16].

The use of catalytic MR for isobutane dehydrogenation has been studied by a number of researchers [17,18,19] that investigated many types of membranes [20] as, for example, γ-alumina, zeolite MFI, Pd/Ag and Pd, dense silica and carbon molecular sieve membranes [21,22,23,24]. The general outcome is that a conversion higher than the one achievable in a traditional reactor can be obtained. In the following analysis, the exploitation of an MR to carry out the direct conversion of n-butane to isobutene was investigated for the reactive system including reactions (R1-R3).

Isobutene production involves many more reactions and chemical species than those included in reactions (R1-R3); the reactions and chemical species lists also depend on the adopted operating conditions and on the catalyst used. However, the simplified reactive scheme allows a first/comprehensive analysis of the hydrogen removal effect on the reactive equilibrium of the reduced chemical system assumed.

Owing to its infinite selectivity toward hydrogen, a Pd-Ag-based membrane has been considered; it allows the recovery of pure hydrogen on the permeate side, thus, no further separation step is required. The shift in equilibrium conversion as a result of the selective extraction of hydrogen in the MR has been evaluated by a thermodynamic analysis, taking into account chemical reaction equilibrium and permeative equilibrium [26] through the membrane. The equilibrium in an MR was described using the same model proposed by [26, 27]. The possibility of defining how much an MR, with respect to a TR, can broaden the thermodynamic constraints for this reaction was analysed. In fact, since the equilibrium conversion is the maximum conversion achievable, it can be useful from a thermodynamic point of view to evaluate the gain that the MR allows.

The effects of temperature, reaction pressure and equilibrium hydrogen pressure on the MR and TR equilibrium conversion have been investigated.

Equilibrium conversions achievable in a membrane and traditional reactors are discussed.

5.1 Thermodynamics

The general criterion of chemical-reaction equilibria is given by the following equation:

$$\sum_i v_i \mu_i = 0$$

Eq. 77

Substituting the expression for chemical potential in function of activity, Eq. 78, and upon rearrangements yield (Eq. 79):

$$\mu_i = G_i^\circ + RT \ln \hat{a}_i$$

Eq. 78

$$\prod_i \hat{a}_i^{v_{i,j}} = K_j$$

Eq. 79

where $\quad K_j \equiv \exp\left(\frac{-\Delta G_j^\circ}{RT}\right)$

The quantity K_j is the chemical-reaction equilibrium constant for reaction j, v_i is the stoichiometric coefficient of the species i and $\Delta G_j°$ is the corresponding standard Gibbs-energy change of reaction, depending only on temperature. It follows that also K_j is only a function of temperature.

For gas phase reaction, the activity can be expressed in term of fugacity coefficient ($\hat{a}_i \equiv \hat{f}_i/f_i^\circ = y_i \hat{\phi}_i p/f_i^\circ$). Moreover, when the phase of an ideal gas can be assumed, $\hat{\phi}_i = 1$, the Eq. 79 becomes:

$$\prod_i y_i^{v_{i,j}} \left(\frac{p}{p^\circ}\right)^{v_j} = K_j$$

Eq. 80

where $v_j \equiv \sum_i v_{i,j}$ and $p°$ is the standard-state pressure of 100 kPa, expressed in the same unit used for p.

This result might also be generalised to a system in which many chemical reactions independently occur and, in particular, has been used in the following analysis where dehydrogenation and isomerisation reaction are considered. The equilibrium composition has been calculated by means of a

suitable stoichiometric method with the concept of a chemical equilibrium constant [25].

The n-butane dehydrogenation is an endothermic reaction occurring with an increment of number of moles, thus the equilibrium conversion is favoured by high temperature and low pressure. To evaluate the number of moles present at the equilibrium, the dehydrogenation and isomerisation can be considered as a series reaction system. The thermodynamic analysis performed was based on significant assumptions including:

> no side-reactions occurring

> only linear butene and isobutene production.

Even though a real reactive system involves more reactions and chemical species, as first step a simplified scheme allows a comprehensive analysis of the conversion shift owing to a selective product removal from the reaction volume.

5.1.1 Thermodynamics of a traditional reactor

The determination of the number of moles in a TR is based on thermodynamic and stoichiometric calculations. Table 54 summarizes the mass balance for the reactive species involved, considering the reactions as a series reaction system. x is the n-butane conversion for the dehydrogenation reaction (R1) and w the n-butene conversion for isomerisation (R2).

At the initial stage only (n_0) moles of n-butane are present. Then dehydrogenation reaction converts ($n_0 x$) moles of n-butane in ($n_0 x$) moles of n-butene and ($n_0 x$) moles of hydrogen (Table 54, Reactive state of reaction 1). The isomerization converts a fraction (w) of the total ($n_0 x$) moles of n-butene in isobutene (Table 54, Reactive state of reaction 2). The moles number of each species at equilibrium are a function of the conversion degrees x and w of both reactions. The mole fractions of all the species involved in the reactions, at equilibrium condition, are reported in Table 55.

The equilibrium conversions can be then evaluated by substituting in the equilibrium constants, Eq. 81 and Eq. 82, the mole fractions, as expressed in Table 55. The expression of equilibrium constant for both reactions are:

$$K_{eq1} = \frac{y_{hydrogen} \quad y_{n\text{-}butene}}{y_{n\text{-}butane}} \, p^{Reaction} = \frac{(1 - x)}{(1 + x)(1 - w)} \, p^{Reaction} = f(T)$$

Eq. 81

$$K_{eq2} = \frac{y_{isobutene}}{y_{n\text{-}butene}} = \frac{w}{(1 - w)} = f(T)$$

Eq. 82

Table 54 Number of moles determination in the reactive state and at equilibrium in a traditional reactor

Moles	n-butane	n-butene	isobutene	hydrogen
initial state	n_0	-	-	-
Reactive state of reaction 1	$- n_0 x$	$n_0 x$	-	$n_0 \, x$
Reactive state of reaction 2		$- n_0 x \, w$	$n_0 \, x \, w$	
Equilibrium state	$n_0 (1 - x)$	$n_0 \, x \, (1 - w)$	$n_0 \, x \, w$	$n_0 \, x$
total number of moles			$n_{total} = n_0 (1 + x)$	

Table 55 Mole fractions in the state of equilibrium of reactions R1 and R2

Species	molar fraction
n-butane	$\dfrac{n_0 \, (1 - x)}{n_0 \, (1 + x)} = \dfrac{(1 - x)}{(1 + x)}$
n-butene	$\dfrac{n_0 \, x \, (1 - w)}{n_0 (1 + x)} = \dfrac{x \, (1 - w)}{(1 + x)}$
isobutene	$\dfrac{n_0 \, x \, w}{n_0 (1 + x)} = \dfrac{x \, w}{(1 + x)}$
hydrogen	$\dfrac{n_0 \, x}{n_0 (1 + x)} = \dfrac{x}{(1 + x)}$

The mass balance at the equilibrium condition, as reported in Table 54, allows to evaluate the composition of a TR, for a given initial condition (n_0), when the conversions (x and w) of reaction 1 and reaction 2 are known.

5.1.2 Thermodynamics of a membrane reactor

The thermodynamic analysis of an MR is similar to the TR ones. The difference between TR and MR is the selective permeation through the membrane of one or more species. In an MR the overall reaction unit can be considered as divided into two compartments: one part is the reaction volume and the other is the permeation volume. In this case the hydrogen selective membrane allows removing the hydrogen from the reaction volume. A part of the produced hydrogen permeates through the membrane into the permeation side. As long as the hydrogen partial pressure in the reaction volume is higher than the partial pressure in the permeate side there is permeating flux. When the partial pressures of hydrogen, on both membrane sides, are equal, no hydrogen permeation happens and then the permeative equilibrium is reached [26]. In the permeative equilibrium state, the partial pressure of hydrogen on both membrane sides is also equal to the equilibrium hydrogen partial pressure; this condition is expressed by Eq. 83.

$$p_{hydrogen}^{Equilibrium} = p_{hydrogen}^{Permeate\ side} = p_{hydrogen}^{Reaction\ side}$$

Eq. 83

Therefore, the thermodynamic equilibrium in an MR is reached if the two following conditions are simultaneously satisfied:

➢ reactive equilibrium in the reaction side

➢ permeative equilibrium between reaction and permeation side.

In this case, hydrogen permeates through a 100% hydrogen-selective membrane, and it is recovered in the permeation side (Table 56): the MR allows the separation from the reaction volume of one of the products. Table 56 reports the reactive states for reaction R1 and R2, as Table 54, but also includes the information for hydrogen permeation through the variable "z".

The latter is the fraction of hydrogen in the permeation side compared to the total hydrogen produced. The difference with respect to TR is introduced by the negative term referred to the hydrogen permeation. Therefore, the moles number of each species at the equilibrium, reactive and permeative, is a function of the conversion degrees of both reactions (x and w) and hydrogen fraction permeated (z).

Table 56 Number of moles determination at reactive and permeative equilibrium in a membrane reactor

Moles	n-butane	n-butene	isobutene	hydrogen
Initial state	n_0	-	-	-
Reactive state of reaction R1	$- n_0 x$	$n_0 x$	-	$n_0 x$
Reactive state of reaction R2		$- n_0 x w$	$n_0 x w$	
Permeation state	-	-	-	$- n_0 x z$
Permeative and reactive equilibrium state	$n_0 (1 - x)$	$n_0 x (1 - w)$	$n_0 x w$	$n_0 x (1 - z)$
total number of moles				$n_0(1 + x - xz)$

Taking into account only the reaction volume, the total moles number for the MR is lower than the TR since part of the hydrogen produced is in the permeation volume (see Table 56, last row).

Table 57 reports the mole fractions of all the species, at reactive and permeative equilibrium condition, as a function of the three variables characterizing the MR equilibrium.

As well as for the traditional reactor, the mass balance on the MR, as reported in Table 56, allows to evaluate the equilibrium composition. In the case of MR the equilibrium condition is achieved when both reactive and permeative equilibrium state are reached; thus the equilibrium composition depends on the equilibrium conversions, x and w, and on the hydrogen fraction permeated, z.

The conversions of reactions R1 and R2 are calculated through the equilibrium constants also including the constraint introduced by Eq. 83 for the permeative equilibrium state.

Table 57 Mole fraction in the equilibrium state

Species	mole fraction
n-butane	$\dfrac{n_0 \, (1 - x)}{n_0 \, (1 + x - xz)} = \dfrac{(1 - x)}{(1 + x - xz)}$
n-butene	$\dfrac{n_0 \, x \, (1 - w)}{n_0(1 + x - xz)} = \dfrac{x \, (1 - w)}{(1 + x - xz)}$
Isobutene	$\dfrac{n_0 \, x \, w}{n_0(1 + x - xz)} = \dfrac{x \, w}{(1 + x - xz)}$
Hydrogen	$\dfrac{n_0 \, x \, (1 - z)}{n_0(1 + x - xz)} = \dfrac{x \, (1 - z)}{(1 + x - xz)}$

The expressions of the equilibrium constants, as a function of x, w, z and reaction pressure, for reactions R1 and R2 are reported in Table 58 and Table 59, respectively. By substituting the molar fractions expression into Eq. 83, the following equation for equilibrium hydrogen partial pressure is obtained:

$$p_{hydrogen}^{Equilibrium} = p^{Reaction\ side} \, \frac{x \, (1 - z)}{(1 + x - xz)}$$

Eq. 84

The mathematical set of equations results in three equations (e.g., Eq. 84, Eq. 85d and Eq. 86d) that can be resolved for obtaining the three variables x, w, z using the equilibrium constants and reaction pressure values as inputs.

Table 58 Equilibrium constant for reaction R1 at reactive and permeative equilibrium, as a function also of x, w and z

$$K_{P1} = \frac{p_{hydrogen}^{Reaction\ side}\ p_{n\text{-}butene}^{Reaction\ side}}{p_{n\text{-}butane}^{Reaction\ side}} \qquad\qquad \text{Eq. 85a}$$

$$K_{P1} = \frac{y_{hydrogen}^{Reaction\ side}\ y_{n\text{-}butene}^{Reaction\ side}}{y_{n\text{-}butane}^{Reaction\ side}}\ P^{Reaction\ side} \qquad\qquad \text{Eq. 85b}$$

$$K_{P1} = \frac{x(1-z)}{(1+x-xz)}\ \frac{x\,(1-w)}{(1+x-xz)}\ \frac{(1+x-xz)}{(1-x)}\ P^{Reaction\ side} \qquad\qquad \text{Eq. 85c}$$

$$K_{P1} = \frac{x^2(1-z)(1-w)}{(1+x-xz)(1-x)}\ P^{Reaction\ side} \qquad\qquad \text{Eq. 85d}$$

Table 59 Equilibrium constant for reaction 2 at reactive and permeative equilibrium, as a function also of x, w and z

$$K_{P2} = \frac{p_{isobutene}^{Reaction\ side}}{p_{n\text{-}butene}^{Reaction\ side}} \qquad\qquad \text{Eq. 86a}$$

$$K_{P2} = \frac{y_{isobutene}^{Reaction\ side}}{y_{n\text{-}butene}^{Reaction\ side}} \qquad\qquad \text{Eq. 86b}$$

$$K_{P2} = \frac{n_0\ x\ w}{n_0\ x\ (1-w)} \qquad\qquad \text{Eq. 86c}$$

$$K_{P2} = \frac{w}{(1-w)} \qquad\qquad \text{Eq. 86d}$$

5.2 Results and discussion

On the basis of the analysis carried out the effects of operating variables such as temperature, reaction pressure and equilibrium hydrogen partial pressure have been investigated. In particular, the equilibrium performance of both traditional and membrane reactor have been calculated, analysing how the operating variable influence the behaviour of both reaction system.

5.2.1 Temperature effect

Figure 56 shows the n-butane equilibrium conversion for the overall reaction (R3) as a function of the temperature, in an MR and in a TR. For both reactors, the conversion increases at a higher temperature because the reaction is endothermic and the MR does not affect the conversion dependence on the temperature. The membrane reactor equilibrium conversion (MREC) is higher than the traditional reactor equilibrium conversions (TREC). Only when the temperature is under 400°C, the TREC exceeds the MREC owing to the back-permeation occurring in the MR. In the permeate the hydrogen partial pressure is, in fact, equal to 0.1 bar. On the other side of the membrane, which is the reaction volume, the partial pressure of hydrogen is lower than 0.1 bar owing to the very low value of conversion; as a consequence, back-permeation occurs. Higher temperatures promote the conversion that increases the partial pressure of hydrogen in the reaction side and thus depleting the back-permeation. In the temperature range between 450 and 600 °C the MR shows the better performance with respect the traditional reactor. At higher temperature, since the dehydroisomerization reaction is endothermic, in both reactors the equilibrium conversion approaches the unitary value. Therefore, an MR allows achieving higher conversion then a traditional reactor, operating also at lower temperature.
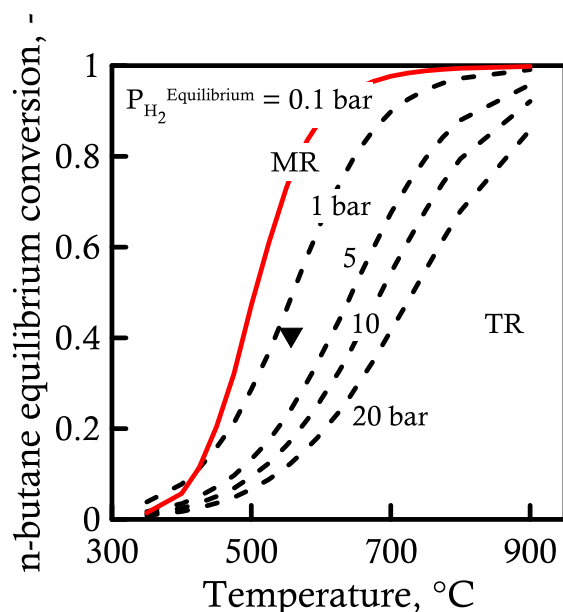
Figure 56 n-Butane dehydroisomerization (R3): equilibrium conversion of a membrane (solid line) and traditional (dashed line) reactors as a function of temperature, at different reaction pressures. For the MR, the equilibrium hydrogen partial pressure is equal to 0.1 bar. Symbols refer to experimental measurement with a feed composition of 10% n-butane, 20% hydrogen, 70% argon (▼) 557°C, 1.8 bar WHSV=9.9 h^{-1} [28].

5.2.2 Pressure effect

As shown in Figure 56, the pressure negatively affects the equilibrium conversion of TR (dashed curves). For instance, at 600°C and 1 bar the equilibrium conversion is around 0.64, but it is much lower (i.e., 0.25) at a reaction pressure of 10 bar. On the contrary, the equilibrium conversion of the MR does not change when the reaction pressure at a set equilibrium hydrogen pressure is varied. The solid curve is the equilibrium conversion achievable in an MR at an equilibrium hydrogen partial pressure of 0.1 bar, for any reaction pressure.

The comparison of MREC and TREC is shown in Figure 57, for an equilibrium hydrogen partial pressure of 1 bar. As a general trend, in the range of reaction pressure between 1 and 20 bar at a low temperature the MR equilibrium conversion is lower than the TR one. Moreover, under these conditions the MREC is always lower than the TREC when the reaction pressure in the TR is low (i.e., 1 bar). As already mentioned, the high

equilibrium hydrogen partial pressure causes the hydrogen back-permeation, which depletes the equilibrium conversion obtainable in an MR. However, at a higher temperature and reaction pressure, the MREC profile exceeds the TREC, also at high $P_{H2}^{Equilibrium}$.
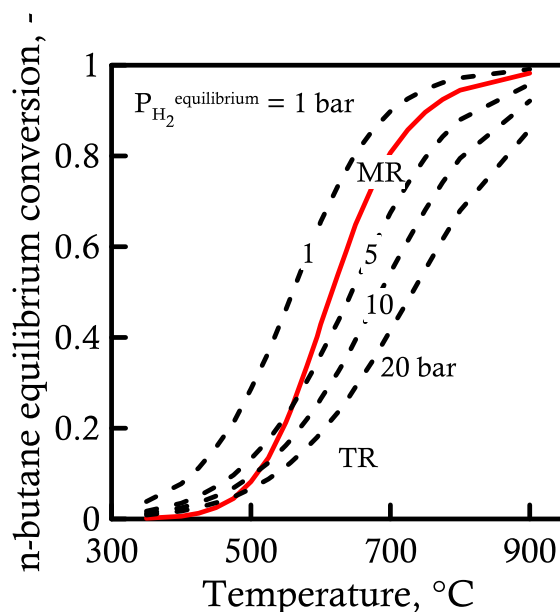

Figure 57 n-Butane dehydroisomerization (R3): equilibrium conversion of membrane (solid line) and traditional (dashed lines) reactors as a function of temperature, at different reaction pressures. For the membrane reactor, the equilibrium hydrogen partial pressure is equal to 1 bar.

The temperature at which the MREC exceeds the TREC is also determined by the reaction pressure: it is higher and higher as the pressure is lower and lower. For instance, 480, 525, 557°C at 20, 10 and 5 bar, respectively.

As already mentioned, the n-butane conversion for the MR depends actually only on the equilibrium hydrogen partial pressure, as shown in Figure 58. The higher the equilibrium hydrogen partial pressure the lower the conversion. This is due to the lower amount of hydrogen transported on the other membrane side. Even though, by increasing equilibrium hydrogen partial pressure MREC profiles seem similar to those shown by the TR, varying the reaction pressure (see Figure 1 dashed curves), the effect of that parameter is quite different. For a clearer understanding, Figure 59 shows

the n-butane equilibrium conversion as a function of the reaction pressure at a set equilibrium hydrogen partial pressure of 1 bar.
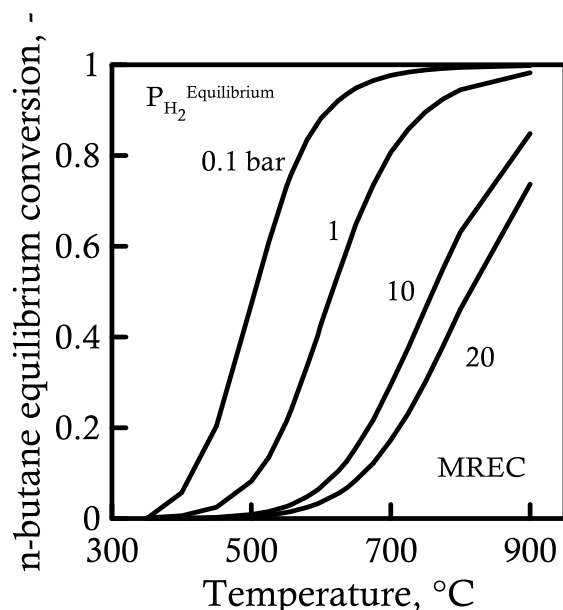

Figure 58 n-Butane dehydroisomerization (R3): membrane reactor equilibrium conversion (MREC) as a function of temperature at different equilibrium hydrogen partial pressure.

The reaction pressure does not affect the MR equilibrium conversion although the TR significantly undergoes the negative effect of the pressure. It does not change the MR conversion owing to the removal of hydrogen from the reaction volume that overtakes this negative effect (Figure 59). Moreover, the MR at a lower temperature achieves the same conversion of a TR, for the same operating pressure. For instance, the MR operating at 550°C has the same conversion of a TR operated at 625°C, for a reaction pressure of 20 bar. Figures 1 and 4 also show the reaction conversions of experimental measurements [14, 23] using two catalysts, for the same feed composition. These values, close to the ones calculated by the thermodynamic analysis, confirm the validity of the assumptions considered in the proposed analysis, in particular, regarding the hypothesis on the reaction scheme assuming linear butene and isobutene as main reaction products.
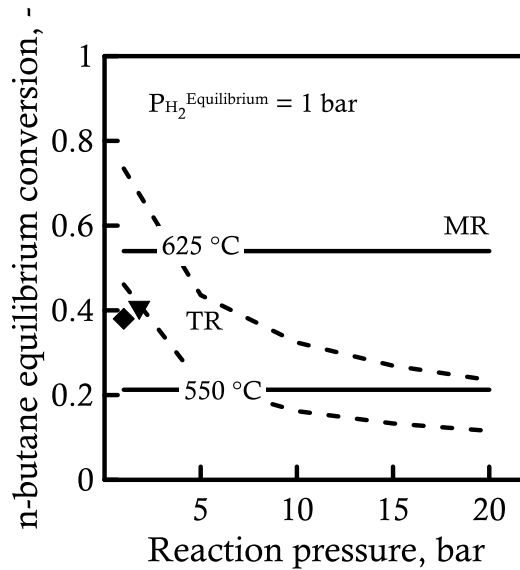
Figure 59 n-Butane dehydroisomerization (reaction 3): equilibrium conversion of membrane (solid lines) and traditional (dashed lines) reactors, at different temperatures, as a function of reaction pressure. The equilibrium hydrogen partial pressure is equal to 1 bar. Symbols refer to an experimental measure with a feed molar composition of 10% n-butane, 20% hydrogen, 70% argon: (▼) 557°C, 1.8 bar, WHSV=9.9 h^{-1} [28]; (♦) 500°C, 1 bar WHSV=23 h^{-1} [29].

5.3   Comparison of MR and TR at equilibrium condition

For estimating the best condition allowing the highest reachable conversions in an MR compared to the traditional one, the evaluation of the distance between the MREC and TREC, operating at the same conditions, appears of interest. A specific index (Eq. 87), already reported in literature [21], was used to quantify this distance; it is defined as the ratio of conversion in an MR and that in a TR calculated in equilibrium condition

$$CI|_{Equilibrium} = \frac{MREC}{TREC}, \quad -$$

Eq. 87

This variable, plotted as a function of the temperature (Figure 60), identifies two regions: one where the MREC is higher than the TREC and another where the opposite behaviour occurs. At high pressure the MREC is higher than the TREC since the MR operates in successful way. The MR, in fact, can operate at a higher pressure, without "paying" any penalty in term of conversion as instead happens for TR. Therefore, the advantages offered by

181

the MR, with respect to the TR, increase by increasing the reaction pressure. The TREC is greater than MREC only in the region of low temperature and pressure, where the MR cannot operate because of the back-permeation. In addition, the maximum improvement in MR conversion, compared to the traditional one, occurs at a temperature of 625°C, for each reaction pressure investigated (Figure 60 left side). The curves, drawn as a function of temperature, show a maximum owing to the thermodynamic effect on the reaction at both low and high temperature. Indeed, at a low temperature the MREC is similar or lower than TREC, because of the thermodynamics and consequentially of the back permeation. In the high temperature range, since the reaction is thermodynamically favoured, both MREC and TREC tend to unitary value thus there is no large margin for MR advantages. At the best condition (625°C and 20 bar) the MREC shows a value more than twice than TREC.

The distance of MREC from TREC is greatly increased for lower equilibrium hydrogen partial pressure. For an equilibrium hydrogen partial pressure of 0.1 bar (Figure 60, right side), in the whole temperature range investigated, the MREC exceeds the TREC also at low reaction pressure: the MREC is 3-7 times higher than TREC. In addition, at this lower equilibrium hydrogen partial pressure, the maximum improvement in the MREC is shifted at lower temperatures (500°C). An MR operating at 500°C, 20 and 0.1 bar as reaction and equilibrium hydrogen pressures respectively allows obtaining an equilibrium conversion approximately equal to 50%, seven times higher than that of a TR, equal to ca. 7%. Considering that the equilibrium conversion is the thermodynamic limit which sets the maximum possible conversion, on the basis of the above analysis it can be concluded that the use of an MR can powerfully enhance these dehydrogenative-type reactions.
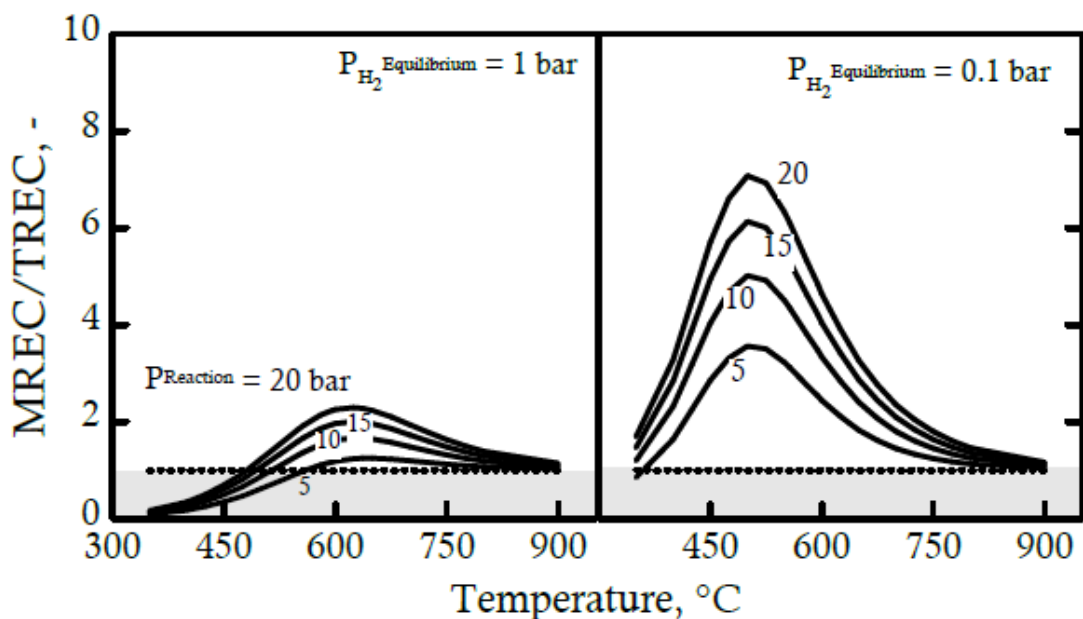
Figure 60 Comparison of membrane reactor equilibrium conversion (MREC) and traditional reactor equilibrium conversion (TREC) as a function of temperature at different reaction pressures. For the membrane reactor, equilibrium hydrogen partial pressure is 1 bar and 0.1 bar for left-side and right-side sections, respectively.

5.4 Conclusion

The shift in equilibrium conversion of dehydroisomerization reactions as a result of selective extraction of hydrogen was evaluated in a membrane reactor by simultaneously taking into account the chemical reaction and permeative equilibria. The n-butane dehydroisomerization is an endothermic reaction and therefore high temperature raises the equilibrium conversion, also in a membrane reactor. The membrane reactor shows the largest improvement with respect to the traditional reactor at high reaction pressure and lowest equilibrium hydrogen partial pressure. The peculiarity of the selective hydrogen removal in the membrane reactor allows the exploitation of the positive effect of the reaction pressure on the hydrogen permeation and consequentially on the conversion. On the contrary, in a traditional reactor increasing the pressure the conversion depletes, since the reaction occurs with an increase in the number of moles. Moreover, the hydrogen partial

pressure at the equilibrium state is another variable affecting the equilibrium conversion in a membrane reactor. A lower equilibrium hydrogen partial pressure leads to a higher removal of the amount of hydrogen from the reaction volume, which promotes the equilibrium shift.

The performed analysis also provides an estimation of the best conditions, in the range of temperature and pressure investigated, which allows achieving the highest reachable conversions in a membrane reactor compared to that of the traditional one. A membrane reactor operating at 500°C, 20 bar and 0.1 bar, reaction and equilibrium hydrogen partial pressures, respectively, shows a conversion seven times higher than that obtainable in a traditional reactor. These results clearly confirm the potentiality of the membrane reactor to carry out this reaction, showing how much the MR application can increase the maximum conversion achievable. An experimental investigation could be therefore performed at the theoretically estimated best operating condition.

List of symbols

N   Total number of moles, -

X n-Butane equilibrium conversion, -

W n-Butene equilibrium conversion, -

Z Hydrogen in the permeate side and hydrogen produced ratio, -

K_P Equilibrium constant expressed in terms of partial pressure

P   Pressure, bar

Y Molar fraction, -

Subscript / superscript

0   Initial referred to

Equilibrium   Equilibrium referred to

total   Total referred to

References

1. Stankiewicz A., Moulijn J. A., Chem. Eng. Prog., 2000, 96(1), 22-23.

2. Stankiewicz A., Moulijn, J. A., Ind. Eng. Chem., Res. 2002, 41(8), 1920-1924.

3. Drioli E., Brunetti A., Di Profio G., Barbieri G., Green Chem., 2012, 14, 1561-1572.

4. Brunetti A., Caravella A., Drioli E., Barbieri G., Chemical Engineering and Technology, 2012, 35, 1238-1248.

5. Barbieri G., Brunetti A., Caravella A., Drioli E. RSC Adv., 2011, 1 (4), 651-661.

6. Weyten H., Luyten J., Keizer K., WillemsL., Leysen R., Catalysis Today, 2000, 56, 3.

7. U.S. Energy Information Administration Home Page. http://www.eia.gov/ (accessed November 20, 2012).

8. Chemeurope Home Page. http://www.chemeurope.com/en/encyclopedia/Isobutylene%2F.html (accessed November 20, 2012).

9. Romanow-Garcia S., Hoffman HL., Petroleum and its products. In Handbook of industrial chemistry and biotechnology Kent J. A, Kent and Riegel's, Eds.,Springer: New York, 2007; pp. 801–842.

10. Obenaus F., Droste W., Neumeister J., Butenes. In: Ullmann's Encyclopedia of Industrial Chemistry, Wiley-VCH: 2005.

11. Buonomo F., Sanfilippo D., Trifirò F., Dehydrogenation reactions, In Handbook of Heterogeneous Catalysis, Ertl, G., Knozinger, H., Weitkamp, J., Eds.; Wiley-VCH: Weinheim. Germany, 1997; vol. 5, pp. 2140–2151.

12. Pirngruber G. D., Seshan K., Lercher J. A., Journal of Catalysis, 2000, 190, 338–351.

13. Li X., Iglesia E., Journal of Catalysis, 2008, 255, 134–137.

14. Scirè S., Burgio G., Crisafulli C., Minicò S., Applied Catalysis A: General, 2004, 274, 151–157.

15. Pirngruber G. D., Seshan K., Lercher J. A., Journal of Catalysis, 1999, 186, 188–200.

16. Bee Derouane-Abd Hamid S., Lambert D, Derouane Eric G., Catalysis Today, 2000, 63, 237–247.

17. van den Bergh J., Gücüyener C., Gascon J., Kapteijn F., Chemical Engineering Journal, 2011, 166, 368–377.

18. Yanglong G., Guanzhong L., Yunsong W., Ren W., Separation and Purification Technology, 2003, 32, 271-279.

19. Babak V. N., Babak T. B., Zakiev, S. E. et. al. Theoretical Foundations of Chemical Engineering, 2009, 43, 74-87.

20. Sanchez, J., Tsotsis T.T., Catalytic Membranes and Membrane Reactors, Wiley-VCH: Weinheim, 2002.

21. Casanave D., Giroir-Fendler A., Sanchez J., Loutaty R., Dalmon J.A., Catalysis Today, 1995, 25, 309.

22. van Dyk L., Miachon S., Lorenzen L., Torres M., Fiaty K., Dalmon J.-A., Catalysis Today, 2003, 82, 167.

23. Liang, W.Q., HughesR., Catalysis Today, 2005, 104, 238.

24. Sznejer G.; Sheintuch M., Chemical Engineering Science, 2004, 59, 2013.

25. Perry RH, Green DW, Maloney JO. Perry's chemical engineers' handbook, (7th Edn), McGraw-Hill, New York 1977.

26. Marigliano G., Barbieri G., Drioli E., Chem. Eng. and Processing, 2003, 42, 231-236.

27. Barbieri G., Marigliano G., Perri G., Drioli E., Ind. Eng. Chem. Res., 2001, 40, 2017.

28. Alireza S., Rezai S., Traa Yof alkanes, J. Membr. Sci., 2008, 319, 279−285.

29. Pirngruber G. D., Seshan K., Lercher J. A., J. Catal., 2000, 190, 396−405.

Conclusion

In this thesis the MR integration in hydrogen production process has been investigated. In particular, the attention has been addressed to the following topics:

1. Design of a pilot scale WGS-MR to produce H_2 by reformate stream upgrading.
2. Integration of WGS-MR in small scale hydrogen generator (100 Nm^3/h H_2) and process plant simulation.
3. Post processing of WGS-MR retentate stream by membrane gas separation technology application for CO_2 recovery.
4. Experimental analysis of a novel WGS catalyst integrated in a membrane reactor.
5. Investigation of the potentiality of MR integration in process involving H_2 production. The isobutene production by n-butane dehydroisomerization has been considered as a case study.

In details, the performed work and results can be summarized as follows.

1.1. For the pilot scale WGS-MR design, the application of a sweep stream or a vacuum pump, both promoting the driving force for the permeation, are required to reach the performance target.

1.2. A preliminary estimation of the required membrane area has been obtained for a fixed permeate H_2 molar flow rate and target permeance, by calculating the permeation driving force through an analogy with heat exchangers. Results from the rigorous MR modelling and simulation, only show a slight difference in terms of required membrane tubes number between the scenarios. Thus, to define the best option between vacuum and sweep scenario, other factors related, for instance, to the operating cost, to ease of designing and operating, have to be considered.

2.1 The WGS-MR integration implies a re-design of the process downstream the membrane reactor, since the permeate and retentate have to be processes in a different way wit respect to the conventional technology.

2.2 In the MR integrated process the hydrogen separation unit is no more required since more than 90% of produced H_2 can be directly recovered in the permeate stream. The recovered hydrogen has to be compressed since the MR delivers a high purity hydrogen stream at slightly above the atmospheric pressure.

2.3 Since the retentate stream is a high-pressure CO_2-rich stream, it can be sent to a membrane separation unit for CO_2 capture, using the remaining offgas as valuable process fuel in the reformer furnace.

2.4 The comparison between sweep and vacuum scenarios showed a small difference in term of H_2 productivity and raw material exploitation but significant difference in the electricity consumption. Therefore, to define the best solution, an H_2 production cost estimation, for both scenarios, is required.

2.5 In the logic of process intensification, the WGS-MR integration results, with respect to the conventional system, in a more "intensified" process since an higher H_2 productivity, enhanced exploitation of raw materials are obtained and less and smaller equipment are needed.

2.6 Behind the proved technical feasibility of WGS-MR integrated system, an economic evaluation is needed to compare both technologies and find in which conditions the MR integrated system is more cost-effective than the traditional one.

3.1. In the post processing of WGS-MR retentate, the technological feasibility of membrane gas separation system application to CO_2 capture has been discussed.

3.2. The application of a membrane with enhanced CO_2/H_2 selectivity (i.e., PEBAX/PEG) allows to achieve the required CO_2 purity target (>95%) in a two stages membrane gas separation unit. The highest purity obtainable with low CO_2/H_2 selectivity (ca. 1) membrane is instead about 85%.

3.3. If the purity target is pursued, a penalty in term of CO_2 recovery his paid. The highest CO_2 recovery achievable is ca. 50%,whereas the target value is in the range of 80- 90%.

3.4. Membrane with tuned selectivity toward H_2, N_2, CH_4 (depending on retentate composition) and large CO_2 permeance value should be developed for this novel application.

4.1. The integration of a novel water gas shift reaction catalyst with a commercial Pd–Ag membrane, investigated in this thesis, resulted in a WGS-MR exhibiting good performance. In particular, operating at high temperature and low GHSV values, higher conversion with respect to the traditional reactor equilibrium conversion was obtained.

4.2. For the same kind of membrane at similar operating condition, novel catalyst showed better performance with respect to the commercial ones reported in the literature.

4.3. The reaction tests repeated after few months confirmed a good stability of the integrated system, membrane and catalyst, showing only a slight reduction of conversion.

5.1. The chemical equilibrium analysis for n-butane dehydroisomerization reaction confirmed the potentiality of MR to carry out reactions involving H_2 production as by-product, showing how much the MR application can increase the maximum conversion achievable.

5.2. Membrane reactor equilibrium conversion up to seven times higher than the one of a traditional reactor can be attained.

5.3. From a thermodynamic point of view, the selective hydrogen removal in the MR makes the equilibrium conversion independent on the reaction pressure. This allows the exploitation of the positive effect of the reaction pressure on the hydrogen permeation and consequentially on the conversion.

Acknowledgment

Appendix

Papers on scientific ISI journals

H. A. Al-Megren, G. Barbieri, I. Mirabelli, A. Brunetti, E. Drioli, M.C. Al-Kinany, "Direct conversion of n-butane to isobutene in membrane reactors: a thermodynamic analysis", Ind. & Eng. Chem. Res., 2013, 52, 10380-10386, http://dx.doi.org/10.1021/ie400006c

G. Barbieri, I. Mirabelli, A. Brunetti, E. Drioli, H. A. Al-Megren, M.C. Al-Kinany, "Direct conversion of n-butane to iso-butene in membrane reactors: a thermodynamic analysis", Chemical Engineering Transaction 2013.

Paper in preparation

Mirabelli, A. Brunetti, G. Barbieri, E. Drioli; "Post processing of WGS-MR streams for CO_2 capture by membrane gas separation system".

"Analysis of WGS membrane reactor integration in small scale hydrogen production unit".

International Conferences

G. Barbieri, I. Mirabelli, A. Brunetti, E. Drioli, H. A. Al-Megren, M.C. Al-Kinany, "Direct conversion of n-butane to iso-butene in membrane reactors: a thermodynamic analysis", ECCE9 – European Congress of Chemical Engineering, April 21-24, Hague (The Netherlands), oral presentation.

G. Barbieri, I. Mirabelli, A. Brunetti, E. Drioli, H. A. Al-Megren, M.C. Al-Kinany, "Direct conversion of n-butane to isobutene in membrane reactors: a thermodynamic analysis", 9th World Conference in Chemical Engineering, Coex Seoul (South Korea), August 18-23, 2013, poster presentation.

G. Barbieri, I. Mirabelli, A. Brunetti, E. Drioli, H. A. Al-Megren, M.C. Al-Kinany, "Direct conversion of n-butane to isobutene in membrane reactors: a thermodynamic analysis", ICHEAP 11 - 11th International Conference on Chemical & Process Engineering 2-5 June 2013 - Milan (Italy), poster presentation.

D. Aiello, I. Mirabelli, F. Testa; "Adsorption of 2-methylbenzoic acid onto MCM-41 materials: a kinetic study" FEZA , 2011, Valencia (Spain), 3-7 July 2011, oral presentation.

National Conferences

G. Barbieri, I. Mirabelli, A. Brunetti, F. Drioli, H. A. Al-Megren , M. C. Al-Kinany; "Direct Conversion of n-Butane to Isobutene in Membrane Reactors: Thermodynamic Analysis"; Convegno congiunto delle sezioni Calabria e Sicilia 2012, 6-7 December 2012 - Arcavacata di Rende Cosenza (Italy); poster presentation.

Encyclopaedia entries

Mirabelli I., "Dehydroisomerization reaction of n-butane to iso butene", Encyclopedia of Membranes edited by Drioli E. and Giorno L., Springer, in press.

Mirabelli I., "n-butane dehydrogenation by membrane reactor", Encyclopedia of Membranes edited by Drioli E. and Giorno L., Springer, in press.

Workshops

"Pd membrane technology scale-up", CACHET-II, CARENA and CoMETHy International Joint Workshop, November 12-14th 2012, Rome (Italy).

"Membranes and Membrane Reactors", CARENA - DEMCAMER Workshop", January 30th 2013, Eindhoven University of Technology (The Netherland).

"Joint Workshop on Scale-up of Pd Membrane Technology From Fundamental Understanding to Pilot Demonstration", November 20-21, 2014, Petten (The Netherlands) Brunetti A., Mirabelli I., Drioli E., Magaud V., Dauriat A., Roses L., Barbieri G., "How membrane reactors can affect hydrogen production", Oral presentation.

Mobility period

November 2013 – July 2014 at HyGear B. V., Arnhem (The Netherlands) under the supervision of Dr. Michael Walter and Dr. Leonardo Roses.

Schools

XXX EMS Summer School on Membranes: "Membranes for liquid separations from an industrial & academic point of view." July 22th-26th 2013, Essen (Germany). (27 hours).

XXIX EMS Summer School on Membranes: "Dense polymeric membranes fundamentals & applications: packaging, barriers & industrial separations". July 10th-13th 2012, Nancy (FRANCE). (27 hours).

PhD school GRICU 2012: "Transport Phenomena and Separation Processes." September 20th – 23rd 2012, Montesilvano, Pescara. (27 hours).

Lectures

"Membranes: Improving Our Standard of living", lecture by Prof. Kang LI, Imperial College of London (United Kingdom), ITM-CNR

"Preparation and Characterization of Polymer Membranes", lecture by Prof. Heiner Strathmann, University of Stuttgart (Germany), ITM-CNR

COMSOL Multiphysics , practical lecture on simulations, UNICAL

Teaching activity

2012/2013 Chemistry course practise at the engineering faculty University of Calabria.